WILEY-VCH

DOI: 10.1002/ ((please add manuscript number))
Article type: ((**Review**))

Emerging Semitransparent Solar Cells: Materials and Device Design

*Qidong Tai and Feng Yan**

Dr. Qidong Tai and Prof. Feng Yan

Department of Applied Physics, The Hong Kong Polytechnic University,

Hung Hom, Kowloon, Hong Kong.

Email: apafyan@polyu.edu.hk

Keywords: (semitransparent, organic solar cells, dye-sensitized solar cells, perovskite solar cell)

Abstract

Semitransparent solar cells can provide not only efficient power-generation but also appealing images and show promising applications in building integrated photovoltaics, wearable electronics, photovoltaic vehicles and so forth in the future. Such devices have been successfully realized by incorporating transparent electrodes in new generation low-cost solar cells, including organic solar cells (OSCs), dye-sensitized solar cells (DSCs) and organometal halide perovskite solar cells (PSCs). In this review, we will summarize the advances in the preparation of semitransparent OSCs, DSCs, and PSCs, focusing on the transparent top electrode materials and the device designs, which are all crucial to the performance of the devices. The techniques for optimizing the efficiency, color and transparency of the devices will be addressed in details. In the end, we will summarize the research field and provide an outlook for the future development.

1. Introduction

Solar energy is a clean and sustainable resource for our future energy needs. The solar energy received on earth's surface per year is about 120,000 terawatts, which is 6-7 thousand times more than the current global energy consumption.[1] Photovoltaic (PV) technology that can directly convert the sunlight into electricity is an efficient way to harness the solar energy. To date, the PV market all over the world has been dominated by inorganic silicon-based solar cells for their advantages of high efficiency and stability. However, some disadvantageous of silicon solar cells, such as the high cost and the environmental concerns in their production, will prohibit their large-scale applications. Therefore, increasing attentions have been drawn to emerging alternative PV technologies.

The representative new generation solar cells, including organic solar cells (OSCs), dye-sensitized solar cells (DSCs) and perovskite solar cells (PSCs), have been investigated by a large number of research groups due to many advantages of the devices over Si-based counterparts. OSCs are devices based on organic semiconductors that can form staggered heterojunctions between them. The first OSC was reported by Tang in 1986, who combined copper phthalocyanine (CuPc) and a perylenetetracarboxylic derivative to form a heterojunction in a device. Although a relative low efficiency (about 1%) was obtained, this is the first demonstration of an organic device with the photovoltaic effect.[2] A substantial improvement in device efficiency was realized by introducing the concept of bulk heterojunction OSCs in polymer-fullerene and polymer-polymer systems by Heeger's and Friend's groups, respectively.[3] DSC is a photoelectrochemical system based on a dye-sensitized photoanode, an electrolyte and a counter electrode. In 1991, O'regan and Grätzel reported their breakthrough work on DSCs for the first time and thus the devices are also known as the Grätzel cells.[4] These two types of solar cells are known for their advantages of easy fabrication, light weight, environmental friendliness, and low cost, and regarded as promising alternatives to silicon solar cells in some applications. Therefore, tremendous

efforts have been spent to improve the efficiency and stability of the devices in the past two decades[1, 5] and both solar cells can reach certified power conversion efficiencies (PCEs) of over 11% now (Fig. 1).[6]

In 2009, Miyasaka's group pioneered the application of methylammoniumlead halide perovskites as sensitizers in liquid-electrolyte DSCs and achieved a 3.8% PCE. However, the device stability was poor since the perovskite materials dissolved rapidly in the organic solvent.[7] In 2012, key advances in the application of the perovskites in solar cells were made by Park's and Snaith's groups when the liquid electrolyte in a DCS was replaced with a solid-state hole transporting material (HTM) 2,2',7,7'-tetrakis(N,N-di-p-methoxyphenylamine)-9,9'-spirobifluorene (Spiro-MeOTAD) and promising PCEs of ~10% in the solar-state devices were first achieved by them.[8] Since then, an unprecedented rapid development of PSCs was witnessed[9] and highlighted by a recently certified PCE of 22.1% (**Figure 1**), which is comparable to those of polycrystalline silicon- and copper indium gallium diselenide (CIGS)- solar cells.[6]

One beauty of the emerging solar cells that outshines conventional silicon solar cells is their possibilities to be made semitransparent (ST), despite state-of-art devices are usually nontransparent because highly reflective metal electrodes (Pt, Al, and Au or Ag) are typically used in the devices. ST solar cells can be easily fabricated by reducing the thickness of the active layers and using transparent top electrodes and they would be appealing for applications in building integrated photovoltaics (BIPVs) as electricity-generating facades, shelters, roofs, and windows.[10] Besides, they may also find broad applications in future solar-powered automotive and wearable electronics. Though ST solar cells typically endure efficiency loss compared to their opaque counterparts, due to the reduced light absorption in the active layers and lack of reflecting light from the top electrodes, they may have higher power generation efficiency for their capabilities of receiving incident light from both

sides.[11] Besides, the ST solar cells can also be conveniently combined with other solar cells to form tandem devices with enhanced light-harvesting in a broader wavelength region and thus lead to a higher efficiency than that of a single-junction device.[12]

Because the efficiency and transparency of ST solar cells typically compromises each other, the major challenge in the fabrication of ST solar cells is how to realize high efficiency and tunable transparency from both sides of the devices, which are closely related to the properties of the two transparent electrodes on the bottom and the top of the devices and the active layers. As summrized in **Table 1**, recent developments of transparent electrodes based on thin films of metal nanowires, graphene, carbon nanotubes (CNTs) and so forth offer great opportunities for preparing high-performance ST solar cells[13]. In fact, many interesting works on the fabrication of ST-OSCs, DSCs, and PSCs have been reported recently. However, the progress achieved in this specific area lags far behind that for normal opaque devices. Hence, we present a comprehensive review here on the developments in this area with a view to inspiring more fantastic ideas on material synthesis and device design that may finally lead to major progress in the fabrication and application of ST solar cells.

2. Basics of semitransparent solar cells

2.1. Performance characterization

To identify the performance of different types of solar cells, devices should be characterized at a standard condition. The important parameters for a solar cell include power conversion efficiencies (PCE), external quantum efficiency (EQE), internal quantum efficiency (IQE) and transparency. The performance of a solar cell is normally characterized under a solar simulator with a spectrum similar to that of solar light. Due to the influence of atmosphere**,** the solar spectrum on earth's surface is different from that in space and varies with the path length that the sunlight passes through the atmosphere. Air mass (AM) refers to the path length of sunlight through the atmosphere normalized to that when sun is directly

overhead (at Zenith).[14] So AM 1.5 (AM=1.5) solar spectrum is defined as the standard reference for the terrestrial testing of solar cells (**Figure 2a**).

Power conversion efficiency The PCE of a solar cell is calculated from its current density (*J*)-voltage (*V*) curve measured under AM 1.5 solar illumination. As illustrated in **Figure 2b**, the PCE is determined by the open-circuit voltage (V_{OC}), short-circuit current density (J_{SC}), fill factor (*FF*) and the power of the incident light (P_{in}):

$$PCE = \frac{V_{OC} * J_{SC} * FF}{P_{in}} \quad (1)$$

The *FF* is defined as the ratio of the maximum power (P_{max}) divided by the product of V_{OC} and J_{SC}:

$$FF = \frac{V_{MP} * J_{MP}}{V_{OV} * J_{SC}} \quad , \quad (2)$$

where V_{MP} and J_{MP} correspond to the voltage and current density at the maximum power point MP shown in Figure 2a, respectively.

External quantum efficiency EQE shows the spectral response of a solar cell in terms of the current output upon illumination by a particular wavelength of light. The corresponding EQE value is given by the ratio between the number of collected photo-generated charges and the number of incident photons. So EQE is determined by a serials of factors related to the charge generation and collection, such as light harvesting efficiency, charge (exciton) generation efficiency, charge (exciton) separation efficiency, charge collection efficiency and so on. *Jsc* can be predicted from EQE by the following equation:

$$J_{SC} = e \int_{\lambda \min}^{\lambda \max} \Phi(x) EQE(\lambda) d\lambda \quad , \quad (3)$$

where *e* is the elementary charge, $\Phi(\lambda)$ is spectral photon flux of the incident light.[15]

Internal quantum efficiency The IQE of a solar cell is defined as the ratio of the number of collected charges to the number of photons absorbed in the active layer. The IQE value is

inversely related to the amount of recombination taking place in the cell, and the spectral shape of the IQE curve can provide information about the exciton harvesting efficiency or the spatial dependence of the charge recombination.[16] The relationship between IQE and EQE can be expressed as:

$$EQE = \eta_A IQE \ , \tag{4}$$

where η_A is the light harvesting efficiency of the active layer. However, the IQE cannot be correctly obtained by measuring the absorption of the bare active layer on glass because the optical field distribution in the active layer of a solar cell does not follow the exponential decay law due to the cavity interference effect caused by the reflective back electrode. Since it is impossible to direct measure the absorption of the active layer in a device, optical simulation (for example, transfer matrix method) has been developed to calculate the absorption of each layer in the device, from which true IQE values could be obtained by subtracting the parasitic absorption in the non-active layers. The typical methods that have been used to determine the IQE values of solar cells are summarized in **Figure 2c**.[17] The IQE response is spectrally flat when the exciton harvesting efficiency is uniform across the device and *vice versa*. Therefore one can evaluate where exciton recombination occurs by comparing the IQE spectrum with the optical field distribution in the device.

Notably, the PCEs, EQEs, and IQEs of ST solar cells can be measured under illumination from either side (bottom or top) of the device, which is different from conventional nontransparent solar cells. A comparison between the different shapes of J-V, EQE and IQE curves measured from different sides could provide valuable insights into device operation and possible loss mechanisms, which is beneficial for device optimization.[18]

2.2. Transmittance, reflectance and color characterization

The transmittance or transparency of ST solar cells, as a unique property of this type of devices, is usually characterized by measuring the average visible transmittance (AVT) of the device in the visible region (370-740 nm) with a spectrophotometer. The requirement of AVT is dependent on real applications. For example, AVT of 25% or higher is required for the applications in windows.[19]

The reflectance of a ST solar cell is important for its practical applications. Moreover, the characterization of the reflectance of a solar cell will help us to better understand the device physics. For example, to obtain the correct IQE value of a solar cell, the reflectance of the device should be considered in device simulation. However, a traditional specular reflection measurement on a solar cell would overestimate the light absorption of the device since a significant amount of light would be diffusively reflected or scattered. Therefore, it is necessary to obtain a more accurate diffusive reflectance that can be measured with a UV-Vis spectrophotometer equipped with an integrating sphere. [16]

Color is another important attribute of ST solar cells, which is typically determined by the photoactive layers and electrodes. Moreover, the color appearance of a ST solar cell can be tuned by optical manipulation, such as the use of metal/dielectric/metal (MDM) microcavity electrodes[20] or dielectric mirrors.[21] The optical perception of ST solar cells by human eyes was first taken into account by Ameri *et al* in 2010 when they studied ST-OSCs,[22] as the transparency color perceptions of ST solar cells by human eyes are usually different from that revealed by instruments. CIE 1931 *xy* chromaticity diagram, which is specially designed for human perception of colors, can be used to evaluate the transparency color properties of ST solar cells. The color coordinate (x,y) of a ST solar cell is calculated from the corresponding transmitted light, represented by the product of incident light spectrum and the transmittance spectrum of the device. Standard daylight illuminant D65 and AM 1.5G solar spectrum are typically chosen as reference light sources (incident light) for determining the color

parameters of ST solar cells. Though colorful semitransparent solar cells may be favorable for decoration purposes, neutral-color semitransparent solar cells with color coordinates close to "white point" (0.3333, 0.3333) or that of illuminant D65 (0.3128,0.3290) and AM 1.5G light (0.3202,0.3324) (**Figure 3**) are generally preferred for window applications, as the natural lighting environment won't be influenced too much.[23]

The color rendering property of ST-OSCs was first considered by Colsmann *et al* in 2011.[24] It is also an importance characteristic for ST solar cells when they are integrated in windows, louvers and overhead shelters. As the color rendering properties of ST solar cells cannot be simply judged from their transparency perception, color rendering index (CRI) is introduced to present the variation degree between the transmitted light and the incident light for the devices. The CRI of a ST solar cell can be calculated from the transmitted light by following the standard CIE procedure and expressed on a scale of 0-100. A higher CRI means better color rendering capacity and thus a higher neutral color degree. The CRI of a ST solar cell is influenced by a series of factors, including device architecture, active material and electrode transmittance. Many methods have been be proposed to improve the CRIs of ST solar cells, such as the use of low bandgap materials,[19, 24] the use of materials with complementary optical absorption,[25] and the incorporation of dye into active layers.[23b] However, in most cases, the CRI value should compromise with device performance. Consequently, novel strategies have been developed to improve the CRIs of ST solar cells without sacrificing device performance. For example, an extra light-coupling/reflecting layer (e.g. dielectric/metal/dielectric (DMD) electrode) has been introduced on top of semitransparent metal anodes of ST-OSCs and led to almost 100% CRIs.[26]

2.3. Optical simulation

Since the optical propeties, such as color and transparency, of ST solar cells are also important in practical applications, optical simulation is needed in optimizing the device

design, which can determine the optical field distribution through each layer at a given wavelength and calculate the light absorption of the active layer and the parasitic absorptions. The common approach for simulating a multilayer structure is the transfer matrix method (TMM) established by Pettersson *et al* in 1999.[27] **Figure 4a** shows the schematic illustration of a multilayer with forward and backward-propagating optical electric field components used for TMM calculation. The optical property of each layer j (j = 1,2,…,m) is described by its thickness (d_j) and complex index of refraction ($N_j=n_j+jk_j$, where n_j and k_j could be obtained using spectroscopic ellipsometry). The optical electric field at any point is composed of two components: one is propagating in the positive direction ($\boldsymbol{E}_j^+(x)$) and the other in the negative direction ($\boldsymbol{E}_j^-(x)$). Assume the multilayer is illuminated from the direction vertical to the surface, the optical electric field in the two outmost layers $j=0$ and $j=m+1$ can be described by the transfer matrix $\boldsymbol{S}$:

$$\begin{bmatrix} \boldsymbol{E}_0^+ \\ \boldsymbol{E}_0^- \end{bmatrix} = \boldsymbol{S} \begin{bmatrix} \boldsymbol{E}_{m+1}^+ \\ \boldsymbol{E}_{m+1}^- \end{bmatrix} \tag{5}$$

$$\boldsymbol{S} = \boldsymbol{I}_{01}\boldsymbol{L}_1\boldsymbol{I}_{12}\ldots\boldsymbol{L}_m\mathbf{I}_{m+1} \tag{6}$$

where $\boldsymbol{I}_{j(j+1)}$ corresponds to the propagation of optical electric field at the interface between layer j and $j+1$,, while $\boldsymbol{L}_j$ is for the propagation in layer j. The matrix $\boldsymbol{I}$ and $\boldsymbol{L}$ are described as follows:

$$\mathbf{I}_{ij} = \frac{1}{t_{ij}} \begin{bmatrix} 1 & t_{ij} \\ r_{ij} & 1 \end{bmatrix} \tag{7}$$

$$\boldsymbol{L}_j = \begin{bmatrix} e^{-i\xi_j d_j} & 0 \\ 0 & e^{i\xi_j d_j} \end{bmatrix}, \tag{8}$$

where r_{ij} and t_{ij} are the Fresnel complex reflection and transmission coefficients at interface *ij*, respectively. Consequently, the optical electric field at an arbitrary position inside layer *j* is given by:

$$\boldsymbol{E}_j(x) = \boldsymbol{E}_j^+(x) + \boldsymbol{E}_j^-(x) = (t_j^+ e^{i\xi x} + t_j^- e^{-i\xi x})\boldsymbol{E}_0^+$$

(9)

The computer code for the calculation is available from McGehee's group.[16]

We have mentioned before that the optical simulation can be used to determine the accurate IQE values of solar cells. Besides, it has been widely used for optimizing the thickness of each functional layer in ST solar cells with a view to obtaining the most balanced photocurrent generation and device transmittance. For instance, Chen *et al* reported that a WO_3/Ag/WO_3 DMD structure was used as transparent top electrodes in inverted ST-OSCs as shown in **Figure 4b** and the optical and electric properties of the devices could be tailored by changing the thickness of the outer WO_3 capping layer. In order to find the optimal thickness of the WO_3 capping layer, optical simulation was conducted to calculate the spatial distribution of the optical field intensity across the solar cells and find the dependence of the photocurrent generation efficiency on the thickness of the WO_3 capping layer (**Figure 4c**). In addition, the influence of the thickness of the WO_3 capping layer on the transmittance of the device was also simulated (**Figure 4d**).[28] They found that the optical simulation was in a good agreement with experimental results. Optical simulation in ST solar cells can also be found in many other reports, which in turn provides a guideline for the optimum design of the devices.[18, 26, 29]

3. Semitransparent organic solar cells (ST-OSCs)

The active layer of an OSC is made of organic donor and acceptor molecules. Some representative donor materials, including poly[2-methoxy-5-(2-ethylhexyloxy)-1,4-

phenylenevinylene] (MEH-PPV), poly(3-hexylthiophene) (P3HT), polythieno[3,4-b]-thiophene/benzodithiophene (PTB7) and the most recently reported poly[(5,6-difluoro-2,1,3-benzothiadiazol-4,7-diyl)-alt-(3,3’’’-di(2-nonyltridecyl)-2,2’;5’,2’’;5’’,2’’’-quaterthiophen-5,5’’’-diyl)] (PffBT4T-C_9C_{13}), have been successfully used in OSCs and the corresponding efficiencies of OSCs were improved from 3% to about 12%.[30] Acceptors previously used in high-efficiency OSCs are mainly fullerene derivatives, such as [6,6]-phenyl C61/71 butyric acid methyl ester ($PC_{61}BM$/$PC_{71}BM$), indene-C_{60}bisadduct (ICBA) and so on,[5h, 5i] while non-fullerene acceptors have attracted much attention recently since the devices based on them also showed efficiencies close to 12%, recently.[31]

Figure 5a depicts the typical structure of a single junction OSC. The device has a bicontinuous intermixed layer of electron donor and acceptor materials that form a bulk heterojuncton (BHJ). The BHJ layer is sandwiched between an anode and a cathode with a selective charge transport layer on each side. The working mechanism of an OSC is mainly attributed to exciton dissociation at the organic heterojunction as illustrated in **Figure 5b**, which has been described in details in many papers.[1b, 5h]The device can be fabricated with either a conventional structure containing indium tin oxide (ITO) as an anode and a low-work-function metal (e.g. Al) as a cathode or an inverted structure using ITO as a cathode and a high-work-function metal (e.g. Au or Ag) as an anode.[1b, 5l]The maximum certified PCE of a single junction OSC has recently been realized by Yan’s group with the value of 11.5%, which however is still far below the Shockley-Queisser limit. One major reason is the loss of V_{OC} due to the thermalization loss of electrons and holes generated by the photons with energy greater than the bandgaps of the donors.[32] Higher PCEs are expected by employing a tandem device structure (**Figure 5c**) consisting of two or more independent active layers with complementary absorption.[33]The corresponding energetic diagram is displayed in **Figure 5d**. Both single junction and tandem OSCs can be made semitransparent when transparent top electrodes are applied. As summarized in **Table 2**, many types of ST-OSCs have been

developed successfully and can be roughly classified according to the transparent top electrode materials since the transparent electrodes are the critical part in the devices, which significantly differentiate the ST-OSCs from normal OSCs.

3.1. Transparent top electrodes for ST-OSCs

Conventional transparent electrodes in OSCs are mainly made of ITO or other transparent conductive oxides (TCOs), which should be prepared at a relatively high temperature. However, the direct deposition of the oxide electrodes on an organic active layer may dramatically degrade the device performance. Therefore, various materials with good conductivity as well as high transparency itemized below have been introduced in ST-PSCs as the transparent top electrodes.

3.1.1. Thin film Au/Ag transparent top electrodes

The most convenient way to prepare transparent top electrodes for OSCs is to deposit ultrathin metal films (*i.e.* Au and Ag) by thermal evaporation, which is similar to the preparation of opaque OSCs, while the thicknesses of the metal films need to be accurately controlled to make them transparent. It is notable that the transparency of the metal films can be very low if their thicknesses are enough for achieving high conductance. So there is a trade-off between the transparency and the conductivity for the metal electrodes and they are normally not the best transparent electrodes for high efficiency ST devices.

Though intensive attention has been paid to OSCs since 1995, ST-OSCs had not been realized until 2006, when the devices with thin film Au electrodes (~12 nm) were first reported by Yang's group.[34] They studied V_2O_5 and Cs_2CO_3 interfacial buffer layers in OSCs based on poly(3-hexylthiophene) (P3HT) and [6,6]-phenyl C60 butyric acid methyl ester ($PC_{60}BM$) blend. Using V_2O_5 as a hole transport layer (HTL), they were able to fabricate a ST-OSC with an inverted structure of ITO/Cs_2CO_3/P3HT:$PC_{61}BM$/V_2O_5/Au, which showed

PCEs of 0.85% and 0.52% under light illumination from the ITO and Au sides, respectively.[34]

In 2009, Koeppe *et al* demonstrated the fabrication of ST-OSCs based on the blend of small-molecule zinc phthalocyanine (ZnPc) or zinc naphthalocyanie (ZnNc) and pyrollidinofullerene (PyF)using thin film Ag electrodes. When the thickness of the Ag electrode is 10nm, the devices showed PCEs of ~0.5% and a peak device transparency of over 60% in the visible region. They also found that ZnPc could be used as an anti-reflection coating (ARC) to further enhance the device transmittance.[35] The modification of the Ag electrode with an Al interlayer and a tris(8-hydroxyquinolinato)-aluminum (Alq3) capping layer could lead to the increase of PCEs to above 2% for the devices based on ZnPc and C_{60}.[36] Then, Meiss *et al* demonstrated a semitransparent tandem solar cell based on fluorinated ZnPc (red absorber), α,ω-bis(dicyanovinyl-sexithiophene-Bu(1,2,5,6) (DCV6T) (green absorber), and C_{60}, which exhibited a much higher PCE of 4.9% at AVT of 24%.[37] In 2012, Jen's group reported the fabrication of inverted ST-OSCs based on low bandgap donor poly{[4,8-bis-(2-ethyl-hexyl-thiophene-5-yl)-benzo[1,2-b:4,5-b′]dithiophene-2,6-diyl]-*alt*-[2-(2′-ethyl-hexanoyl)-thieno[3,4-b]thiophen-4,6-diyl]}(PBDTTT-C-T) and $PC_{71}BM$ as shown in **Figure 6a**. It was found that when the thicknesses of the Ag electrodes increased from 6 to 60 nm, the PCEs of the devices increased from 4.25 to 7.56%, while the corresponding AVT decreased from 35.9 to 2%. So the optimized device showed a promising PCE of ~6% with intermediate AVT of ~25%. It is worth noting that all of the devices showed very high CRIs close to 100%, despite their color coordinates moved toward blue when the Ag electrodes became thicker (**Figure 6b,c**).[19] In a followed study by the same group, a PCE of 5% and a remarkable device AVT as high as 47.3%were achieved in a device using a fluoro-containing low bandgap polymer poly[2,6-(4,4-bis(2-ethylhexyl)-4H-cyclopenta[2,1-b;3,4-b']dithiophene)-alt-4,7-(5-fluoro-2,1,3-benzothia-diazole)] (PCPDTFBT).[38] They also reported a poly(indacenodithiphene-co-phenanthro[9,10-

b]quinoxaline) (PIDT-PhanQ) and $PC_{71}BM$ based ST-OSC by using a transparent fullerene surfactant/Ag hybrid top electrode, which showed a PCE of 4.2% at AVT of ~32%.[29d]

Similarly, Silva *et al* reported a flexible ST-OSC based on the blend of poly[(4,40-bis(3-(2-ethyl-hexyl)dithieno[3,2-b:30-d]silole)-2,6-diyl-alt-(2,5-(3-(2-ethylhexyl)thiophen-2-yl)thiazolo[5,4-d]thiazole)) (PSEHTT) and ICBA using an Ag transparent electrode. Instead of p-type metal oxides, polyaniline (PANI) film was used as the HTL and buffer beneath the Ag electrode. An 18 nm PANI film was found to be optimal and the corresponding device showed a considerable PCE of 6.87% with AVT of 36%.[39]

The high reflectance of thin film metal electrodes limits the transmittance and top-illuminated efficiency of ST-OSCs. To solve this problem, Ren*et al* proposed a hybrid optical nanostructure of metal/nanoparticle/dielectric (M/NP/D) to replace the metal transparent electrodes of ST-OSCs. The device employing a Ag/Si NPs/Alq3 electrode and an active layer based on a low bandgap polymerpoly(2,6'-4,8-bis(5-ethylhexylthienyl)benzo[1,2-b;3,4-b]thiophene-alt-5-dibutyloctyl-3,6-bis(5-bromothiophen-2-yl)pyrrolo[3,4-c]pyrrole-1,4-dione)(PDBTT-DPP) and $PC_{71}BM$showed remarkable 61% and 34% enhancement of the AVT and top-illuminated PCE, respectively, compared to a control device based on a bare Ag (10nm) electrode.[40]In addition, Shen's group has done serial studies on improving the transmittance and efficiencies of ST-OSCs with an inverted structure of ITO/TiO_2/BHJ blend/HTL (WO_3, MoO_3, V_2O_5)/Ag, by introducing one-dimensional photonic crystals (1DPCs) as reflecting layers (composed of multi-layered WO_3/LiF film)[26, 41]or a light coupling layer (e.g. V_2O_5) on top of the Ag electrode.[29b, 42] In the latter case, a dielectric/metal/dielectric (DMD) microcavity was formed, which is a convenient strategy to enhance the transparency of ST-OSCs.[28, 43] Besides, non-periodic photonic crystals (composed of multilayer dielectric structure[44]) were applied on top of thin film Ag electrodes to enhance the light-harvesting of PTB7:$PC_{71}BM$ -based ST-OSCs, while high device transparency was maintained. Consequently, a PCE of 5.6% was obtained at the device AVT

close to 30%. It was also demonstrated that this kind of photonic structure could be used to tune the color of ST-OSCs.[29c]

3.1.2. Transparent conductive oxide (TCO) based transparent top electrodes

ITO is better than a thin film metal electrode in achieving high device transmittance. However, an ITO electrode can only be prepared by a high-energy sputtering method, which may cause undesired damage to the organic layer. Inverted OSCs employing hole selective metal oxides including V_2O_5/VO_x, WO_3/WO_x, MoO_3/MoO_x and NiO/NiO_x HTLs, can withstand the sputter deposition of ITO electrode, due to the protective role of metal oxides. For example, Schmidt et al successfully fabricated a ST-OSC with inverted structure of ITO glass/TiO_2/P3HT:$PC_{61}BM$/MoO_3/ITO (sputtered), which showed a PCE of 1.9% and transmittance of ~80% in the red region of the visible spectrum.[45]

In another work reported by Yang's group, they demonstrated ST-OSCs based on the same active layer prepared by a facile lamination way illustrated in **Figure 7**.The devices showed PCEs of ~3% under standard AM 1.5 ($100mWcm^{-2}$) illumination, which are comparable to the performance of normal opaque devices.[46] One key step in the lamination process is to use D-sorbitol doped poly(ethylenedioxythiophene):poly(styrene-sulfonate)(PEDOT:PSS) as both HTL and electric glue to enhance the electric contact between laminated components.

Al:ZnO (AZO) has been widely explored as alternative bottom electrodes to ITO in OSCs, however, very little study can be found on the application of AZO as transparent top electrodes for ST-OSCs. Similar to the case of ITO top electrodes, sputtering is required for preparing transparent AZO top electrodes. Therefore, a protecting underlayer beneath an AZO top electrodeis necessary in the fabrication of efficient ST-OSCs. In 2012, Bauer *et al* reported the fabrication of ST-OSCs with AZO electrodes based on the active layer of

poly[[9-(1-octylnonyl)-9h-carbazole-2,7-diyl]-2,5-thiophenediyl-2,1,3-benzothiadiazole-4,7-diyl-2,5-thiophenediyl] (PCDTBT) and $PC_{71}BM$.Solution-processed TiO_x layer was used as both electron selective layer and protective layer. However, it was found that the direct contact of AZO and TiO_x could lead to the formation of visible cracks in the AZO layer caused by the chemical instable interface. Therefore, Al interlayer was introduced between AZO and TiO_x layer. Under the optimal condition, an average PCE of ~4% was obtained with average device transmittance of ~34% in the 300-1300 nm region.[47]

3.1.3. Silver nanowire (AgNW)-based transparent top electrodes

AgNWs are considered to be good alternative electrode material for preparing high performance ST-OSCs, for their advantages of high conductivity and transparency (capable of achieving 90% transmittance with sheet resistance below 15 Ωsq^{-1}), high flexibility, low temperature and solution processability.[13a, 48] Transparent AgNW top electrodes can be integrated into ST-OSCs via lamination,[49] drop casting,[50] doctor blading,[51] inkjet printing[52] and spray coating.[25, 53] Among these methods, spray coating turns out to be the most used one, because it is easy, scalable and more importantly, its impact on the underlying organic layer is minimum.

The application of AgNWs in P3HT:$PC_{61}BM$ based ST solar cells resulted in PCEs of ~2%, under illumination from either ITO or AgNW side.[53b]A 2-fold enhanced PCE (4%) was achieved by Yang's group, with a visibly transparent OSC (~66% transmittance at 550 nm) based on the blend of PDBTT-DPP and $PC_{61}BM$ and an AgNW-based composite transparent top electrode (**Figure 8a, b**).The AgNW-based composite electrode is prepared by a multi-step process, in which the AgNWs were first spray-coated on the active layer, followed by the coating of a TiO_2 sol-gel solution to enhance the connection between AgNWs and the adhesion of AgNWs to the underlying active layer. Finally, ITO nanoparticles (NPs) were used to fill the empty space in the AgNW network to improve the charge collecting efficiency

of the AgNW electrode.[53a] In a further study by the same group, this type composite transparent electrodes were applied to ST tandem OSCs, in which $PC_{61}BM$, $PC_{71}BM$ and two infrared (IR) sensitive polymers PBDTT-FDPP-C_{12}, PBDTT-SeDPP were used as active materials (PBDTT-FDPP-C_{12}:$PC_{61}BM$ for front subcell, PBDTT-SeDPP:$PC_{61}BM$/$PC_{71}BM$ for back subcell) and multiple layers of poly[(9,9-di(3,3'- N,N' - trimethylammonium)propylfluorenyl-2,7-diyl)-*alt*-(9,9-dioctylfluorenyl-2,7-diyl)] diiodide salt (PFN) /TiO_2/PEDOT:PSS were used as interconnecting layer (**Figure 8c**). The color of the tandem solar cells could be altered from light green to light brown by replacing the $PC_{61}BM$ in the back subcell with $PC_{71}BM$. The greenish devices showed PCEs of ~6% with AVT of ~40%, while the brownish devices showed PCEs of ~7% with AVT of ~30% (**Figure 8d,e**).[25]

The high carrier density of ITO NPs would cause parasitic optical absorption when they are used as fillers in AgNW-based transparent electrodes. As proposed by Beiley *et al*, this problem could be overcome by replacing the ITO NPs with ZnO NPs since the conductivity of the filling materials does not need to be very high. Such a AgNW-ZnO NP composite transparent electrode reached a sheet resistance of 14 Ωsq^{-1}at AVT >90%, resulting in PCEs of 4-5% in a ST-OSC with an active layer composed of poly(di(2-ethylhexyloxy)benzo[1,2-b:4,5-b']dithiophene-co-octylthieno[3,4-c]pyrrole-4-6-dione)(PBDTTPD) and $PC_{71}BM$.[53c]

In 2015, Guo *et al* reported a remarkable progress in fabricating large-scale ST-OSC modules on both glass and plastic substrates by using AgNWs as transparent top electrodes (**Figure 9a,b**). One key advance reported in their work was the application of a high-precision laser patterning system, which could effectively improve the electric contacts between individual cells and reduce the dead area in the module, thus allowing the fabrication of large-area ST-OSC module (64 cm^2) with an electric FF as high as ~63% and geometric FF over 95%.This method is promising for future commercial fabrication of ST-OSC modules.[51b]

Most recently, Min *et al* reported for the first time solution-processed small-molecule based ST-OSCs using AgNW top electrodes. The device structure is illustrated in **Figure 9c**, in which a ZnO/perylenediimide derivative (PDINO) bilayer was used as cathode buffer and four small molecules with different absorptions (colors) were employed as electron donors (**Figure 9d**), and $PC_{71}BM$ was used as electron acceptor. Under optimized conditions, the ST-OSC employing the 2D-conjugated molecule based on alylthio-thienyl-conjugated side chain (BDTT-S-TR) gave the highest PCE of 3.62%. In addition, the transparency perceptions of these solar cells by human eyes were also analyzed and all the devices showed color coordinates close to white light (**Figure 9e**).[53e]

3.1.4. CNT-based transparent top electrodes

CNTs are one of the most promising materials for preparing transparent electrodes, for their advantages of high carrier mobility and conductivity, high flexibility, and high chemical and mechanical stability.[13a] CNT-based transparent conducting films have been widely studied in many types of optoelectronic devices, including OSCs.[13c, 54]However, most of the studies have focused on the application of transparent CNT films as bottom electrodes to replace ITO. There are few reports on the use of transparent CNT films as top electrodes for ST-OSCs. In 2012, Kim *et al* reported a small-molecule ZnPc and C_{60}-based ST-OSC with laminated free-standing multi-walled CNT (f-CNT) top electrode, which was prepared by a chemical vapor deposition (CVD) method (**Figure 10**). The as-laminated CNT electrode should be densified for improved transparency and conductivity (by immersing the whole device into orthogonal liquid hydrofluoroether for several seconds). Under optimal conditions, the final device showed PCEs of 1.5% and 1% with illumination from the ITO and CNT sides, respectively. In addition, better stability was observed for the CNT-based device compared to Ag-based control device.[29a]Besides, the transparent f-CNT electrodes were also used to fabricate ITO-free ST-OSCs by the same group, which will be discussed later.[55]

Very recently, Jeon *et al* reported the fabrication of ST-OSCs with laminated transparent single-walled CNT films based on an inverted device structure of ITO/ZnO/PTB7:$PC_{71}BM$/MoO_3/CNT. The CNT films were prepared via aerosol CVD method and p-doped by HNO_3 or MoO_x to improve the film conductivity and transmittance. When thin CNT films with 90% transmittance at 550 nm were used, 3.7 and 3.1% PCEs were obtained from the HNO_3 and MoO_x-doped devices, respectively, with illumination from ITO sides. Higher PCEs of 4.1 and 3.4% were observed when thicker CNT films (60% transmittance at 550 nm) were used. In comparison, the reference device employing an opaque Ag top electrode showed a PCE of 7.8%.[56]

3.1.5. Graphene-based transparent top electrodes

Graphene, the thinnest two-dimensional carbon material, has been extensively explored as transparent conductive electrodes for optoelectronic devices in recent years, for its advantages of high transparency and conductivity (transmittance of 90% and a sheet resistance of less than 30 Ωsq^{-1}), excellent mechanical flexibility and chemical stability.[13a, 13d]Up to now, graphene-based transparent electrodes have been successfully used in OSCs as both bottom and top electrodes.

In 2011, Lee et al reported a ST-OSC using a top laminated graphene electrode with an inverted structure of ITO/ZnO/P3HT:$PC_{61}BM$/graphene oxide (GO)/graphene, where the GO serves as HTL. They found that the sheet resistance of the graphene film decreased remarkably with the increasing number of graphene layers, whereas the film transmittance was reduced for about 2-3% with each layer of graphene added. The final device reached the best PCE of 2.5% with a 10-layer graphene electrode when illuminated from the ITO side, while the best device performance (2.04%)under illumination from graphene sides was obtained when the layer number of graphene was 8.[57]

Our group found that the conductivity of graphene film could be significantly enhanced by $HAuCl_4$ and PEDOT:PSS doping due to the modification of the Fermi level in the graphene layer. For example, an over 80% reduced sheet resistance (from ~ 580 to 96 Ωcm^{-2}) was observed in our lab for a single-layer graphene film coated with a PEDOT:PSS layer. This observation allowed us to fabricate ST-OSCs with single-layer graphene top electrodes (**Figure 11a, b**). The devices (based on P3HT and $PC_{61}BM$) showed PCEs of ~3% when illuminated from the graphene side, which were higher than that obtained from the ITO side (**Figure 11c**), owing to the excellent transmittance (AVT >90%) of the single layer graphene electrode. Since the multi-step film transfer process is no longer necessary for preparing graphene electrode, this method should be appealing for large-scale preparation of graphene-based ST devices.[58] In addition, we found the devices employing graphene top electrodes showed excellent device stability, which could be attributed to the package effect of the graphene film.[59] Recently, our group further developed a fully transparent neutral-color OSC with graphene as both bottom and top electrodes (**Figure 11d, e**). By using PTB7 as electron donor and $PC_{71}BM$ as electron acceptor, PCEs up to ~3.4% and transmittance of ~40% were obtained with illumination from either side (**Figure 11f**). It is worth noting that the devices were mainly made of carbon-based materials. To the best of our knowledge, the obtained PCE is the highest value reported for all carbon-based solar cells.[60]

3.1.6. PEDOT:PSS-based transparent top electrodes

PEDOT:PSS is one of the most popular highly-conductive polymer available in the market.[61] Large-area PEDOT:PSS thin films can be easily prepared on various substrate by solution process with high transparency (>90%) in the visible region and low sheet resistance. It is interesting to find that the conductivity of PEDOT:PSS film is greatly related to the organic solvent in the precursor and the processing condition, and the maximum conductivity can be up to ~4000 Scm^{-1},[62] which is good enough for a electrode material for solar cells.

Therefore, PEDOT:PSS films have been used as electrodes in optoelectronic devices when they are prepared at optimum conditions with high conductivities although the major application of PEDOT:PSS is for HTLs in OSCs and PSCs. Moreover, the application of PEDOT:PSS based electrodes in optoelectronic devices is challenged by the stability of PEDOT:PSS upon exposure to high temperature, humidity, and UV light.[13a]

Till now, PEDOT:PSS based transparent top electrodes have only been applied tofewP3HT and $PC_{61}BM$ -based ST-OSCs. The corresponding devices typically exhibited PCEs of 1-3%, depending on the transparency of the PEDOT:PSS films and the methods for cell fabrication.[63] Typically, when highly conductive PEDOT:PSS film is used as a top electrode, an extra PEDOT:PSS HTL is still required for obtaining good device performance. However, Zhou *et al* found it possible to fabricate ST-OSCs with a single layer of PEDOT:PSS mixtures consisting of hole-selective (H. C. Starck CLEVIOS, CPP 105D) and high-conductivity (H. C. Starck CLEVIOS, PH1000) PEDOT:PSS solutions. Different volume ratios of CPP-PEDOT and PH1000 were studied and the ratio of 1:3 was found to give the highest PCE of 2.4% in a P3HT:$PC_{61}BM$ -based inverted ST device.[63d] This work offers an easier way for preparing transparent PEDOT:PSS top electrodes for ST solar cells.

Though transparent PEDOT:PSS electrodes have been successfully used in small-size ST-OSCs, they are not suitable for preparing large-size devices, as their sheet resistance could increase significantly at large scale when they were made thin and transparent, which limits practical applications of them. One strategy to improve the conductivity of PEDOT:PSS films and maintain high film transmittance is the integration of current-collecting metal grids on top of them. For example, Galagan *et al* reported that screen-printed Ag grid was used to fabricate transparent electrode in combination with PEDOT:PSS film and a sheet resistance of $1 \Omega sq^{-1}$ could be obtained with only 6.4-8% surface coverage. Such a composite electrode was used to replace ITO as bottom electrode for fabricating flexible OSC (opaque) with an active area of 4 cm^2, which showed a much higher efficiency than a similar ITO-based device. This kind of

composite electrode should also be promising for application as top electrodes in ST-OSCs.[64] It is notable that the density, width, and spacing of the metal grid lines should be fully considered for the best balancing of the transparency and conductivity of the PEDOT:PSS/metal grid composite electrodes.

3.2 ITO-free ST-OSCs

Apart from being used as top electrodes in ST-OSCs, the above mentioned transparent electrodes are also of potential to be used as bottom electrodes, thus allowing the fabrication of ITO-free ST-OSCs with proper combinations (bottom and top) of them. In 2009, Hau *et al* reported an ITO-free ST-OSC, in which highly conductive PEDOT:PSS films were used as both bottom and top electrodes and blend of P3HT:$PC_{61}BM$ was used as an active layer. However, only a PCE of 0.47% was obtained.[63a] A much higher PCE of 1.8% was achieved by Zhou *et al* with a similar device configuration in 2010.[63c] Kim *et al* have investigated various electrode combinations for ST and ITO-free OSCs based on the blend of ZnPc:C_{60} with Ag (opaque), ITO, PEDOT:PSS and AgNWs as bottom electrodes, thin film Ag (t-Ag) and f-CNTfilm as top electrodes. AgNWs_t-Ag, PEDOT:PSS_t-Ag, and PEDOT:PSS_f-CNT were identified as potential combinations for ITO-free ST-OSCs.[55] In 2013, Guo *et al* demonstrated an ITO-free ST-OSC using AgNWs as both bottom and top electrodes and a ternary blend consisting of poly[(4,40-bis(2-ethylhexyl)dithieno[3,2-b:2′,3′-d]-silole)-2,6-diyl-alt-(4,7-bis(2-thienyl)-2,1,3-benzothiadiazole)-5,5′-diyl] (Si-PCPDTBT), P3HT, and $PC_{61}BM$ as an active layer. The resulting device showed a PCE of 2.2% at AVT of 33%, which was comparable to a reference device using ITO bottom electrode (**Figure 12a, b**).[51a] In a further study, they obtained a 2.9% PCE together with a much higher AVT of 41% based on the BHJ blend of pDDP5T-2:$PC_{61}BM$ (**Figure 12c, d**).[65] Similarly, Yim *et al* reported a P3HT:$PC_{61}BM$ -based ST-OSC employing transparent AgNWs film as bottom electrode and PEDOT:PSS as top electrode. The final device showed an excellent visible transparency and

reasonable PCEs of 2.3% and 2.2% under the illumination from AgNWs and PEDOT:PSS sides, respectively (**Figure 12e, f**).[66] It is notable that Yusoff *et al* recently demonstrated an efficient ITO-free tandem ST-OSC based on the device structure of graphene-mesh/PEDOT:PSS/PSEHTT:$IC_{60}BA$/ZnO/PEDOT:PSS/PBDTT-DPP:$PC_{71}BM$/TiO_2/AgNWs. Upon optimizing the fabrication parameters for both front- and back subcells, they finally realized a remarkable AVT of ~45%, together with PCEs of 8.02% and 6.47% obtained from the graphene and AgNWs sides, respectively.[67]

More recently, Wilken *et al* reported a P3HT:$PC_{61}BM$ -based ITO-free OSC with AZO and MoO_3/Au/MoO_3 as bottom and top electrodes, respectively. On top of the AZO electrode, a ZnO overlayer was coated to enhance the electron collection efficiency. Two thicknesses of AZO electrodes (625 and 1270 nm) were studied. It was found that the devices with thinner AZO electrodes showed slightly higher J_{SC} than those with thicker ones possibly due to their higher average transmittance, while no statistical evidence for this observation was presented. Meanwhile, the thicker AZO electrodes showed clearly smaller series resistance (R_S) than the thinner ones for their reduced sheet resistance. Consequently, the final PCEs of these solar cells were very similar. The thickness of active layers was optimized in devices using 1270 nm AZO bottom electrodes and MoO_3 (12 nm)/Au (12 nm)/MoO_3(50 nm) top electrodes. An optimized PCE of ~2% was obtained under bottom illumination with the maximum device transmittance of 60% for wavelengths above 650 nm, corresponding to an active layer thickness of 140 nm.[18]

3.3. Stability Study of ST-OSCs.

Considerable long-term stability under operation conditions is a prerequisite for practical applications of photovoltaic devices. Although the stability of conventional nontransparent OSCs has been widely concerned, very little attention has been paid to ST-OSCs. In a study of Kim *et al* in 2013,transparent PEDOT:PSS electrodes based on PH1000 as mentioned in

section 3.1.6 were used to fabricate ST-OSCs with the inverted structure of ITO/ZnO/P3HT:PCBM/PEDOT:PSS/PH1000. A solution-processed WO_x film was coated on top of the PH1000 electrode to enhance the thermal stability of the device. It was found that the device without WO_x lost 78% of its original efficiency (from 2.49 to 0.55%) after been annealed at 95°C for 8h, while the WO_x-coated device maintained 53% of its original efficiency (from 2.45 to 1.3%). The observed better stability of the WO_x-coated device was attributed to the enhanced thermal stability of the PH1000/WO_x electrode as its conductivity decreased slower than that of a PH1000 electrode under a thermal annealing. However, the underlying mechanism was not addressed by the authors. We speculate that it is presumably due to p-type doping in PEDOT:PSS films by WO_x.[68]

Recently, Romero-Gomez et al performed stability test (according to ISOS-standards) of PTB7:$PC_{71}BM$ -based ST-OSCs with structures of standard semitransparent (Std-ST, ITO/PEDOT:PSS/PTB7:$PC_{71}BM$/BCP/Ag/MoO_3), inverted semitransparent (Inv-ST, ITO/ZnO/PTB7:$PC_{71}BM$/MoO_3/Ag/MoO_3), and inverted semitransparent with multilayer trapping structure (Inv-ML-ST, ITO/ZnO/PTB7:$PC_{71}BM$/MoO_3/Ag/(MoO_3/MgF_2)).It was found that Inv-ML-ST solar cells showed the longest lifetime, which was almost 8 and 400 times longer than that of Inv-ST and Std-ST solar cells, respectively. The better stability of Inv-ML-ST solar cells was resulted from better device isolation from external agents such as oxygen and moisture, while the rapid degradation of Std-ST solar cells was related to the acidic nature of PEDOT:PSS in contact with the ITO electrodes. In addition, similar degradation behaviors were observed in ST devices and corresponding opaque ones, indicating that thinner metal electrode would not degrade the device lifetime.[69]

Finally, it should be emphasized that the difference between ST-OSCs and nontransparent ones lies on the top electrodes only, which means that the stability issues related to the active layers of ST-OSCs should be similar to those of nontransparent ones. Thus special attention

should be paid to the influence of the transparent top electrodes on the device stability in the future.

4. Semitransparent dye-sensitized solar cells (ST-DSCs)

DSCs, being photoelectrochemical cells, have been investigated for more than 20 years. As shown in **Figure 13a**, a standard DSC is composed of a mesoporous TiO_2 film (mp-TiO_2), a monolayer of sensitizing dye *e.g* N3, N719 ruthenium dyes and YD2-o-C8, SM315 Zinc porphyrin dyes, an electrolyte containing a redox couple, e.g. I^-/I_3^- and $[Co(bpy)_3]^{2+/3+}$ (or a solid state HTM layer), and a counter electrode (cathode) that is typically made of platinized F-doped SnO_2 (FTO) glass. The operation mechanism of DSC is summarized in **Figure 13b**; the detailed description of the charge transfer processes will not be addressed here, as it can be easily found in previous reports and review papers.[5a, 5b] Since the dye-sensitized TiO_2 film can be conveniently made transparent or semitransparent, the fabrication of ST-DSCs relies mainly on the transparency of counter electrodes (CEs).

When DSC works, the CE accounts for catalyzing the reduction of oxidative species in the redox electrolyte and passing electrons to external circuits, which therefore means reasonable conductivity and catalytic activity are both required for CE materials. The catalytic activity of CE can be evaluated from its exchange current density (j_0) as expressed in eqn (10):

$$j_0 = \frac{RT}{nFR_{CT}} \quad , \tag{10}$$

where R is the gas constant, T is temperature, n is the number of electrons involved in the charge transfer process (n=2 for I^-/I_3^- redox couple), F is Faraday constant, and R_{CT} is the charge transfer resistance at the CE/electrolyte interface (R_{CT} can be obtained *via* electrochemical impedance measurement).[70] To avoid electron loss at the CE, the redox couple reduction rate should be comparable to the dye regeneration rate, which means j_0

should be comparable to J_{SC}. Considering a J_{SC} value of20 mA $cm^{-2}$for state-of-the-art DSCs, the ideal R_{CT} for CEs is estimated to be 1.3Ωcm^2. Typically, R_{CT} value of < 10 Ωcm^2 was considered to be enough for high performance DSCs.[71] For this reason, Pt has been used as benchmark CEs in DSCs. However, Pt is not preferable for large-scale commercial applications due to its high cost and scarce source. Therefore, many efforts have been made to develop alternative CEs for more cost-effective DSCs based on carbon materials, conducting polymers, and inorganic metal compounds etc.[72] Some of these materials have shown great potential in fabricating ST- or bifacial DSCs as summarized in **Table 3**. Bifacial DSCs are the devices that can be operated with illumination from both FTO and CE sides but are not necessarily semitransparent.

4.1 Transparent CEs for ST-DSCs

4.1.1. Transparent Pt CEs

Pt CEs are usually prepared on FTO glass via sputtering or thermal decomposition (with H_2PtCl_6 precursor) method. Due to the intrinsic high catalytic activity and conductivity, a Pt film with a thickness of 1-2 nm is sufficient to achieve high device efficiency,[73] which is semitransparent in such case. In 2008, Ito *et al* reported a bifacial DSC based on an ionic liquid electrolyte and a transparent Pt CE, which showed PCEs of ~6% under illumination from either FTO or Pt side. This might be the first report of bifacial DSCs, while the semitransparent property of the device was not characterized.[74] Although ST-DSCs were fabricated with ST-Pt CEs later,, much more efforts have been spent on the development of Pt-free transparent CEs for the high cost of Pt.[75]

4.1.2. Carbon-based transparent CEs

Traditional carbon materials, such as carbon black, activated carbon, graphite and their composites, have been widely used as alternative CEs in DSCs. However, these carbon CEs

have been rarely made transparent.[72b] Although CNTs and graphene are promising for transparent and conductive electrodes, both materials suffer from their intrinsic low catalytic activity toward the reduction of I_3^- due to the lack of catalytic sites (edge defects and oxidic groups), which limits their performance in conventional I-mediated ST-DSCs.[70] The catalytic activities of CNT and graphene CEs can be simply improved by increasing the film thickness (for increased catalytic sites) while a compromise in the film transmittance is inevitable. This dilemma can be alleviated by using CNT micro-balls[76] or graphene nanoplatelets (GNPs)[77] in CEs with tunable densities or by improving their intrinsic catalytic activities through chemical doping.[78] On the other hand, both CNT and graphene CEs show much better catalytic activities in Co-mediated DSCs, which are comparable or even superior to Pt CE, because the electrochemical kinetics of $Co^{+2/+3}$ redox couples were found to be faster on carbon electrode than Pt.[70] For example, PCEs > 9% were achieved by Kavan *et al* in DSCs using GNP-based transparent CEs prepared on FTO substrates(~66% transmittance at 550nm) in combination with a triphenylamine-based Y123 dye and $[Co(bpy)_3]^{+2/+3}$ (bpy = 2,2'-bipyridine)or $[Co(bpy\text{-}pz)_3]^{+2/+3}$ (bpy-pz = 6-(1H-pyrazol-1-yl)- 2,2'-bipyridine) redox couples.[79] Despite the transparency of the completed devices was not shown by the authors in their works, these results did indicate promising applications of GNP- based transparent CEs in ST-DSCs.

In a further study of Kavan *et al*, the adhesion between GNP film and FTO substrate was taken into account, as it could become poor in some cases and thus undermining the performance and stability of DSCs. They proposed to enhance the mechanical stability of GNP CEs by incorporating graphene oxide (GO) into GNP films for the stronger interaction of GO and FTO. The GO showed almost no catalytic activity towards $[Co(bpy)_3]^{+2/+3}$ redox couple before it was activated by thermal or hydrazine reduction and the thermal reduction was found to give better device performance. Under optimal condition, the GO-modified GNP CE (containing 50wt% GO) showed a remarkable 9.1% PCE (from FTO side) with

80%transmittance at 550 nm.[80]Pure thermal reduced GO nanoplatelets (rGNPs) could also be used to prepare transparent CEs for DSCs, however the device performance was much worse than that based on Pt CE, due to the poor electronic connection between the rGNPs and FTO glass.[81] It was found that the electronic contact at the rGNPs/FTO interface could be significantly improved by introducing Ni NPs interlayer between them due to the enhanced restoration of graphene double bonds. The Ni-modified rGNP CE showed a transmittance as high as 91% at 550nm and a PCE of 7.54% in I-mediated DSC, which was higher than that for Pt CE (7.45%).[82]

Recently, Zhao's group reported a novel carbon-based transparent CE prepared by an *in situ* carbonization method with an organic precursor containing Triton X-100 as a carbon source, isopropanol as a solvent, and acetylacetone as a dispersant (**Figure 14a**). Under optimal condition, the carbon CE showed not only excellent transparency (AVT = ~70%) but also good catalytic activity and mechanical stability. The best performed ST-DSC based on this kind of carbon CE demonstrated PCEs of 6.07% (from FTO side) and 5.04% (from carbon CE side), in comparison with that for Pt CE (6.89%), as shown in **Figure14b**. In addition, the device also showed promising long-term stability.[83] This work offers a new avenue for preparing efficient transparent carbon CEs for ST-DSCs and better device performance would be expectable by further optimizing the composition of the organic precursor. However, this method is probably not compatible with plastic substrates.

4.1.3. Conducting polymers for transparent CEs

Conducting polymers, such as polyaniline (PANI), polypyrrole (PPy), PEDOT and so on, have been identified as promising alternative CEs for DSCs in recent years for their advantages of low cost, ease of preparation, good catalytic activity, high conductivity, solution and low-temperature processability, excellent flexibility and environmental stability. Conducting polymer-based CEs are usually prepared on FTO substrates and the polymer films

can be deposited with either *in situ* polymerization method or *ex situ* spin-coating/doctor-blade method. It is noteworthy that *in situ* polymerization method is quite useful for preparing transparent polymer films with good adhesion to the FTO substrates.[72b]

In 2011, Zhao's group demonstrated an efficient ST-DSC based on transparent PANI CE (**Figure 15a**), which was prepared by *in situ* chemical polymerization of the aniline monomer on FTO glass. As shown in **Figure 15b**, the obtained PANI film was quite porous at nanoscale, which rendered it high surface area and thus good catalytic activity comparable to that of Pt CE. The corresponding ST-DSC showed PCEs of 6.54% and 4.26% under illumination from the FTO- and PANI sides, respectively (**Figure 15c**), which is superior to the devices based on transparent PANI CEs prepared by other methods, such as spin-coating and electrochemical deposition. In comparison, PCE of 6.69% was obtained in a similar device using Pt CE.[84]In a followed study, Wu *et al* showed that the photoelectric performance of PANI CE could be improved by the modification of 4-aminothiphenol (4-ATP) and PCEs of 6.7% (FTO side) and 4.15% (PANI side) were obtained. Interestingly, they demonstrated a higher output power when the device was simultaneously illuminated from both sides (by using a reflecting mirror), which was ~24.6% higher than that under the illumination from FTO side only.[85] In fact, it is generally expected that ST or bifacial solar cells are able to generate up to 50% more electrical power when they are applied with reflecting devices. Besides, polyvinylpyrrolidone (PVP) additive has been recently introduced to improve the uniformity and adhesion of the transparent PANI film for better device performance.[86]It is worth noting that the light absorption of PANI film is complementary with the most used ruthenium dyes, which should be beneficial for light harvesting from the PANI side and may be useful for fabricating neutral color ST-DSCs.

In 2012, Zhao's group reported another ST-DSC based on transparent PPy CE (**Figure 15d**), which was prepared with a similar *in situ* chemical deposition method used for preparing transparent PANI CE. The influence of the monomer concentration (MC) on the

photoelectric performance of PPy CEs was studied and the best condition was found to be 0.3 M MC. As shown in **Figure 15e**, the resulting PPy film also exhibited a rough microstructure. The final device showed PCEs of 5.74% and 3.06% under illumination from FTO and PPy sides, respectively, which are lower than the PCE of 6.76% for a Pt-based device (**Figure 15f**).[87] Recently, Hwang *et al* reported the fabrication of transparent PPy CEs with ultrathin polypyrrole nanosheets (UPNSs), which were synthesized by chemical oxidation *via* organic single crystal surface induced polymerization (OCSP) using sodium decylsulfonate as a template. HCl vapor post-treatment was applied to enhance the photoelectric properties of UPNS CEs and it was found that the conductivity of UPNS film was slightly increased from 31 to 39σcm^{-1} after HCl treatment, while the R_{CT} was significantly reduced from 91 to 4.4 Ω (compared to 5.6 Ω of Pt), indicating a greatly enhanced catalytic activity, due to the increased N doping level. The HCl-treated UPNS CEs with 55.2-67.2% transmittance at 500-700 nm gave an average PCE of 6.8% in DSCs, which was ~19% higher than the untreated ones and comparable to the PCE (7.8%) for Pt CEs.[88]Though the authors didn't mention whether the devices were semitransparent or not, promising application of this kind of transparent PPy CEs in ST-DSCs is expected.

Commercial PEDOT:PSS solution can be easily used to prepare CEs for DSCs. However, the resulting PEDOT:PSS films are thin and dense, which implies the lack of catalytic active area. Therefore, the corresponding device performance typically turned out to be much worse than that of Pt-based devices unless very thick PEDOT:PSS films were used.[89] For this reason,SiO_2 NPs were added into PEDOT:PSS solution for obtaining high performance transparent PEDOT:PSS CEs by Song *et al*. It was found that the incorporation of SiO_2 NPs resulted in an increase of not only the transmittance but also the catalytic activity of PEDOT:PSS CEs, due to the change of the optical property and the increase of the surface area of the PEDOT:PSS films, respectively. Finally, the DSC based on a SiO_2-modified

PEDOT:PSS transparent CE (~80% AVT) showed a PCE ~55% higher than that of the device based on pure PEDOT:PSS CE with similar transmittance.[90]

On the other hand, *in situ* polymerized PEDOT CEs (on FTO substrates) were reported to give excellent device performance, being comparable to Pt CEs.[91] However, it was usually difficult to obtain a PEDOT film with both high transparency and high catalytic activity through conventional electro-polymerization method using 3,4-ethylenedioxythiophene (EDOT) monomer. Li *et al* managed to solve this problem by using 2,2'-bis(3,4-ethylenedioxythiophene) (bis-EDOT) monomer. Considered that the optical absorption of I^-/I_3^- electrolyte in the visible region would undermine the light harvesting from the CE side, a colorless thiolate/disulfate (AT^-/BAT) electrolyte was developed and used to fabricate ST-DSCs with transparent PEDOT CEs (**Figure 16a, b**). The final devices showed a PCE ~10% higher than that using I^-/I_3^- electrolyte under illumination from the PEDOT side, suggesting that the idea of developing new colorless electrolytes could be an efficient way to improve the overall performance of ST-DSCs.[92]Besides, highly conductive (800 S cm^{-1}) and transparent (88% transmittance at 550 nm) PEDOT films have been used in FTO-free DSCs by Lee et al, using a pre-solution/in situ polymerization method, which showed a PCE of 5.08% slightly lower than that for Pt CE (5.88%).[93]

4.1.4. Inorganic transparent CEs

Recently, inorganic transition metal sulfides, nitrides, carbides, and oxides have been explored as potential alternative CEs for DSCs due to their advantages of low cost, high catalytic activity, and high stability.[72] Among them, only a few sulfide-based CEs, such as NiS, CoS, and MoS_2 electrodes, have been reported to be transparent and, typically, PCEs of ~6-7 % were obtained in the devices using the CEs with transmittance of 70-80% at 550nm.[94] However, the PCEs from the CE sides were not shown in these studies. Besides, transparent FeS_2 CEs, which were prepared by spin coating a FeS_2 nanocrystal (NC) ink on

indium tin oxide (ITO) substrates, were used to fabricate bifacial DSCs by Wang *et al*. A promising PCE of 7.31% was achieved from the ITO side, which is very close to that obtained with Pt CE (7.52%). However, the PCE from the FeS_2 CE side was rather lower (4.17%) due to the relative poor transmittance of the FeS_2 film (AVT = ~60%). Benefiting from the low-temperature solution method, FeS_2 CE was also prepared on flexible substrate, which demonstrated a 6.36% PCE in DSC. It is worth noting that remarkable electrochemical stability was observed in FeS_2 CEs upon more than 500 consecutive cyclic voltammetric scans.[95]

In addition, metal selenide alloys (M-Se, M= Co, Ni, Cu, Fe, Ru) have been recently identified as promising transparent CEs for bifacial DSCs. For example, PCEs of 6.43% (4.24%), 7.64% (5.05%), 7.85% (4.37%), 8.30% (4.63%), and 9.22% (5.90%) were obtained with transparent $Cu_{0.5}Se$, FeSe, $Ni_{0.85}Se$, $Co_{0.85}Se$, and $Ru_{0.33}Se$ CEs, respectively, under illumination from FTO (CE) sides, which are better than that of the device with a Pt CE (6.18% (3.56)). All of the alloy CEs had shown considerable transparency in visible region (AVT>70%), which should be beneficial to the efficiency of bifacial and STDSCs.[96]

4.1.5. AgNWs for transparent CEs

Generally, Silver cannot be used as CEs in liquid-electrolyte DSCs, due to its poor stability in corrosive electrolyte solution, while it can be used as top electrodes in solid-state DSCs (ssDSCs). In this regard, AgNWs are promising for the applications in ST-ssDSCs. In 2013, Margul is *et al* reported for the first time the fabrication of ST-ssDSCs using spray-coated AgNWs network as transparent top electrodes together with a triphenylamine-based organic dye (D35) and Spiro-MeOTAD as HTM. It was found that the direct deposition of AgNW electrode on Spiro-MeOTAD layer led to only a PCE of 1.33% due to the poor electric contact and energetic mismatch between AgNWs and Spiro-MeOTAD. Therefore, a PEDOT:PSS interfacial layer was proposed to ensure the ohmic contact between AgNWs and

Spiro-MeOTAD due to better work function match between PEDOT:PSS (5.0 eV) and Spiro-MeOTAD (5.2 eV) than that between AgNWs (4.5 eV) and Spiro-MeOTAD. On the other hand, PEDOT:PSS could act as filling material as mentioned before to enhance the lateral charge transport in AgNW network. Consequently, a much higher PCE of 3.6% was obtained, which was comparable to a reference device using an opaque Ag electrode prepared by thermal evaporation (3.7%).[97]

4.1.6. Composite materials for transparent CEs

Considering the difficulty to obtain desired transparency, conductivity, and catalytic activity in an individual CE material, the strategy of using composite materials offers an alternative way to fabricate efficient transparent CEs for ST-DSCs. Though pure Pt CE is not favorable as we discussed before, Pt NPs have been widely used to enhance the performance of non-Pt transparent CEs such as CNTs,[98] graphene,[99] PANI,[100] and CoS.[101] These Pt-loaded composite transparent CEs can exhibit similar performance to pure Pt CEs in DSCs with high visible transmittance. It is noteworthy that the increase in the cost is negligible since very little amount of Pt is loaded (1-2 μg cm^{-2}).[72b] In addition, graphene has been frequently used as a functional component to prepare Pt-free composite transparent CEs with other non-Pt CE materials due to its excellent transparency and conductivity. For example, PEDOT:PSS/graphene,[89b] MoS_2/graphene-nanosheet[102], PEDOT/N-doped graphene,[103] PANI/rGO,[104] and CoS/rGO[105] composite films have been explored as transparent CEs for DSCs and the devices showed better performance than those without graphene. Besides, transparent PANI/CNT composite CE with acceptable performance was also reported.[106]

4.2. Dye engineering for ST-DSCs

The transparency of a ST-DSC is related to not only the transparent electrodes but also the dye used in the device. For example, although bipyridine ruthenium dyes have been widely

used as sensitizers for DSCs, their optical absorption lies mainly in the high-eye-sensitivity range of 500-600 nm, making it difficult to balance the transparency and light harvesting (or PCE) of ST-DSCs. In order to solve this problem, Zhang *et al* proposed to use a cocktail dye system composed of a UV-sensitive dye and a near infrared (NIR) sensitive dye, so that the light absorption in the high-eye-sensitivity region could be avoided, which can achieve high device transparency, while the light harvesting in the UV and NIR regions are sufficient enough to generate desired photocurrent. Following this design rule, they demonstrated a highly transparent DSC with a donor-π-acceptor (D-π-A) Y1 dye and a squaraine HSQ5 dye, which showed a promising PCE of 3.66% at a remarkable device transmittance of 60.3% at 500-600 nm region (**Figure 16c-e**).[107] Alternatively, dielectric mirror (photonic crystal) was also used to increase the light harvesting and keep the device transparency of ST-DSCs.[108]

5. Semitransparent perovskite solar cells (ST-PSCs)

The general crystal structure of organometal halide perovskite materials is illustrated in **Figure 17a**.The unit cell of a perovskite material with a formula of ABX_3 is composed of five atoms in a cubic structure, in which cation A has twelve nearest neighbors and cation B has six nearest-neighbor anion X. To form an ideal cubic structure, the lattice constants a, b, c should be the same, which means:

$$\frac{r_A + r_X}{\sqrt{2}} = r_B + r_X \quad , \tag{11}$$

where r_A and r_B are the ionic radii of the A and B cations, r_X is the ionic radius of the X anion. Similarly, Goldschmidt's tolerance factor (t) is defined as:

$$t = \frac{r_A + r_X}{\sqrt{2}(r_B + r_X)} \tag{12}$$

When *t* is 0.9-1, ideal cubic structure can be formed. Otherwise, distorted structures, such as orthorhombic, rhombohedral, and tetragonal, are likely to be formed.[9l, 9n]As shown in **Figure**

17b, the bandgaps of perovskite materials are dependent on their compositions. Currently, methylammonium ($CH_3NH_3^+$, MA) and formamidinium ($HC(NH_2)_2^+$, FA) based lead halides ($MAPbX_3$ and $FAPbX_3$, where X= I^-, Cl^-, Br^-or mixture thereof) are most used perovskite materials for PSCs. Typically, perovskite films can be prepared by the reaction of PbX_2 and MAX or FAX *via* one-step or two-step deposition methods (**Figure 17c**).[9k, 9l] PSCs can be fabricated using either mesoporous structures or planar structures; the latter can be further classified into regular structures (n-i-p) and inverted structures (p-i-n) (**Figure 17d**).[9m] Generally, mesoporous structures are favorable for device efficiency and can lead to little J-V hysteresis, while planar structures are simpler and devices based on them can be fabricated at low temperature. Similar to the properties of ST-OSCs and ST-DSCs, the performance of ST-PSCs relies mainly on the transparency of the top electrodes as well. The recent developments of ST-PSCs are summarized in **Table** 4.

5.1.Transparent top electrodes for ST-PSCs

5.1.1. Thin film Au/Ag top electrodes

In principle, ST-PSCs can be simply fabricated with thin film Au/Ag top electrodes if the transparency of the metal thin films is high enough. For example, Roldán-Carmona *et al* reported the fabrication of ST-PSCs with the inverted structure of ITO/PEDOT:PSS/$MAPbI_3$/$PC_{61}BM$/Au and the device transmittance was controlled by the thickness of the perovskite layer. It was found that the energy loss at the Au electrode could be reduced by introducing a LiF capping layer, which thus led to an improved device transparency. The final devices with the active layer thicknesses of 180 and 100 nm showed PCEs of 7.3%and 6.4% at AVT of 22% and 29%, respectively.[109] Due to the strong optical absorption of perovskite, it is usually difficult to tailor the device transmittance by changing the thickness of the perovskite active layer. For better transparency control, Aharon *et al* proposed the use of perovskite grid prepared by mesh-assisted assembly of perovskite

solution in ST-PSCs. The transparency of the perovskite grid could be controlled by the perovskite solution concentration and the mesh opening. Finally, ST-PSCs based on the device structure and thin film Au electrodes with AVT of 20-70% were realized and the maximum PCE of 5% was achieved at 20% AVT.[110] Moreover, in order to reduce the high reflectance of Au films, transparent MoO_3/Au/MoO_3 DMD electrodes were employed for fabricating devices with better performance by Gaspera *et al*. The thicknesses of the Au, bottom, and top MoO_3 layers were optimized to be 10, 5, and 35 nm, respectively. The resulting devices showed PCEs of 5.3-13.6% with the corresponding AVT of 31-7%.[111] Very recently, MoO_3/Au/Ag/MoO_3/Alq_3DMD electrodes were used to fabricate flexible ITO-free ST-PSCs by Ou *et al,* in which ultrathin Au -based bottom electrodes were employed to replace the commonly used ITO electrodes for better device bendability. The thicknesses of the Au, Ag, Alq_3, bottom and top MoO_3 layers were fixed at 1, 7, 50, 2, and 5 nm, respectively. The influence of the thickness of the Au bottom electrodes on the photovoltaic performance and the transmittance of the ST-PSCs was investigated. It was found that the PCE and AVT values of the devices were inversely dependent on the thickness of the Au electrodes. The highest PCE of 8.67 % (AVT = 15.94%) was obtained with a 30 nm Au electrode, while the highest AVT of 31.61% (PCE = 4.11%) was achieved with a 15 nm Au electrode.[112]

Jung *et al* reported that thin film Ag electrodes with bis-C_{60}buffer layers could be used in inverted ST-PSCs and CuSCN was employed to replace PEDOT:PSS as HTLs for its better transparency in the UV-Vis-NIR region. The CuSCN layer was prepared from its solution in diethylsulfide *via* a spin-coating method and its optimal thickness was found to be about 40 nm. Different device transmittance was obtained by changing the thickness of the perovskite film and promising PCEs over 10% were achieved with the device AVT of around 25%, which corresponds to the thick of 180 nm for the perovskite film.[113]It is notable that that the bis-C_{60} buffer layers were introduced to guarantee the uniform growth of the thin Ag

electrodes because the direct deposition of Ag atoms on a dielectric surface typically would lead to the formation of island-like film morphology, which is detrimental to the film conductivity. This issue was also considered by Chang *et al* when they fabricated inverted ST-PSCs and they proposed the use of thiol-containing cationic surfactant (11-mercaptoundecyl)trimethylammonium bromide (MUTAB) as a butter layer since Ag-S bonds can be formed at the interface to enhance the interfacial electric contact and the stability of the Ag electrodes. The final device showed a PCE as high as 11.8% at the AVT of 20.8%, together with good ambient and thermal stability.[114]

Considering the difficulty to produce high quality and pinhole-free thin perovskite films on PEDOT:PSS surface, Bag *et al* proposed to modify the PEDOT:PSS surface in p-i-n type ST-PSCs with thiourea by vapor assisted surface treatment (VAST). Since Pb and I in $MAPbI_3$perovskite are highly polarizable, the modification of PEDOT:PSS surface with soft, polarizable chalcogenide species could lead to a favorable surface interaction between perovskite and PEDOT:PSS and thus improve the perovskite film coverage. With the semitransparent perovskite films prepared with this method, ST-PSCs were fabricated by using transparent thin Ag electrodes and C_{60} and 11-amino-1-undecanethiol hydrochloride (AUH) interfacial layers. PCEs of 9.4% and 8.2% were obtained at the device AVT of 29% and 34%, corresponding to the perovskite film thicknesses of 150 and 110 nm, respectively.[115] Moreover, semitransparent perovskite films with remarkable centimeter-scale uniformity were demonstrated by Qi's group with a hybrid vapor deposition method with $PbCl_2$ and MAI precursors, where the nominal stoichiometry of $PbCl_2$ and MAI could be well controlled by monitoring the vapor partial pressure of MAI using a quartz crystal monitor. A PCE of 9.9% was obtained when the thickness of the semitransparent perovskite film is ~135 nm. This method is of great potential for the fabrication of efficient large-area ST-PSCs.[116]

5.1.2. TCO-based top electrodes

TCOs, including ITO,[117] hydrogen-doped indium oxide (IO:H),[118] indium zinc oxide (IZO),[119] and aluminum-doped zinc oxide (AZO)[120], have been explored as transparent electrodes for ST-PSCs. These electrodes are usually prepared *via* sputtering and thus inorganic buffer layers (*e.g.* MoO_3 or MoO_x) are required for protecting the underlying perovskite layer from being damaged.[121] It is notable that most of the studies are focusing on the fabrication of NIR-transparent ST-PSCs for applications in tandem solar cell.

In 2015, Heo *et al* reported the fabrication of planar ST-PSCs with the device structure of FTO/TiO_2/$MAPbI_3$/P3HT(or PTAA)/PEDOT:PSS/ITO, where the ITO electrode was introduced by a lamination method using PEDOT:PSS as an interfacial layer. When P3HT was used as the HTM, the devices showed an average PCE of 12.8%.However,the optical transparency of the devices was poor due to the absorption of P3HT. In comparison, the devices with PTAA as the HTM showed better device transparency(AVT of 6.3-17.3%) and exhibited PCEs of 15.8-12.55%.In addition, the devices without encapsulation showed excellent stability (>20 days) in humid air.[117a]

Löper *et al* reported the application of sputtered ITO top electrodes in ST-PSCs with a normal device structure. To protect the perovskite active layer, MoO_x was coated by thermal evaporation before the deposition of ITO and acted as a hole-collecting buffer layer in the devices as well. However, the ST-PSCs showed a PCE of only 6.2%.[117b] With the same sputtered ITO top electrodes, Bush *et al* prepared inverted devices with a much higher PCE of 12.3% recently by using solution processed AZO layer as a buffer beneath the ITO electrodes. The ambient and thermal stability of the devices was also improved substantially by the ITO electrodes on the top.[117c]

IO:H is also an excellent TCO material, which can be used as transparent electrodes in ST solar cells. Fu *et al* prepared ST-PSCs with a planar structure of FTO/ZnO/$PC_{61}BM$/$MAPbI_3$/MoO_3/IO:H, which showed PCEs of 14.1% and 9.5% under

illumination from FTO and IO:H sides, respectively.[118] Besides, IO:H/ITO bilayers were also used in ST-PSCs with improved PCEs (16.3%) probably due to the better conductivity of the electrodes.[122]

In 2015, Wener *et al* reported the fabrication of ST-PSCs with sputtered IZO electrodes based on a normal mesoporous structure. The device showed a PCE of 9.7% when the IZO was directly deposited on Spiro-MeOTAD while a higher PCE of 10.36% was achieved when a thin MoO_x buffer layer was introduced beneath the IZO electrodes.[119] Recently, Kranz et al fabricated mesoporous ST-PSCs with sputtered AZO transparent electrodes and demonstrated a promising PCE of 12.1%. As mention above, AZO can also be used as an electron-selective buffer layer for the deposition of other TCO electrode.[120]

5.1.3. AgNW-based transparent electrodes

AgNWs have been widely employed in transparent top electrodes of ST-PSCs. In 2014, Guo *et al* reported for the first time the application of AgNW electrodes in ST-PSCs with the inverted structure of ITO/PEDOT:PSS/$MAPbI_3$/$PC_{61}BM$/ZnO /AgNWs (**Figure 18a**), in which the ZnO layer was used to ensure an ohmic contact between $PC_{61}BM$ and the AgNWs and protect the underlying perovskite layer from being damaged during the deposition of AgNWs. The final device showed an 8.5% PCE and a reasonable AVT of 28.4% (**Figure 18b, c**).[123] In a followed study, an atomic layer deposited ZnO layer (ALD-ZnO) was directly used as ETL instead of $PC_{61}BM$ in ST-PSCs by Chang *et al* (**Figure 18d**). The ST-PSCs showed an average PCE of 10.15% and AVT of 25.5%. However, the devices were found to degrade quickly in ambient condition (30°C, 65% relative humidity) due to the degradation of AgNWs in air. Then polyethylene terephthalate (PET) coated with ALD-Al_2O_3wasemployed as encapsulation layers, which resulted in a significant improvement of the device stability while the device efficiency and transparency were barely influenced, leading to an average PCE of 10.55 % and AVT of 22.5) (**Figure 18e, f**).[124]

Recently, Dai *et al* reported that the potential reaction between AgNWs and the underlying halides may lead to the decomposition of Ag electrodes. Since a traditional semiconducting charge transport layer cannot fully prevent the migration of halide ions, they proposed an Au/AgNWs bilayer electrode that could separate AgNWs from the underlying halides by the Au interlayer. Upon optimizing the thickness of Au and AgNW layers, the devices with a normal mesoporous structure showed high device stability and the highest PCEs of 11.07% and 6.1% under illumination from the FTO and AgNWs sides, respectively.[125]

Noticeably, Quiroz *et al* reported an unprecedented AVT of 46% and a PCE of 3.55% for a ST-PSC using a transparent AgNWs electrode, in which the semitransparent $MAPbI_3$filmwas prepared by a facile annealing-free solvent-solvent extraction (SSE) method. By controlling the active layer thickness, the PCE of the devices was improved to 8.12% with the decrease of the AVT to 28% (**Figure 18g, h**). It is notable that the SSE method is compatible with other transparent top electrodes and suitable for preparing flexible ST-PSCs.[126]

5.1.4. CNT-based transparent electrodes

In 2014, Wong's group reported the synthesis of free-standing CNT films by a floating catalyst CVD method.[127] The CNT films were directly laminated on top of the active layers of PSCs with the structure of FTO/compact TiO_2/mp-TiO_2/$MAPbI_3$/CNT as anodes, which showed a PCE of 6.87%. The PCE of the devices was further improved to 9.9% when Spiro-MeOTAD was incorporated into the CNT network. More importantly, the CNT films could be used as transparent electrodes for ST-PSCs. In a followed study, they used the transparent CNT films in ST-PSCs based on $MAPbBr_3$and obtained a PCE of 4.84% only. Higher PCE of 5.33% was obtained when a thin layer of poly(methyl methacrylate) (PMMA) was coated on top of a CNT electrode due to the reduced contact resistance at the CNT/perovskite interface.

A further increase of the PCE to 5.76% was demonstrated by the deposition of Au finger electrodes while the device transmittance was compromised.[128]

5.1.5. Graphene-based transparent electrodes

Similar to ST-OSCs, ST-PSCs with graphene transparent electrodes were successfully fabricated by our group in 2015, as shown in **Figure 19a**. The graphene electrodes were prepared by a CVD method on copper foils and transferred on the active layer of PSCs with the structure of FTO/compact TiO_2/mp-TiO_2/$MAPbI_{3-x}Cl_x$/Spiro-MeOTAD/PEDOT:PSS/graphene by a lamination method. The PEDOT:PSS layer was modified on the graphene surface to increase the conductivity of the graphene electrodes by modulating the Fermi level in graphene. Even though, the conductivity of the graphene electrodes is not high enough for high performance PSCs. Then the performance of the devices was further optimized by changing the layer number of multilayer graphene electrodes and 2-layer graphene was found to be the most suitable condition for the devices. Then the influence of the thickness of $MAPbI_{3-x}Cl_x$perovskite layer on the transparency and performance of ST-PSCs was investigated. As shown in **Figure 19b-d**, the device transmittance increased with the decrease of film thickness while the device performance changed oppositely. The optimized devices showed PCEs of 10-12% with the transmittance of 35-20% at 700nm. This work suggests that graphene is an excellent candidate material for the transparent electrodes of ST-PSCs.[129]

5.1.6. PEDOT:PSS-based transparent electrodes

Although transparent PEDOT:PSS films are usually used as HTLs in inverted PSCs,[9m] there are few reports on the application of them as transparent top electrodes in ST-PSCs because the direct deposition of aqueous PEDOT:PSS solutions on top of the water-sensitive perovskite layer is not allowed. By using a film-transfer lamination method, Bu *et al*

fabricated ST-PSCs with transparent PEDOT:PSS top electrodes. The resulting devices with an active area of 0.06 cm^2showed the highest PCE of 10.1% at AVT of 7.3%while the device efficiency was decreased to only 2.9% for a bigger device with the active area of 2.4 cm^2 due to the low conductivity of the PEDOT:PSS layer. It is expected that better device performance can be achieved by increasing the conductivity of the PEDOT:PSS electrode and reducing the contact resistance between the PEDOT:PSS film and the underlying active layer.[130]

5.2 Color tuning of ST-PSCs

5.2.1. Neutral color ST-PSCs

Neutral color ST solar cells are appealing for window applications. However, a typical perovskite film normally shows reddish brown color, making it difficult to fabricate neutral color ST-PSCs. Recently, Snaith's group reported the fabrication of neutral color $MAPbI_3$ film by replacing the full-covered perovskite layer with discontinuous perovskite "islands" (**Figure 20a,b**). The film transmittance was tuned by changing the coverage of perovskite (**Figure 20c**) and the resulting ST-PSCs showed PCEs of 8-3.5% at AVT of 7-30%. However, the completed devices were not color-neutral anymore as thin film Au electrodes were used.[131] In a further study, they demonstrated a neutral color ST-PSC with a novel nickel-mesh-based transparent laminated cathode (TLC) and an active layer of $FAPbI_3$ perovskite. The final device showed a promising PCE of 5.2% at AVT of 28% (**Figure 20d-g**), which is a significant improvement on their previous report.[132] One critical problem for this kind of ST-PSC is the direct contact of HTM and TiO_2 (ETL) at the perovskite-free region, which could reduce the open-circuit voltage (Voc),the fill factor (FF) and thus the PCE of the device due to the increased recombination (shunt) pathways. It was proposed by Hörantner *et al* that these shunting paths could be effectively blocked byalkyl silane passivation, such as octadecyl-siloxane (OTS). The OTS insulating layer could be easily introduced by dipping the perovskite film on a TiO_2 substrate into a toluene solution of OTS for a couple of minutes (e.g.

10 min) and the OTS molecules would preferentially attach to the uncovered TiO_2 surface. Upon OTS passivation, the maximum PCE of 5.9% (average PCE of $4.6 \pm 0.8\%$) was obtained in the devices with Au top electrodes, being higher than that (4.3%)for control devices (average PCE of $3.2 \pm 1.4\%$). When Au electrodes were replaced with transparent TLC electrodes, a PCE of 6.1% was achieved with a decent device AVT close to 40%.[133]

Islands-like perovskite films were also used to fabricate neutral-color ST-PSCs by Heo *et al* with a device structure of FTO/TiO_2/$MAPbI_3$/PTAA/PEDOT:PSS/ITO, in which a polystyrene (PS) passivation layer was used to block the direct contact of bare $TiO_2$with PTAA. The PS passivation layer was introduced by the direct spin-coating of PS toluene solution on top of the perovskite film and then the PS on perovskite was removed by a spin-washing process with pure toluene. However, the spin-washing process is difficult to be controlled.PS on both TiO_2 and perovskite could be washed out if the spin coating speed was low (4000 rpm)while PS on perovskite only would be removed when the spin coating speed was increased to 7000 rpm. Upon PS passivation, the average PCE of the devices was greatly improved from 2.93 ± 1.57 to $6.17 \pm 2.32\%$, together with the maximum value of over 10%. The device AVT was also slightly improved from 18.6 to 20.9%. Besides, the sandwiched ST-PSCs showed good long-term stability as mentioned in a previous section.[134]

Recently, Zhang *et al* reported near-neutral-colored perovskite films prepared by a combined method of colloidal self-assembly and plasma etching. Firstly, a PS colloidal monolayer was prepared by air-water interface self-assembly and transferred onto a FTO/TiO_2 substrate. Then O_2 plasma was applied for a certain of time to etch the PS layer to form a non-close packed hexagonally ordered template, followed by spin-coating an ethanol solution of 20 nm SiO_2 NPs on top of it. The film was then sintered to remove the PS layer and form a stable SiO_2 honeycomb scaffold. Finally, a $MAPbI_3$ perovskite film was coated and showed a neutral color. The transmittance of the perovskite film could be controlled by the plasma

etching period of the PS layer besides the precursor concentration. It was found that the transmittance of perovskite films increased with the increase of the etching time from 0 to 8 min and then decreased at longer etching time when 600 nm PS spheres were used. The resulted PSCs showed the maximum PCE of 10.3 % together with a considerable AVT of 38%for the active layer. However, the final devices were not semitransparent since thick Ag electrodes were used. Anyway, neutral-colored ST-PSCs are expected to be fabricated by using perovskite active layers prepared by this method as well as transparent nickel mesh-based TLC or graphene electrodes.[135]

5.2.2. Different color of ST-PSCs

Colorful ST-PSCs would be favorable for aesthetic applications on buildings, vehicles and wearable electronics. The color of a perovskite layer is dependent on the light absorption spectrum and the bandgap of the perovskite material.[9l, 136]Besides the compositional engineering of perovskite films, optical methods have been developed to tune the color of ST-PSCs without changing the inherent properties of perovskite films. For example, a metal/dielectric/metal (MDM) microcavity electrode was proposed by Lee *et al*. The color of ST-PSCs could be easily tuned by changing the thickness of the dielectric layer of the electrode. They demonstrated red, green, and blue -colored ST-PSCs using Ag/WO_3/Ag electrodes and obtained the highest PCE of 3.86%in the red-colored device, in which each Ag layer was deposited on a thin film of perylenetetracarboxylicbis-benzimidazole (PTCBI).[20b] Similarly, Lu *et al* reported the fabrication of colorful ST-PSCs with Ag/ITO/Ag microcavity electrodes (**Figure 21a**). The color of the device could be continuously tuned from reddish-orange to blue by changing the thickness of the ITO layer (**Figure 21b-d**) and the highest PCE of 7.6% was obtained in a bluish-green device.[20c]

In 2016, Quiroz *et al* reported the color tailoring of ST-PSCs with dielectric mirrors (**Figure 21e, f**), which are composed of alternating layers with a high refractive index (HRI)

and a low refractive index (LRI). The optical response of the dielectric mirror is determined by the refractive indices as well as the number and the thicknesses of the corresponding dielectric layers. It was found that the appearance of ST-PSCs could be tailored to almost any desired color except bright green. Besides, dielectric mirrors could enhance the light harvesting of the ST-PSCs and the best combination of efficiency and transparency was predicted to be obtained for colors of light green, light blue, and light orange for a full stack of ST-PSCs and dielectric mirrors. The highest PCE of 4.2% PCE was obtained for alight orange device at AVT of 31%.[21]

5.3. ST-PSCs for tandem solar cells

It is worth noting that ST-PSCs can be used to form tandem solar cells with low bandgap crystalline Silicon (c-Si)- and CIGS- solar cells due to larger bandgaps of perovskite materials, which offers a convenient and economical way to boost the efficiencies of solar cells.[12]For example, PCEs over 30% have been predicted for perovskite/c-Si tandem solar cells, which are much higher than the current record efficiency (25.6%) of c-Si solar cells.[117b] In the fabrication of efficient tandem solar cells, excellent NIR transparency is required for the ST-PSCs on top of the inorganic solar cells.

The tandem device can be fabricated in either a four-terminal way by the mechanical stacking of top (ST-PSCs) and bottom (c-Si/CIGS) cells,[12, 117b, 117c, 118-120, 122, 137] or a two-terminal monolithic way.[122, 138]A four-terminal device can be easily fabricated and tested in a laboratory. By now the highest reported PCEs for four-terminal perovskite/c-Si and perovskite/CIGS tandem solar cells are 25.2% and 20.5%, respectively.[12, 118, 122]A two-terminal monolithic device requires a complicated fabrication process while it is more suitable for commercial production and applications. In 2015, Werner *et al* reported a monolithic perovskite/c-Si tandem solar cell with the structure of Ag/ITO/c-Si/IZO/PCBM/PEIE/$MAPbI_3$/Spiro-MeOTAD/MoO_x/IO:H/ITO, in which IZO was an

intermediate layer and IO:H/ITO was a transparent electrode. Devices with the active areas of 0.17 and 1.22 cm^2demonstrated PCEs of 21.2% and 19.2%, respectively.[138c] By optimizing the fabrication of perovskite top cells, they further improved the PCE to 20.5% for a larger device with the area of 1.43 cm^2. Todorov *et al* reported a monolithic tandem solar cell based on a CIGS cell with the structure of glass/Si_3N_4/Mo/CIGS/CdS/ITO/PEDOT:PSS/$MAPbI_3$/PCBM/BCP/Ca and obtained a PCE of 10.98 %. Although the efficiency of the device is relatively low, the device performance is expected to be improved by optimizing the transparency of the perovskite top cell and using a CIGS cell with better performance.[138a]

5.4. Stability study of ST-PSCs

The stability issue of PSCs has attracted much attention in recent years due to the importance to their long-term commercial applications.[139] The degradation mechanisms of perovskite materials under light, moisture, heat, and other operational conditions have been extensively studied. However, almost all of these studies are based on opaque PSCs and there's little report on the stability study of the ST-PSCs.

Recently, polyvinylpyrrolidone (PVP) was used as an additive to improve the air and thermal stability of ST-PSCs by Guo *et al* for the first time. They found that the molecular weight (M_w) and the amount of PVP could influence the device performance. The highest PCE was obtained for a M_w of 40K and the addition level of 3wt%. To further enhance the stability of the ST-PSCs, a thin layer of fluorous polymer CYTOP was coated on the perovskite film. As shown in **Figure 22**, the resulting ST-PSC showed a PCE of 5.36% at AVT of 34% and a promising lifetime of more than 800 h in air, which was almost 40 times longer than that of a control device that retained the same efficiency. The improved stability was mainly attributed to the protection of perovskite nanocrystals by PVP molecules.[140] Similarily, other functional additives such as butylphosphonic acid 4-ammonium chloride (4-

ABPACl)[141] and polyethylene glycol (PEG)[142] which have been used as additives in perovskite layers to improve their moisture stability in conventional opaque PSCs, should also be useful in ST-PSCs.

In addition, the following approaches are proposed to improve the stability of ST-PSCs, based on the stability study of opaque PSCs: (1) *Compositional engineering.* It was reported that the incorporation of Br^- ions into $MAPbI_3$ perovskite led to an improved device stability.[9c, 136] Similar effects were observed when pseudohalide SCN^- ions were introduced in the perovskite materials, as reported by Xu's and our groups.[143] Recently, greatly enhanced stability was observed in Cs^+ containing perovskites[144] and 2D Ruddlesden-Popper perovskites formed by using large-size alkylammonium as spacer.[9j, 145] In addition, a fluorinated alkylammonium $CF_3CH_2NH_3^+$ has been incorporated into $MAPbI_3$ to improve the environmental stability of PSCs.[146] (2) *Inorganic charge transport layers.* PEDOT:PSS and $PC_{61}BM$ are usually used as HTLs and ETLs in inverted PSCs, respectively, while Spiro-MeOTAD is normally used as HTLs in PSCs with normal structures. However, the organic charge transport layers are unstable in air. So they should be replaced with some inorganic counterparts to improve device stability.[9f, 147] (3) *Hydrophobic passivation and encapsulation.* Encapsulation methods are very effective and straightforward, which can be used together with the abovementioned methods.[148]

6. Conclusions and Outlook

In summary, OSCs, DSCs and PSCs are representative emerging photovoltaic technologies, which have drawn tremendous attention from the solar cell community in the past two decades. Compared to conventional inorganic silicon- and thin film solar cells, one distinguished advantage of the emerging solar cells is their prospect of being made semitransparent, which will enable many novel applications of the devices.

In the fabrication of the ST solar cells, two transparent electrodes (CE for DSCs) on both sides are needed, which is different from the case of normal opaque solar cells. Though thin film metal electrodes were first used in device fabrication (Au or Ag for ST-OSCs and ST-PSCs, Pt for ST-DSCs), they are not idea candidate for high-performance devices. The trade-off between the transmittance and conductivity of the metal electrodes and their high reflectance are detrimental to the device performance. Promising results have been obtained in ST devices with alternative transparent electrodes based on AgNWs, graphene, CNTs, TCOs and conductive polymers, although the fabrication techniques of these materials are yet to be optimized. Actually, the conductivity of graphene, CNTs and conductive polymers is still not high enough for such applications. Most of the transparent electrodes can be conveniently assembled into ST-OSCs and ST-PSCs by lamination and coating methods, which pay a way for the mass production of large-area devices. For CEs of ST-DSCs, in addition to transparency and conductivity, reasonable catalytic activity is required on their surfaces. Therefore, the CEs can be modified with some nanomaterials with higher catalytic activity without scarifying their transmittance and conductivity. Besides, PANI, PPy and few metal sulfides and metal selenide alloys have also been explored as potential transparent CEs for ST-DSCs.

PCE, transparency and color are all important properties for ST solar cells. In addition, human perceptions of color and transparency should be taken into account in the fabrication and characterization of the devices, which however have been rarely reported for ST-DSCs. It is generally considered that neutral color ST solar cells with high CRIs are favorable for window applications. On the other hand, colorful ST devices could be appealing in some cases for their aesthetic functionalities. However, color tailoring of the active layer via composition or bandgap engineering sometimes may lead to the compromise in device efficiency. Therefore optical methods have been proposed to tune the color of ST solar cells, for example by using MDM electrodes (e.g. Ag/ITO/Ag) or dielectric mirrors.

Although remarkable progress has been made in developing efficient ST solar cells based on OSCs, DSCs, and PSCs as reviewed above, the performance of the devices still lag far behind that of the state-of-art opaque ones. It is expected that the efficiency and transparency of the ST solar cells can be further improved by incorporating novel materials for active layers and ideal transparent electrodes in the devices. Particular attention should be paid to novel device designs and fabrication techniques of ST solar cells, especially the light management approaches that can enhance light absorption and tune the color of the devices. For the future work, we thus need to optimize the device performance and fabrication techniques in the following aspects.

First, highly transparent and conductive materials for the top electrodes of OPVs/PSCs and counter electrodes of DSCs are urgently needed. Although transparent electrodes based on ultrathin metal (Au, Ag, Pt) and TCOs have been successfully used in devices with acceptable performance, the transparency and conductance of the metal films cannot meet the requirements of the devices simultaneously while TCOs cannot be used as top electrodes. The poor stability of the metal electrodes is also a drawback for some devices especially PSCs. So we need to develop transparent electrodes based on nanomaterials, including AgNWs, graphene, other carbon-based materials and the mixture of them. AgNWs electrodes have already shown the sheet resistance of less than 15 Ωsq^{-1} and transmittance higher than 90%, which are good enough for high-performance solar cells. We still need to optimize the size and aspect ratio of AgNWs, tackle the processing conditions in device fabrication and realize large-area uniform films with high conductivity as well as high transparency. Suitable interfacial layers between the electrodes and active layers should be pursued with a view to enhancing electron or hole transfer from the active layers to the electrodes. It is notable that AgNWs are unstable in liquid-electrolyte and thus, for DSCs, they can only be used in solid electrolytes. Carbon-based electrodes, including graphene, CNT and conductive polymers, are more stable and cheaper in comparison with AgNWs, and can be easily coated by solution

processes. However the reported conductivity and transparency of the carbon-based materials are not enough for high-efficiency ST solar cells. Considering that graphene has very high carrier mobilities, a feasible approach to improving the conductivity of graphene is to increase the carrier density by effective doping techniques. Some possible doping techniques, including the surface modification of metal nanoparticles, organic molecules and acids, are recommended to investigate in the future.

Second, the improvement of device performance will rely on novel designs of device structures and materials. Nanostructures and functional materials can be introduced in certain layers of the devices with different device structures (e.g. normal or inverted structures for PSCs and OSCs). The feasible approaches include: (a) Photonic structures (e.g. plasmonic metal nanoparticles [30]) can be incorporated in the interfacial or active layers of the devices to optimize the optical properties and enhance the light absorption of the devices. The transparency and color of the devices are expected to be tuned by changing the nanostructures in the devices. (b) More suitable active materials of OSCs/PSCs and dyes of DSCs specifically for ST solar cells should be developed. Both the electrical and optical properties of the materials are the major concerns in material design. In device fabrication, the color and transparency of the devices can also be tuned by changing the active materials and the compositions (e.g. ratio of donor and acceptor in OPVs). Particular attention should be paid to the fabrication of neutral color devices, which are expected to find applications in solar windows and building integrated photovoltaics.

Third, the long-term stability of the solar cells is the prerequisite for real applications, which should be substantially improved in the future study. Graphene and other carbon-based materials have shown promising effects in improving the device stability when they are used as top electrodes. Graphene is impermeable to gas and water and it is thus a good candidate material for not only the transparent electrodes but also the encapsulation layers of solar cells.[59] Therefore, carbon-based transparent electrodes should be further developed for

highly stable devices. On the other hand, the stability of the active and interfacial layers in the devices should be improved. A good example is to introduce more stabe inorganic charge transport layers in PSCs, which leads to much better stability than using organic layers.

Forth, large-area fabrication of ST solar cells should be investigated, which has been rarely reported until now. We can further develop the fabrication techniques previously used in normal large-area OSCs, PSCs, and DSCs, mainly focusing on the application of roll-to-roll (R2R) and printing techniques on solution-processed ST solar cells. The available fabrication techniques for large-area devices include inkjet printing, doctor blading, gravure printing, spray coating and R2R processing. It is notable that R2R is a continuous, low-cost and solution-based manufacturing method, which is only applicable for flexible devices. So the devices on rigid substrates cannot be prepared by R2R process. Spray coating and doctor blading are convenient approaches for the mass production of multilayer devices on both flexible and rigid substrates. Since the quality of each layer of the devices is critical to the device performance, the processing conditions, such as the choice of solvent, the viscosity and temperature of precursors and the surface properties of substrates, should be carefully optimized at each step.

Due to their unique properties, the emerging ST solar cells are expected to complement the market of Si-based photovoltaics and find applications in many niche areas. With the development of fabrication techniques, we would be able to use the colorful ST devices integrated with buildings, clothes and even vehicles in the near future, which will not only generate electricity but also exhibit eye-catching appearances.

Acknowledgements

This work is financially supported by the Research Grants Council of Hong Kong, China (project No. T23-713/11), The Hong Kong Polytechnic University (project No. 1-ZVGH) and the National Natural Science Foundation of China (grant Nos. 21403089, 61575085).

Received: ((will be filled in by the editorial staff))
Revised: ((will be filled in by the editorial staff))
Published online: ((will be filled in by the editorial staff))

References

[1] a）M. Grätzel, Acc. Chem. Res. **2009**, 42, 1788; b）K. A. Mazzio, C. K. Luscombe, Chem. Soc. Rev. **2015**, 44, 78.

[2] C. W. Tang, Appl. Phys. Lett. **1986**, 48, 183.

[3] a）G. Yu, J. Gao, J. C. Hummelen, F. Wudl, A. J. Heeger, Science **1995**, 270, 1789; b）J. J. M. Halls, C. A. Walsh, N. C. Greenham, E. A. Marseglia, R. H. Friend, S. C. Moratti, A. B. Holmes, Nature **1995**, 376, 498.

[4] B. O'Regan, M. Gratzel, Nature **1991**, 353, 737.

[5] a）M. Gratzel, Nature **2001**, 414, 338; b）A. Hagfeldt, G. Boschloo, L. Sun, L. Kloo, H. Pettersson, Chem. Rev. **2010**, 110, 6595; c）A. Yella, H.-W. Lee, H. N. Tsao, C. Yi, A. K. Chandiran, M. K. Nazeeruddin, E. W.-G. Diau, C.-Y. Yeh, S. M. Zakeeruddin, M. Grätzel, Science **2011**, 334, 629; d）I. Chung, B. Lee, J. He, R. P. H. Chang, M. G. Kanatzidis, Nature **2012**, 485, 486; e）S. Mathew, A. Yella, P. Gao, R. Humphry-Baker, F. E. CurchodBasile, N. Ashari-Astani, I. Tavernelli, U. Rothlisberger, K. NazeeruddinMd, M. Grätzel, Nat. Chem. **2014**, 6, 242; f）S. Günes, H. Neugebauer, N. S. Sariciftci, Chem. Rev. **2007**, 107, 1324; g）M. Jørgensen, K. Norrman, S. A. Gevorgyan, T. Tromholt, B. Andreasen, F. C. Krebs, Adv. Mater. **2012**, 24, 580; h）G. Li, R. Zhu, Y. Yang, Nat. Photon. **2012**, 6, 153; i）L. Lu, T. Zheng, Q. Wu, A. M. Schneider, D. Zhao, L. Yu, Chem. Rev. **2015**, 115, 12666; j）L. Lu, M.

A. Kelly, W. You, L. Yu, Nat. Photon. **2015**, 9, 491; k）P. Cheng, X. Zhan, Chem. Soc. Rev. **2016**, 45, 2544; l）K. Wang, C. Liu, T. Meng, C. Yi, X. Gong, Chem. Soc. Rev. **2016**, 45, 2937.

[6] http://www.nrel.gov/ncpv/images/efficiency_chart.jpg.

[7] A. Kojima, K. Teshima, Y. Shirai, T. Miyasaka, J. Am. Chem. Soc. **2009**, 131, 6050.

[8] a）H. S. Kim, C. R. Lee, J. H. Im, K. B. Lee, T. Moehl, A. Marchioro, S. J. Moon, R. Humphry-Baker, J. H. Yum, J. E. Moser, M. Gratzel, N. G. Park, Sci Rep **2012**, 2, 591; b）M. M. Lee, J. Teuscher, T. Miyasaka, T. N. Murakami, H. J. Snaith, Science **2012**, 338, 643.

[9] a）J. Burschka, N. Pellet, S.-J. Moon, R. Humphry-Baker, P. Gao, M. K. Nazeeruddin, M. Gratzel, Nature **2013**, 499, 316; b）M. Liu, M. B. Johnston, H. J. Snaith, Nature **2013**, 501, 395; c）N. J. Jeon, J. H. Noh, Y. C. Kim, W. S. Yang, S. Ryu, S. I. Seok, Nat. Mater. **2014**, 13, 897; d）A. Mei, X. Li, L. Liu, Z. Ku, T. Liu, Y. Rong, M. Xu, M. Hu, J. Chen, Y. Yang, M. Grätzel, H. Han, Science **2014**, 345, 295; e）H. Zhou, Q. Chen, G. Li, S. Luo, T.-b. Song, H.-S. Duan, Z. Hong, J. You, Y. Liu, Y. Yang, Science **2014**, 345, 542; f）W. Chen, Y. Wu, Y. Yue, J. Liu, W. Zhang, X. Yang, H. Chen, E. Bi, I. Ashraful, M. Grätzel, L. Han, Science **2015**, 350, 944; g）N. J. Jeon, J. H. Noh, W. S. Yang, Y. C. Kim, S. Ryu, J. Seo, S. I. Seok, Nature **2015**, 517, 476; h）W. S. Yang, J. H. Noh, N. J. Jeon, Y. C. Kim, S. Ryu, J. Seo, S. I. Seok, Science **2015**, 348, 1234; i）X. Li, D. Bi, C. Yi, J.-D. Décoppet, J. Luo, S. M. Zakeeruddin, A. Hagfeldt, M. Grätzel, Science **2016**, 353, 58; j）H. Tsai, W. Nie, J. C. Blancon, C. C. Stoumpos, R. Asadpour, B. Harutyunyan, A. J. Neukirch, R. Verduzco, J. J. Crochet, S. Tretiak, L. Pedesseau, J. Even, M. A. Alam, G. Gupta, J. Lou, P. M. Ajayan, M. J. Bedzyk, M. G. Kanatzidis, A. D. Mohite, Nature **2016**; k）M. A. Green, A. Ho-Baillie, H. J. Snaith, Nat Photon **2014**, 8, 506; l）H. S. Jung, N.-G. Park, Small **2015**, 11, 2; m）L. Meng, J. You, T. F. Guo, Y. Yang, Acc. Chem. Res. **2016**, 49, 155; n）Y. Zhao, K. Zhu, Chem. Soc.

Rev. **2016**, 45, 655.

[10] a）B. Petter Jelle, C. Breivik, H. Drolsum Røkenes, Sol. Energy Mater. Sol. Cells **2012**, 100, 69; b）G. Tranell, B. P. Jelle, C. Breivik, Energy Procedia **2012**, 20, 68.

[11] J. Bisquert, Nat Photon **2008**, 2, 648.

[12] D. P. McMeekin, G. Sadoughi, W. Rehman, G. E. Eperon, M. Saliba, M. T. Hörantner, A. Haghighirad, N. Sakai, L. Korte, B. Rech, M. B. Johnston, L. M. Herz, H. J. Snaith, Science **2016**, 351, 151.

[13] a）D. S. Hecht, L. Hu, G. Irvin, Adv. Mater. **2011**, 23, 1482; b）J. Lee, I. Lee, T. S. Kim, J. Y. Lee, Small **2013**, 9, 2887; c）M. F. De Volder, S. H. Tawfick, R. H. Baughman, A. J. Hart, Science **2013**, 339, 535; d）Z. Liu, S. P. Lau, F. Yan, Chem. Soc. Rev. **2015**, 44, 5638; e）Y. H. Kim, C. Sachse, M. L. Machala, C. May, L. Müller-Meskamp, K. Leo, Adv. Funct. Mater. **2011**, 21, 1076.

[14] C. Riordan, R. Hulstron, "What is an air mass 1.5 spectrum? [solar cell performance calculations]", presented at *Photovoltaic Specialists Conference, 1990., Conference Record of the Twenty First IEEE*, 21-25 May 1990, 1990.

[15] Q. Tai, F. Yan, in *Organic Solar Cells: Materials and Device Physics*, (Ed: C. H. W. Choy), Springer London, London 2013, 243.

[16] G. F. Burkhard, E. T. Hoke, M. D. McGehee, Adv. Mater. **2010**, 22, 3293.

[17] A. Armin, M. Velusamy, P. Wolfer, Y. Zhang, P. L. Burn, P. Meredith, A. Pivrikas, ACS Photonics **2014**, 1, 173.

[18] S. Wilken, V. Wilkens, D. Scheunemann, R. E. Nowak, K. von Maydell, J. Parisi, H. Borchert, ACS Appl. Mater. Interface **2015**, 7, 287.

[19] K.-S. Chen, J.-F. Salinas, H.-L. Yip, L. Huo, J. Hou, A. K. Y. Jen, Energy Environ. Sci. **2012**, 5, 9551.

[20] a）Y. H. Chen, C. W. Chen, Z. Y. Huang, W. C. Lin, L. Y. Lin, F. Lin, K. T. Wong, H.

W. Lin, Adv. Mater. **2014**, 26, 1129; b）K.-T. Lee, M. Fukuda, S. Joglekar, L. J. Guo, J. Mater. Chem. C **2015**, 3, 5377; c）J.-H. Lu, Y.-L. Yu, S.-R. Chuang, C.-H. Yeh, C.-P. Chen, J. Phys. Chem. C **2016**, 120, 4233.

[21] C. O. Ram ŕez Quiroz, C. Bronnbauer, I. Levchuk, Y. Hou, C. J. Brabec, K. Forberich, ACS Nano **2016**, 10, 5104.

[22] T. Ameri, G. Dennler, C. Waldauf, H. Azimi, A. Seemann, K. Forberich, J. Hauch, M. Scharber, K. Hingerl, C. J. Brabec, Adv. Funct. Mater. **2010**, 20, 1592.

[23] a）J. Mescher, S. W. Kettlitz, N. Christ, M. F. G. Klein, A. Puetz, A. Mertens, A. Colsmann, U. Lemmer, Org. Electron. **2014**, 15, 1476; b）J. Czolk, A. Puetz, D. Kutsarov, M. Reinhard, U. Lemmer, A. Colsmann, Adv. Energy Mater. **2013**, 3, 386.

[24] A. Colsmann, A. Puetz, A. Bauer, J. Hanisch, E. Ahlswede, U. Lemmer, Adv. Energy Mater. **2011**, 1, 599.

[25] C.-C. Chen, L. Dou, J. Gao, W.-H. Chang, G. Li, Y. Yang, Energy Environ. Sci. **2013**, 6, 2714.

[26] a）W. Yu, X. Jia, Y. Long, L. Shen, Y. Liu, W. Guo, S. Ruan, ACS Appl. Mater. Interface **2015**, 7, 9920; b）W. Yu, X. Jia, M. Yao, L. Zhu, Y. Long, L. Shen, Phys. Chem. Chem. Phys. **2015**, 17, 23732.

[27] L. A. A. Pettersson, L. S. Roman, O. Ingan äs, J. Appl. Phys. **1999**, 86, 487.

[28] C. Tao, G. Xie, F. Meng, S. Ruan, W. Chen, J. Phys. Chem. C **2011**, 115, 12611.

[29] a）Y. H. Kim, L. M üller-Meskamp, A. A. Zakhidov, C. Sachse, J. Meiss, J. Bikova, A. Cook, A. A. Zakhidov, K. Leo, Sol. Energy Mater. Sol. Cells **2012**, 96, 244; b）L. Shen, S. Ruan, W. Guo, F. Meng, W. Chen, Sol. Energy Mater. Sol. Cells **2012**, 97, 59; c）R. Betancur, P. Romero-Gomez, A. Martinez-Otero, X. Elias, M. Maym ó, J. Martorell, Nat. Photon. **2013**, 7, 995; d）C.-C. Chueh, S.-C. Chien, H.-L. Yip, J. F. Salinas, C.-Z. Li, K.-S.

Chen, F.-C. Chen, W.-C. Chen, A. K. Y. Jen, Adv. Energy Mater. **2013**, 3, 417; e）Y. Jiang, I. Almansouri, S. Huang, T. Young, Y. Li, Y. Peng, Q. Hou, L. Spiccia, U. Bach, Y.-B. Cheng, M. A. Green, A. Ho-Baillie, J. Mater. Chem. C **2016**, 4, 5679.

[30] a）Y. Liang, Z. Xu, J. Xia, S. T. Tsai, Y. Wu, G. Li, C. Ray, L. Yu, Adv. Mater. **2010**, 22, E135; b）Y. Liu, J. Zhao, Z. Li, C. Mu, W. Ma, H. Hu, K. Jiang, H. Lin, H. Ade, H. Yan, Nat. Commun. **2014**, 5, 5293; c）S. Liu, P. You, J. Li, J. Li, C.-S. Lee, B. S. Ong, C. Surya, F. Yan, Energy Environ. Sci. **2015**, 8, 1463; d）S. Liu, R. Jiang, P. You, X. Zhu, J. Wang, F. Yan, Energy Environ. Sci. **2016**, 9, 898; e）J. Zhao, Y. Li, G. Yang, K. Jiang, H. Lin, H. Ade, W. Ma, H. Yan, Nat. Energy **2016**, 1, 15027.

[31] W. Zhao, D. Qian, S. Zhang, S. Li, O. Inganäs, F. Gao, J. Hou, Adv. Mater. **2016**, 28, 4734.

[32] a）M. C. Scharber, N. S. Sariciftci, Prog Polym Sci **2013**, 38, 1929; b）M. C. Scharber, Adv. Mater. **2016**, 28, 1994.

[33] a）J. You, L. Dou, K. Yoshimura, T. Kato, K. Ohya, T. Moriarty, K. Emery, C. C. Chen, J. Gao, G. Li, Y. Yang, Nat. Commun. **2013**, 4, 1446; b）T. Ameri, N. Li, C. J. Brabec, Energy Environ. Sci. **2013**, 6, 2390; c）J. You, L. Dou, Z. Hong, G. Li, Y. Yang, Prog. Polym. Sci. **2013**, 38, 1909.

[34] G. Li, C. W. Chu, V. Shrotriya, J. Huang, Y. Yang, Appl. Phys. Lett. **2006**, 88, 253503.

[35] R. Koeppe, D. Hoeglinger, P. A. Troshin, R. N. Lyubovskaya, V. F. Razumov, N. S. Sariciftci, ChemSusChem **2009**, 2, 309.

[36] a）J. Meiss, N. Allinger, M. K. Riede, K. Leo, Appl. Phys. Lett. **2008**, 93, 103311; b）J. Meiss, M. K. Riede, K. Leo, J. Appl. Phys. **2009**, 105, 063108.

[37] J. Meiss, T. Menke, K. Leo, C. Uhrich, W.-M. Gnehr, S. Sonntag, M. Pfeiffer, M. Riede, Appl. Phys. Lett. **2011**, 99, 043301.

[38] C.-Y. Chang, L. Zuo, H.-L. Yip, Y. Li, C.-Z. Li, C.-S. Hsu, Y.-J. Cheng, H. Chen, A. K. Y. Jen, Adv. Funct. Mater. **2013**, 23, 5084.

[39] W. J. da Silva, H. P. Kim, A. Rashid bin Mohd Yusoff, J. Jang, Nanoscale **2013**, 5, 9324.

[40] X. Ren, X. Li, W. C. H. Choy, Nano Energy **2015**, 17, 187.

[41] a）W. Yu, S. Ruan, Y. Long, L. Shen, W. Guo, W. Chen, Sol. Energy Mater. Sol. Cells **2014**, 127, 27; b）W. Yu, L. Shen, Y. Long, P. Shen, W. Guo, W. Chen, S. Ruan, Org. Electron. **2014**, 15, 470; c）W. Yu, L. Shen, P. Shen, Y. Long, H. Sun, W. Chen, S. Ruan, ACS Appl. Mater. Interface **2014**, 6, 599.

[42] a）F. Li, S. Ruan, Y. Xu, F. Meng, J. Wang, W. Chen, L. Shen, Sol. Energy Mater. Sol. Cells **2011**, 95, 877; b）L. Shen, Y. Xu, F. Meng, F. Li, S. Ruan, W. Chen, Org. Electron. **2011**, 12, 1223.

[43] a）C. Tao, G. Xie, C. Liu, X. Zhang, W. Dong, F. Meng, X. Kong, L. Shen, S. Ruan, W. Chen, Appl. Phys. Lett. **2009**, 95, 053303; b）J. M. Cho, S. K. Lee, S.-J. Moon, J. Jo, W. S. Shin, Curr. Appl. Phys. **2014**, 14, 1144.

[44] F. Pastorelli, P. Romero-Gomez, R. Betancur, A. Martinez-Otero, P. Mantilla-Perez, N. Bonod, J. Martorell, Adv. Energy Mater. **2015**, 5, 1400614.

[45] H. Schmidt, H. Flügge, T. Winkler, T. Bülow, T. Riedl, W. Kowalsky, Appl. Phys. Lett. **2009**, 94, 243302.

[46] J. Huang, G. Li, Y. Yang, Adv. Mater. **2008**, 20, 415.

[47] A. Bauer, T. Wahl, J. Hanisch, E. Ahlswede, Appl. Phys. Lett. **2012**, 100, 073307.

[48] L. Hu, H. S. Kim, J.-Y. Lee, P. Peumans, Y. Cui, ACS Nano **2010**, 4, 2955.

[49] J. Y. Lee, S. T. Connor, Y. Cui, P. Peumans, Nano Lett **2010**, 10, 1276.

[50] M. Reinhard, R. Eckstein, A. Slobodskyy, U. Lemmer, A. Colsmann, Org. Electron. **2013**, 14, 273.

[51] a）F. Guo, X. Zhu, K. Forberich, J. Krantz, T. Stubhan, M. Salinas, M. Halik, S. Spallek, B. Butz, E. Spiecker, T. Ameri, N. Li, P. Kubis, D. M. Guldi, G. J. Matt, C. J. Brabec, Adv. Energy Mater. **2013**, 3, 1062; b）F. Guo, P. Kubis, T. Przybilla, E. Spiecker, A. Hollmann, S. Langner, K. Forberich, C. J. Brabec, Adv. Energy Mater. **2015**, 5, 1401779.

[52] H. Lu, J. Lin, N. Wu, S. Nie, Q. Luo, C.-Q. Ma, Z. Cui, Appl. Phys. Lett. **2015**, 106, 093302.

[53] a）C.-C. Chen, L. Dou, R. Zhu, C.-H. Chung, T.-B. Song, Y. B. Zheng, S. Hawks, G. Li, P. S. Weiss, Y. Yang, ACS Nano **2012**, 6, 7185; b）J. Krantz, T. Stubhan, M. Richter, S. Spallek, I. Litzov, G. J. Matt, E. Spiecker, C. J. Brabec, Adv. Funct. Mater. **2013**, 23, 1711; c）Z. M. Beiley, M. G. Christoforo, P. Gratia, A. R. Bowring, P. Eberspacher, G. Y. Margulis, C. Cabanetos, P. M. Beaujuge, A. Salleo, M. D. McGehee, Adv. Mater. **2013**, 25, 7020; d）Y.-J. Kang, D.-G. Kim, J.-K. Kim, W.-Y. Jin, J.-W. Kang, Org. Electron. **2014**, 15, 2173; e）J. Min, C. Bronnbauer, Z.-G. Zhang, C. Cui, Y. N. Luponosov, I. Ata, P. Schweizer, T. Przybilla, F. Guo, T. Ameri, K. Forberich, E. Spiecker, P. Bäuerle, S. A. Ponomarenko, Y. Li, C. J. Brabec, Adv. Funct. Mater. **2016**, 26, 4543.

[54] C. Wang, K. Takei, T. Takahashi, A. Javey, Chem. Soc. Rev. **2013**, 42, 2592.

[55] Y. H. Kim, C. Sachse, A. A. Zakhidov, J. Meiss, A. A. Zakhidov, L. Müller-Meskamp, K. Leo, Org. Electron. **2012**, 13, 2422.

[56] I. Jeon, C. Delacou, A. Kaskela, E. I. Kauppinen, S. Maruyama, Y. Matsuo, Sci Rep **2016**, 6, 31348.

[57] Y.-Y. Lee, K.-H. Tu, C.-C. Yu, S.-S. Li, J.-Y. Hwang, C.-C. Lin, K.-H. Chen, L.-C. Chen, H.-L. Chen, C.-W. Chen, ACS Nano **2011**, 5, 6564.

[58] Z. Liu, J. Li, Z. H. Sun, G. Tai, S. P. Lau, F. Yan, ACS Nano **2012**, 6, 810.

[59] Z. Liu, J. Li, F. Yan, Adv. Mater. **2013**, 25, 4296.

[60] Z. Liu, P. You, S. Liu, F. Yan, ACS Nano **2015**, 9, 12026.

[61] X. Fan, B. Xu, S. Liu, C. Cui, J. Wang, F. Yan, ACS Appl. Mater. Interface **2016**, 8, 14029.

[62] N. Kim, H. Kang, J.-H. Lee, S. Kee, S. H. Lee, K. Lee, Adv. Mater. **2015**, 27, 2317.

[63] a）S. K. Hau, H.-L. Yip, J. Zou, A. K. Y. Jen, Org. Electron. **2009**, 10, 1401; b）Q. Dong, Y. Zhou, J. Pei, Z. Liu, Y. Li, S. Yao, J. Zhang, W. Tian, Org. Electron. **2010**, 11, 1327; c）Y. Zhou, H. Cheun, S. Choi, W. J. Potscavage, C. Fuentes-Hernandez, B. Kippelen, Appl. Phys. Lett. **2010**, 97, 153304; d）Y. Zhou, H. Cheun, S. Choi, C. Fuentes-Hernandez, B. Kippelen, Org. Electron. **2011**, 12, 827; e）A. Colsmann, M. Reinhard, T.-H. Kwon, C. Kayser, F. Nickel, J. Czolk, U. Lemmer, N. Clark, J. Jasieniak, A. B. Holmes, D. Jones, Sol. Energy Mater. Sol. Cells **2012**, 98, 118; f）J.-W. Kang, Y.-J. Kang, S. Jung, D. S. You, M. Song, C. S. Kim, D.-G. Kim, J.-K. Kim, S. H. Kim, Org. Electron. **2012**, 13, 2940.

[64] Y. Galagan, J.-E. J.M. Rubingh, R. Andriessen, C.-C. Fan, P. W.M. Blom, S. C. Veenstra, J. M. Kroon, Sol. Energy Mater. Sol. Cells **2011**, 95, 1339.

[65] F. Guo, P. Kubis, T. Stubhan, N. Li, D. Baran, T. Przybilla, E. Spiecker, K. Forberich, C. J. Brabec, ACS Appl. Mater. Interface **2014**, 6, 18251.

[66] J. H. Yim, S.-y. Joe, C. Pang, K. M. Lee, H. Jeong, J.-Y. Park, Y. H. Ahn, J. C. de Mello, S. Lee, ACS Nano **2014**, 8, 2857.

[67] A. R. b. M. Yusoff, S. J. Lee, F. K. Shneider, W. J. da Silva, J. Jang, Adv. Energy Mater. **2014**, 4, 1301989.

[68] H. P. Kim, H. J. Lee, A. R. b. Mohd Yusoff, J. Jang, Sol. Energy Mater. Sol. Cells **2013**, 108, 38.

[69] P. Romero-Gomez, R. Betancur, A. Martinez-Otero, X. Elias, M. Mariano, B. Romero, B. Arredondo, R. Vergaz, J. Martorell, Sol. Energy Mater. Sol. Cells **2015**, 137, 44.

[70] S. Ahmad, E. Guillén, L. Kavan, M. Grätzel, M. K. Nazeeruddin, Energy Environ. Sci. **2013**, 6, 3439.

[71] A. Hauch, A. Georg, Electrochim. Acta **2001**, 46, 3457.

[72] a）S. Yun, A. Hagfeldt, T. Ma, Adv. Mater. **2014**, 26, 6210; b）Q. Tai, X.-Z. Zhao, J. Mater. Chem. A **2014**, 2, 13207.

[73] a）X. Fang, T. Ma, G. Guan, M. Akiyama, T. Kida, E. Abe, J. Electroanal. Chem. **2004**, 570, 257; b）Y.-L. Lee, C.-L. Chen, L.-W. Chong, C.-H. Chen, Y.-F. Liu, C.-F. Chi, Electrochem. Commun. **2010**, 12, 1662.

[74] S. Ito, S. M. Zakeeruddin, P. Comte, P. Liska, D. Kuang, M. Gratzel, Nat Photon **2008**, 2, 693.

[75] A. Iefanova, J. Nepal, P. Poudel, D. Davoux, U. Gautam, V. Mallam, Q. Qiao, B. Logue, M. F. Baroughi, Thin Solid Films **2014**, 562, 578.

[76] S. I. Cha, B. K. Koo, S. H. Seo, D. Y. Lee, J. Mater. Chem. **2010**, 20, 659.

[77] L. Kavan, J. H. Yum, M. Grätzel, ACS Nano **2011**, 5, 165.

[78] G. Wang, Y. Fang, Y. Lin, W. Xing, S. Zhuo, Mater. Res. Bull. **2012**, 47, 4252.

[79] a）L. Kavan, J. H. Yum, M. Gratzel, Nano Lett **2011**, 11, 5501; b）L. Kavan, J.-H. Yum, M. K. Nazeeruddin, M. Grätzel, ACS Nano **2011**, 5, 9171.

[80] L. Kavan, J. H. Yum, M. Graetzel, ACS Appl. Mater. Interface **2012**, 4, 6999.

[81] R. Cruz, D. A. Pacheco Tanaka, A. Mendes, Solar Energy **2012**, 86, 716.

[82] R. Cruz, J. P. Araújo, L. Andrade, A. Mendes, J. Mater. Chem. A **2014**, 2, 2028.

[83] C. Bu, Y. Liu, Z. Yu, S. You, N. Huang, L. Liang, X. Z. Zhao, ACS Appl. Mater. Interface **2013**, 5, 7432.

[84] Q. Tai, B. Chen, F. Guo, S. Xu, H. Hu, B. Sebo, X.-Z. Zhao, ACS Nano **2011**, 5, 3795.

[85] J. Wu, Y. Li, Q. Tang, G. Yue, J. Lin, M. Huang, L. Meng, Sci Rep **2014**, 4, 4028.

[86] J. Gao, Y. Yang, Z. Zhang, J. Yan, Z. Lin, X. Guo, Nano Energy **2016**, 26, 123.

[87] C. Bu, Q. Tai, Y. Liu, S. Guo, X. Zhao, J. Power Sources **2013**, 221, 78.

[88] D. K. Hwang, D. Song, S. S. Jeon, T. H. Han, Y. S. Kang, S. S. Im, J. Mater. Chem. A

2014, 2, 859.

[89] a）J.-G. Chen, H.-Y. Wei, K.-C. Ho, Sol. Energy Mater. Sol. Cells **2007**, 91, 1472; b）W. Hong, Y. Xu, G. Lu, C. Li, G. Shi, Electrochem. Commun. **2008**, 10, 1555.

[90] D. Song, M. Li, Y. Li, X. Zhao, B. Jiang, Y. Jiang, ACS Appl. Mater. Interface **2014**, 6, 7126.

[91] a）J. Xia, N. Masaki, K. Jiang, S. Yanagida, J. Mater. Chem. **2007**, 17, 2845; b）S. Ahmad, J.-H. Yum, Z. Xianxi, M. Grätzel, H.-J. Butt, M. K. Nazeeruddin, J. Mater. Chem. **2010**, 20, 1654; c）J. M. Pringle, V. Armel, D. R. MacFarlane, Chem. Commun. **2010**, 46, 5367.

[92] X. Li, Z. Ku, Y. Rong, G. Liu, L. Liu, T. Liu, M. Hu, Y. Yang, H. Wang, M. Xu, P. Xiang, H. Han, Phys. Chem. Chem. Phys. **2012**, 14, 14383.

[93] K. S. Lee, H. K. Lee, D. H. Wang, N.-G. Park, J. Y. Lee, O. O. Park, J. H. Park, Chem. Commun. **2010**, 46, 4505.

[94] a）H. Sun, D. Qin, S. Huang, X. Guo, D. Li, Y. Luo, Q. Meng, Energy Environ. Sci. **2011**, 4, 2630; b）Z. Ku, X. Li, G. Liu, H. Wang, Y. Rong, M. Xu, L. Liu, M. Hu, Y. Yang, H. Han, J. Mater. Chem. A **2013**, 1, 237; c）S.-Y. Tai, C.-F. Chang, W.-C. Liu, J.-H. Liao, J.-Y. Lin, Electrochim. Acta **2013**, 107, 66; d）J.-Y. Lin, S.-W. Chou, Electrochem. Commun. **2013**, 37, 11; e）B. Lei, G. R. Li, X. P. Gao, J. Mater. Chem. A **2014**, 2, 3919; f）J. Zhang, S. Najmaei, H. Lin, J. Lou, Nanoscale **2014**, 6, 5279.

[95] Y. C. Wang, D. Y. Wang, Y. T. Jiang, H. A. Chen, C. C. Chen, K. C. Ho, H. L. Chou, C. W. Chen, Angew. Chem. Int. Ed. **2013**, 52, 6694.

[96] Y. Duan, Q. Tang, J. Liu, B. He, L. Yu, Angew. Chem. Int. Ed. **2014**, 53, 14569.

[97] G. Y. Margulis, M. G. Christoforo, D. Lam, Z. M. Beiley, A. R. Bowring, C. D. Bailie, A. Salleo, M. D. McGehee, Adv. Energy Mater. **2013**, 3, 1657.

[98] H.-Y. Chen, J.-Y. Liao, B.-X. Lei, D.-B. Kuang, Y. Fang, C.-Y. Su, Chem.- Asian J.

2012, 7, 1795.

[99] a）F. Gong, H. Wang, Z.-S. Wang, Phys. Chem. Chem. Phys. **2011**, 13, 17676; b）V.-D. Dao, L. V. Nang, E.-T. Kim, J.-K. Lee, H.-S. Choi, ChemSusChem **2013**, 6, 1316; c）H.-S. Jang, J.-M. Yun, D.-Y. Kim, S.-I. Na, S.-S. Kim, Surf. Coat. Technol. **2014**, 242, 8; d）P.-T. Shih, R.-X. Dong, S.-Y. Shen, R. Vittal, J.-J. Lin, K.-C. Ho, J. Mater. Chem. A **2014**, 2, 8742.

[100] S. Peng, J. Liang, S. G. Mhaisalkar, S. Ramakrishna, J. Mater. Chem. **2012**, 22, 5308.

[101] F. De Rossi, L. Di Gaspare, A. Reale, A. Di Carlo, T. M. Brown, J. Mater. Chem. A **2013**, 1, 12941.

[102] J.-Y. Lin, C.-Y. Chan, S.-W. Chou, Chem. Commun. **2013**, 49, 1440.

[103] P.-Y. Chen, C.-T. Li, C.-P. Lee, R. Vittal, K.-C. Ho, Nano Energy **2015**, 12, 374.

[104] Y.-S. Wang, S.-M. Li, S.-T. Hsiao, H. Wei, S.-Y. Yang, H.-W. Tien, C.-C. M. Ma, C.-C. Hu, J. Power Sources **2014**, 260, 326.

[105] J. Huo, J. Wu, M. Zheng, Y. Tu, Z. Lan, Electrochim. Acta **2016**, 187, 210.

[106] H. Zhang, B. He, Q. Tang, L. Yu, J. Power Sources **2015**, 275, 489.

[107] K. Zhang, C. Qin, X. Yang, A. Islam, S. Zhang, H. Chen, L. Han, Adv. Energy Mater. **2014**, 4, 1301966.

[108] C. Lopez-Lopez, S. Colodrero, H. Miguez, Phys. Chem. Chem. Phys. **2014**, 16, 663.

[109] C. Roldán-Carmona, O. Malinkiewicz, R. Betancur, G. Longo, C. Momblona, F. Jaramillo, L. Camacho, H. J. Bolink, Energy Environ. Sci. **2014**, 7, 2968.

[110] S. Aharon, M. Layani, B.-E. Cohen, E. Shukrun, S. Magdassi, L. Etgar, Adv. Mater. Interfaces **2015**, 2, 1500118.

[111] E. Della Gaspera, Y. Peng, Q. Hou, L. Spiccia, U. Bach, J. J. Jasieniak, Y.-B. Cheng, Nano Energy **2015**, 13, 249.

[112] X.-L. Ou, M. Xu, J. Feng, H.-B. Sun, Sol. Energy Mater. Sol. Cells **2016**, 157, 660.

[113] J. W. Jung, C.-C. Chueh, A. K. Y. Jen, Adv. Energy Mater. **2015**, 5, 1500486.

[114] C.-Y. Chang, Y.-C. Chang, W.-K. Huang, K.-T. Lee, A.-C. Cho, C.-C. Hsu, Chem. Mater. **2015**, 27, 7119.

[115] S. Bag, M. F. Durstock, Nano Energy **2016**, 30, 542.

[116] a）M. R. Leyden, L. K. Ono, S. R. Raga, Y. Kato, S. Wang, Y. Qi, J. Mater. Chem. A **2014**, 2, 18742; b）L. K. Ono, S. Wang, Y. Kato, S. R. Raga, Y. Qi, Energy Environ. Sci. **2014**, 7, 3989; c）M. R. Leyden, M. V. Lee, S. R. Raga, Y. Qi, J. Mater. Chem. A **2015**, 3, 16097; d）S. Wang, L. K. Ono, M. R. Leyden, Y. Kato, S. R. Raga, M. V. Lee, Y. Qi, J. Mater. Chem. A **2015**, 3, 14631.

[117] a）J. H. Heo, H. J. Han, M. Lee, M. Song, D. H. Kim, S. H. Im, Energy Environ. Sci. **2015**, 8, 2922; b）P. Loper, S. J. Moon, S. M. de Nicolas, B. Niesen, M. Ledinsky, S. Nicolay, J. Bailat, J. H. Yum, S. De Wolf, C. Ballif, Phys. Chem. Chem. Phys. **2015**, 17, 1619; c）K. A. Bush, C. D. Bailie, Y. Chen, A. R. Bowring, W. Wang, W. Ma, T. Leijtens, F. Moghadam, M. D. McGehee, Adv. Mater. **2016**.

[118] F. Fu, T. Feurer, T. Jager, E. Avancini, B. Bissig, S. Yoon, S. Buecheler, A. N. Tiwari, Nat. Commun. **2015**, 6, 8932.

[119] J. Werner, G. Dubuis, A. Walter, P. Löper, S.-J. Moon, S. Nicolay, M. Morales-Masis, S. De Wolf, B. Niesen, C. Ballif, Sol. Energy Mater. Sol. Cells **2015**, 141, 407.

[120] L. Kranz, A. Abate, T. Feurer, F. Fu, E. Avancini, J. Lockinger, P. Reinhard, S. M. Zakeeruddin, M. Gratzel, S. Buecheler, A. N. Tiwari, J. Phys. Chem. Lett. **2015**, 6, 2676.

[121] H. Kanda, A. Uzum, A. K. Baranwal, T. A. N. Peiris, T. Umeyama, H. Imahori, H. Segawa, T. Miyasaka, S. Ito, J. Phys. Chem. C **2016**, 120, 28441.

[122] J. Werner, L. Barraud, A. Walter, M. Bräuninger, F. Sahli, D. Sacchetto, N. Tétreault, B. Paviet-Salomon, S.-J. Moon, C. Allebé, M. Despeisse, S. Nicolay, S. De Wolf, B. Niesen, C. Ballif, ACS Energy Lett. **2016**, 474.

[123] F. Guo, H. Azimi, Y. Hou, T. Przybilla, M. Hu, C. Bronnbauer, S. Langner, E.

Spiecker, K. Forberich, C. J. Brabec, Nanoscale **2015**, 7, 1642.

[124] C.-Y. Chang, K.-T. Lee, W.-K. Huang, H.-Y. Siao, Y.-C. Chang, Chem. Mater. **2015**, 27, 5122.

[125] X. Dai, Y. Zhang, H. Shen, Q. Luo, X. Zhao, J. Li, H. Lin, ACS Appl. Mater. Interface **2016**, 8, 4523.

[126] C. O. Ramírez Quiroz, I. Levchuk, C. Bronnbauer, M. Salvador, K. Forberich, T. Heumüller, Y. Hou, P. Schweizer, E. Spiecker, C. J. Brabec, J. Mater. Chem. A **2015**, 3, 24071.

[127] Z. Li, S. A. Kulkarni, P. P. Boix, E. Shi, A. Cao, K. Fu, S. K. Batabyal, J. Zhang, Q. Xiong, L. H. Wong, N. Mathews, S. G. Mhaisalkar, ACS Nano **2014**, 8, 6797.

[128] Z. Li, P. P. Boix, G. Xing, K. Fu, S. A. Kulkarni, S. K. Batabyal, W. Xu, A. Cao, T. C. Sum, N. Mathews, L. H. Wong, Nanoscale **2015**.

[129] P. You, Z. Liu, Q. Tai, S. Liu, F. Yan, Adv. Mater. **2015**, 27, 3632.

[130] L. Bu, Z. Liu, M. Zhang, W. Li, A. Zhu, F. Cai, Z. Zhao, Y. Zhou, ACS Appl. Mater. Interface **2015**, 7, 17776.

[131] G. E. Eperon, V. M. Burlakov, A. Goriely, H. J. Snaith, ACS Nano **2014**, 8, 591.

[132] G. E. Eperon, D. Bryant, J. Troughton, S. D. Stranks, M. B. Johnston, T. Watson, D. A. Worsley, H. J. Snaith, J. Phys. Chem. Lett. **2015**, 6, 129.

[133] M. T. Hörantner, P. K. Nayak, S. Mukhopadhyay, K. Wojciechowski, C. Beck, D. McMeekin, B. Kamino, G. E. Eperon, H. J. Snaith, Adv. Mater. Interfaces **2016**, 3, 1500837.

[134] J. H. Heo, M. H. Jang, M. H. Lee, H. J. Han, M. G. Kang, M. L. Lee, S. H. Im, J. Mater. Chem. A **2016**, 4, 16324.

[135] L. Zhang, M. T. Hörantner, W. Zhang, Q. Yan, H. J. Snaith, Sol. Energy Mater. Sol. Cells **2017**, 160, 193.

[136] J. H. Noh, S. H. Im, J. H. Heo, T. N. Mandal, S. I. Seok, Nano Lett. **2013**, 13, 1764.

[137] a）C. D. Bailie, M. G. Christoforo, J. P. Mailoa, A. R. Bowring, E. L. Unger, W. H. Nguyen, J. Burschka, N. Pellet, J. Z. Lee, M. Grätzel, R. Noufi, T. Buonassisi, A. Salleo, M.

D. McGehee, Energy Environ. Sci. **2015**, 8, 956; b）B. Chen, Y. Bai, Z. Yu, T. Li, X. Zheng, Q. Dong, L. Shen, M. Boccard, A. Gruverman, Z. Holman, J. Huang, Adv. Energy Mater. **2016**, 6, 1601128; c）F. Fu, T. Feurer, Thomas P. Weiss, S. Pisoni, E. Avancini, C. Andres, S. Buecheler, Ayodhya N. Tiwari, Nat. Energy **2016**, 2, 16190; d）J. Peng, T. Duong, X. Zhou, H. Shen, Y. Wu, H. K. Mulmudi, Y. Wan, D. Zhong, J. Li, T. Tsuzuki, K. J. Weber, K. R. Catchpole, T. P. White, Adv. Energy Mater. **2017**, 7, 1601768.

[138] a）T. Todorov, T. Gershon, O. Gunawan, Y. S. Lee, C. Sturdevant, L.-Y. Chang, S. Guha, Adv. Energy Mater. **2015**, 5, 1500799; b）S. Albrecht, M. Saliba, J. P. Correa Baena, F. Lang, L. Kegelmann, M. Mews, L. Steier, A. Abate, J. Rappich, L. Korte, R. Schlatmann, M. K. Nazeeruddin, A. Hagfeldt, M. Grätzel, B. Rech, Energy Environ. Sci. **2016**, 9, 81; c）J. Werner, C. H. Weng, A. Walter, L. Fesquet, J. P. Seif, S. De Wolf, B. Niesen, C. Ballif, J. Phys. Chem. Lett. **2016**, 7, 161.

[139] a）M. Gratzel, Nat. Mater. **2014**, 13, 838; b）T. Leijtens, G. E. Eperon, N. K. Noel, S. N. Habisreutinger, A. Petrozza, H. J. Snaith, Adv. Energy Mater. **2015**, 5, 1500936; c）Y. Rong, L. Liu, A. Mei, X. Li, H. Han, Adv. Energy Mater. **2015**, 5, 1501066; d）G. Niu, X. Guo, L. Wang, J. Mater. Chem. A **2015**, 3, 8970; e）T. A. Berhe, W.-N. Su, C.-H. Chen, C.-J. Pan, J.-H. Cheng, H.-M. Chen, M.-C. Tsai, L.-Y. Chen, A. A. Dubale, B.-J. Hwang, Energy Environ. Sci. **2016**, 9, 323; f）N. H. Tiep, Z. Ku, H. J. Fan, Adv. Energy Mater. **2016**, 6, 1501420; g）D. Bryant, N. Aristidou, S. Pont, I. Sanchez-Molina, T. Chotchunangatchaval, S. Wheeler, J. R. Durrant, S. A. Haque, Energy Environ. Sci. **2016**, 9, 1655; h）Z. Song, A. Abate, S. C. Watthage, G. K. Liyanage, A. B. Phillips, U. Steiner, M. Graetzel, M. J. Heben, Adv. Energy Mater. **2016**, 6, 1600846.

[140] Y. Guo, K. Shoyama, W. Sato, E. Nakamura, Adv. Energy Mater. **2016**, 6, 1502317.

[141] X. Li, M. I. Dar, C. Yi, J. Luo, M. Tschumi, S. M. Zakeeruddin, M. K. Nazeeruddin,

H. Han, M. Gratzel, Nat. Chem. **2015**, 7, 703.

[142] Y. Zhao, J. Wei, H. Li, Y. Yan, W. Zhou, D. Yu, Q. Zhao, Nat. Commun. **2016**, 7.

[143] a）Q. Jiang, D. Rebollar, J. Gong, E. L. Piacentino, C. Zheng, T. Xu, Angew. Chem. Int. Ed. **2015**, 54, 7617; b）Q. Tai, P. You, H. Sang, Z. Liu, C. Hu, H. L. W. Chan, F. Yan, Nat. Commun. **2016**, 7.

[144] a）J.-W. Lee, D.-H. Kim, H.-S. Kim, S.-W. Seo, S. M. Cho, N.-G. Park, Adv. Energy Mater. **2015**, 5, 1501310; b）M. Saliba, T. Matsui, J.-Y. Seo, K. Domanski, J.-P. Correa-Baena, M. K. Nazeeruddin, S. M. Zakeeruddin, W. Tress, A. Abate, A. Hagfeldt, M. Grätzel, Energy Environ. Sci. **2016**, 9, 1989; c）R. J. Sutton, G. E. Eperon, L. Miranda, E. S. Parrott, B. A. Kamino, J. B. Patel, M. T. Hörantner, M. B. Johnston, A. A. Haghighirad, D. T. Moore, H. J. Snaith, Adv. Energy Mater. **2016**, 6, 1502458; d）W. Li, W. Zhang, S. Van Reenen, R. J. Sutton, J. Fan, A. A. Haghighirad, M. B. Johnston, L. Wang, H. J. Snaith, Energy Environ. Sci. **2016**, 9, 490; e）R. E. Beal, D. J. Slotcavage, T. Leijtens, A. R. Bowring, R. A. Belisle, W. H. Nguyen, G. F. Burkhard, E. T. Hoke, M. D. McGehee, J. Phys. Chem. Lett. **2016**, 7, 746; f）M. Kulbak, S. Gupta, N. Kedem, I. Levine, T. Bendikov, G. Hodes, D. Cahen, J. Phys. Chem. Lett. **2016**, 7, 167.

[145] I. C. Smith, E. T. Hoke, D. Solis-Ibarra, M. D. McGehee, H. I. Karunadasa, Angew. Chem. Int. Ed. **2014**, 53, 11232.

[146] D. Bi, P. Gao, R. Scopelliti, E. Oveisi, J. Luo, M. Gratzel, A. Hagfeldt, M. K. Nazeeruddin, Adv. Mater. **2016**, 28, 2910.

[147] J. You, L. Meng, T.-B. Song, T.-F. Guo, Y. Yang, W.-H. Chang, Z. Hong, H. Chen, H. Zhou, Q. Chen, Y. Liu, N. De Marco, Y. Yang, Nat Nano **2016**, 11, 75.

[148] a）T. Leijtens, G. E. Eperon, S. Pathak, A. Abate, M. M. Lee, H. J. Snaith, Nat. Commun. **2013**, 4, 2885; b）S. N. Habisreutinger, T. Leijtens, G. E. Eperon, S. D. Stranks, R.

J. Nicholas, H. J. Snaith, Nano Lett. **2014**, 14, 5561; c）S. M. Kang, N. Ahn, J.-W. Lee, M. Choi, N.-G. Park, J. Mater. Chem. A **2014**, 2, 20017; d）I. Hwang, I. Jeong, J. Lee, M. J. Ko, K. Yong, ACS Appl. Mater. Interface **2015**, 7, 17330.

Figures

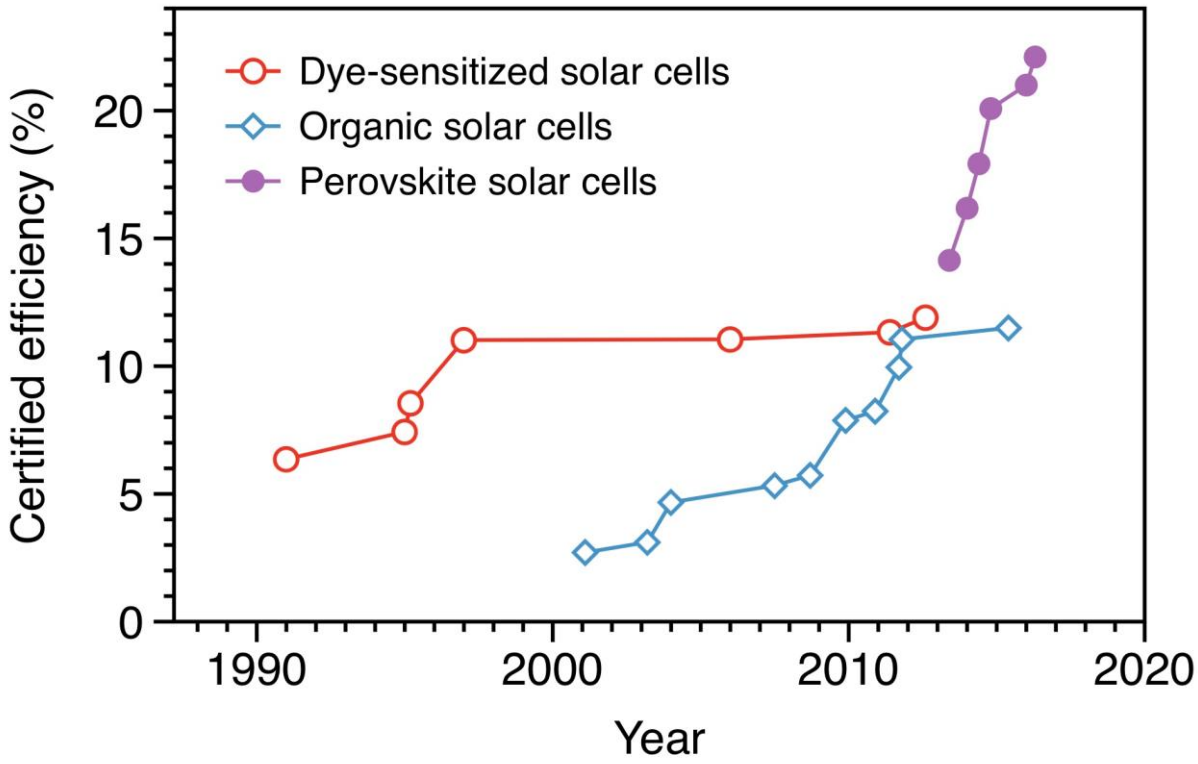

Figure 1. Evolution of the record efficiencies of OSCs, DSCs, and PSCs.[6]

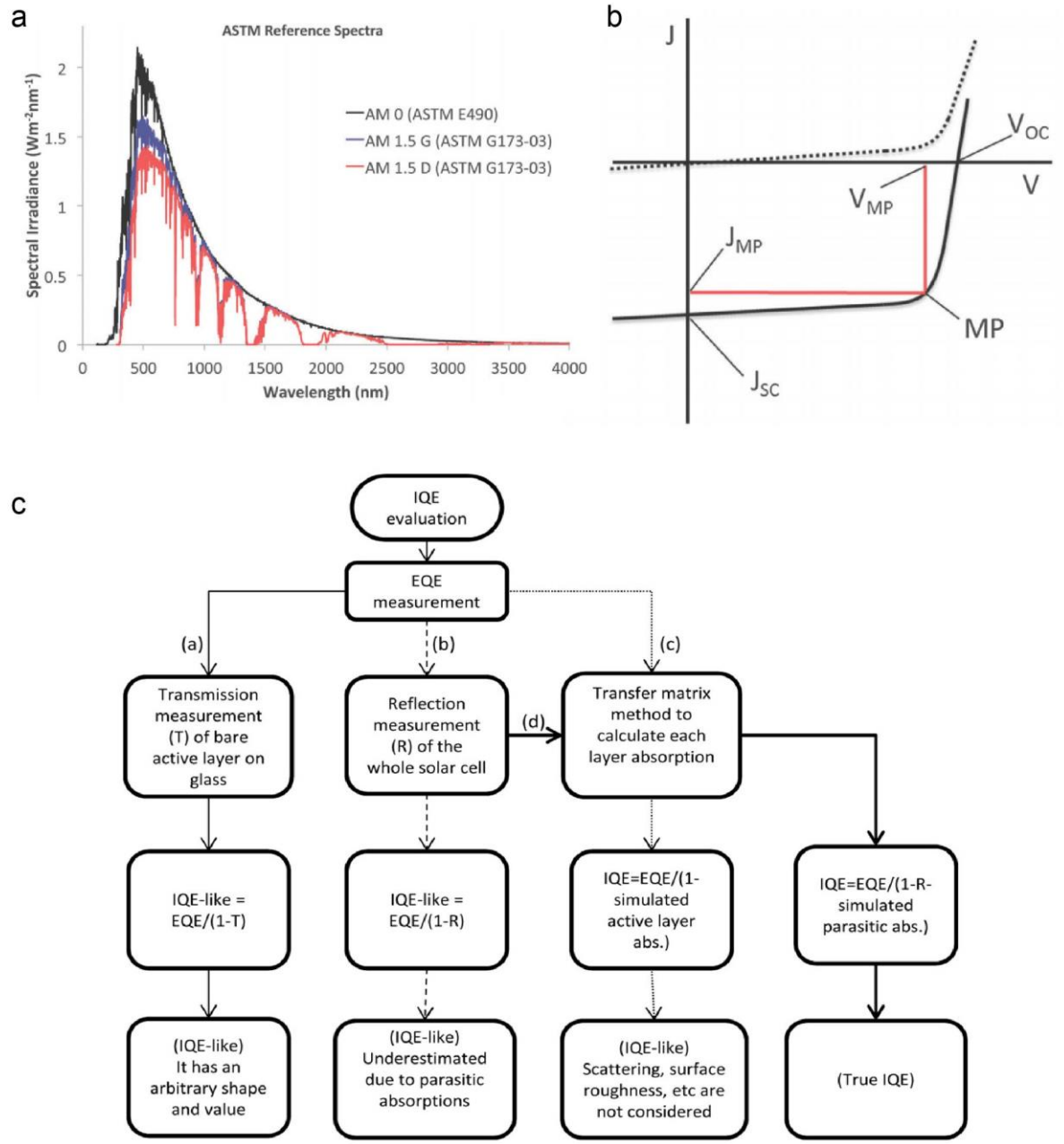

Figure 2. (a) AM 0 and AM 1.5 solar spectrum. (b) A typical J-V curve of a solar cell. Reproduced with permission.[1b] Copyright 2015, Royal Society of Chemistry. (c) Illustration of different approaches commonly used for IQE evaluation in thin film solar cells. Reproduced with permission.[17] Copyright 2014, American Chemical Society.

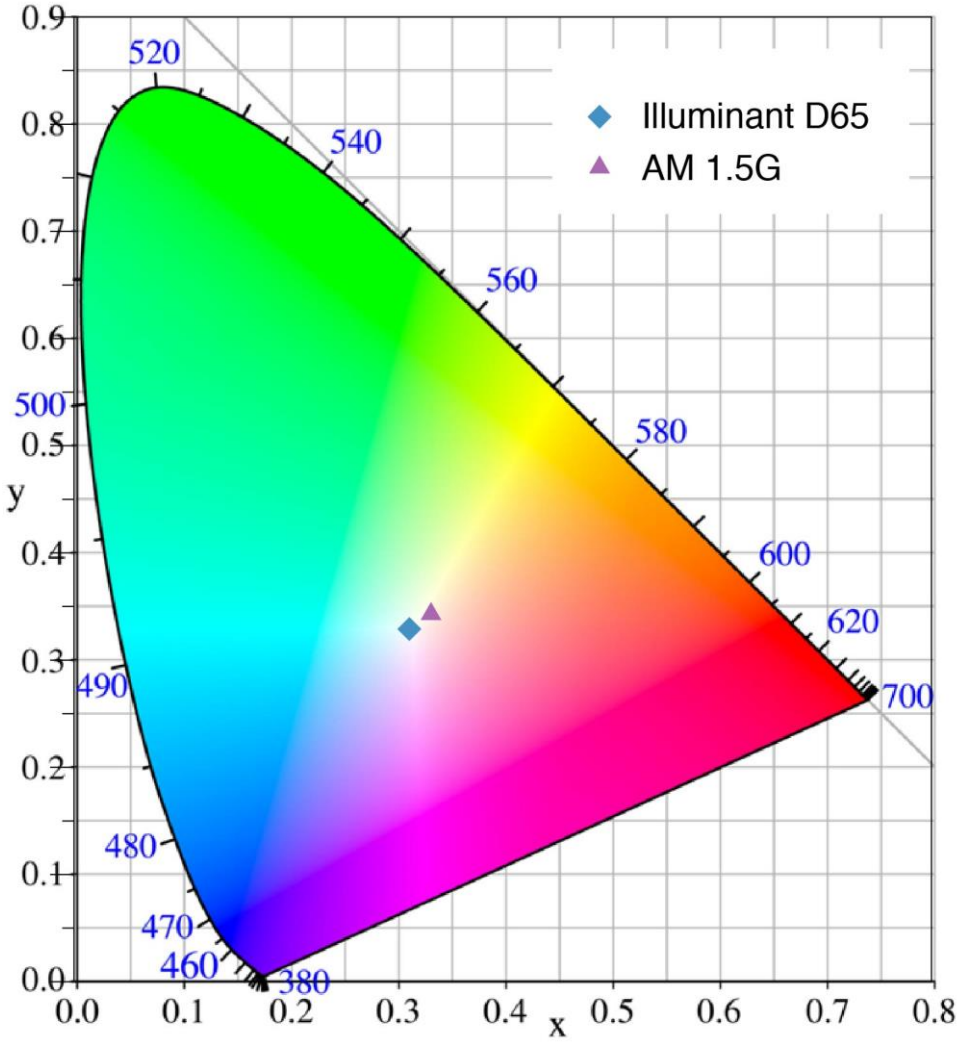

Figure 3. Color coordinates of Illuminant D65 and AM 1.5G light in CIE xy 1931 chromaticity diagram.

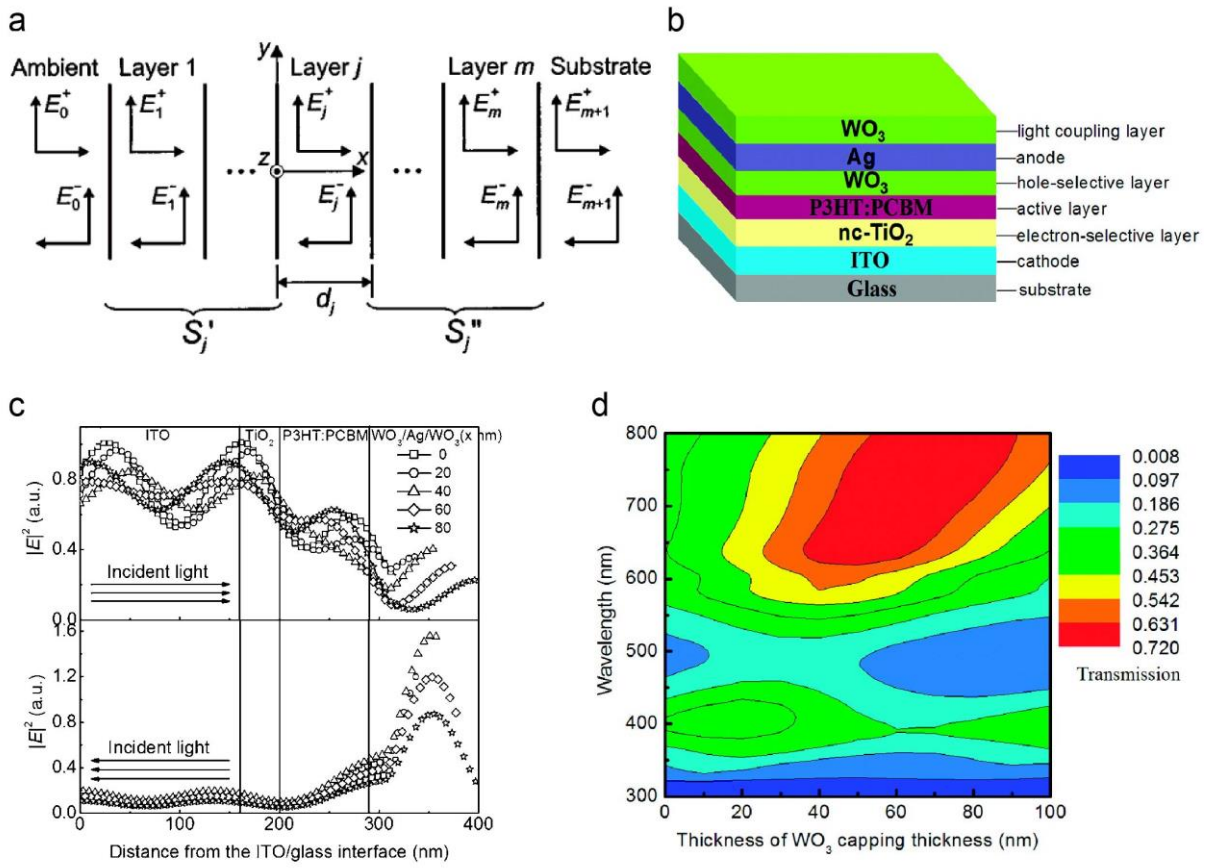

Figure 4. (a) Schematic illustration of a multilayer having m layers between a semi-infinite transparent ambient and a semi-infinite substrate with forward and backward-propagating optical electric field components used for TMM calculation. Reproduced with permission.[27] Copyright 1999, American Institute of Physics. (b) Schematic of the device structure of the inverted ST-OSC employing WO_3/Ag/WO_3 as transparent top electrode, (c) calculated distribution of the optical field intensity in the devices with different thickness of the WO_3 capping layer at 520 nm incident light, (d) simulated total transmittance of the device depending on the thickness of the WO_3 capping layer. Reproduced with permission.[28] Copyright 2011, American Chemical Society.

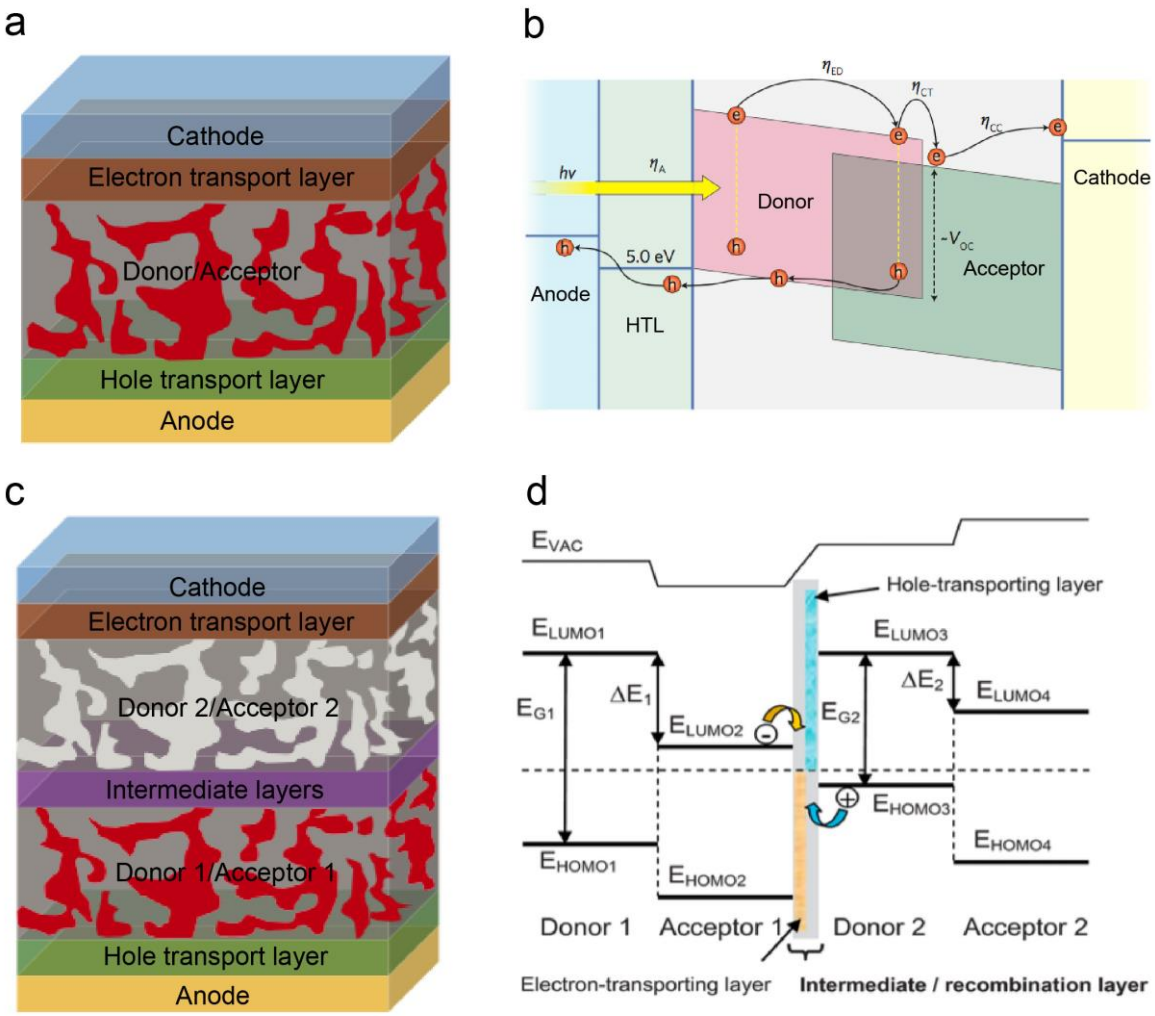

Figure 5. General device structures and the corresponding energy diagrams of single junction (a, b) and tandem (c, d) BHJ OSCs. Reproduced with permission.[5h, 5j, 33b] Copyright 2012, 2015, Nature Publishing Group; Copyright 2013, Royal Society of Chemistry.

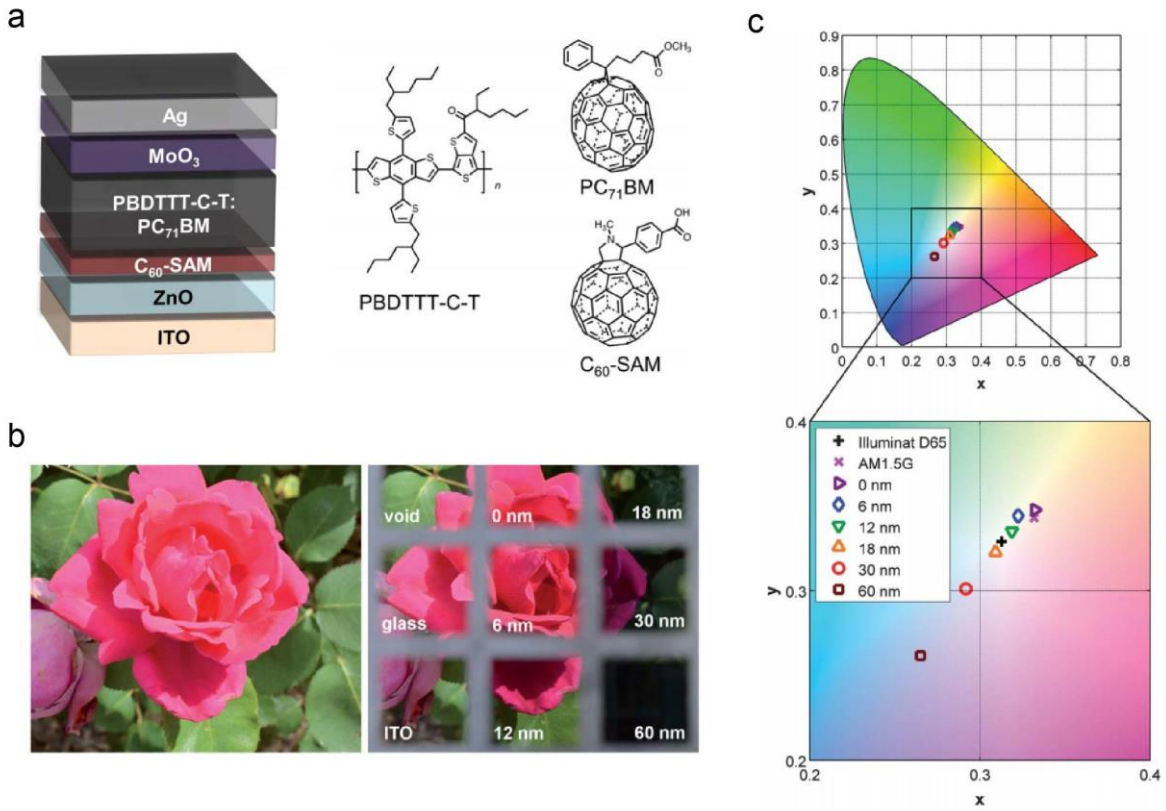

Figure 6. (a) Device structure and chemical structures of active materials. (b) Comparison of the photos taken through different semitransparent devices, and (c) color coordinates of ST-OSCs with different thickness of Ag electrodes under AM 1.5 G illumination in CIE xy 1931 chromaticity diagram. Reproduced with permission.[19] Copyright 2012, Royal Society of Chemistry.

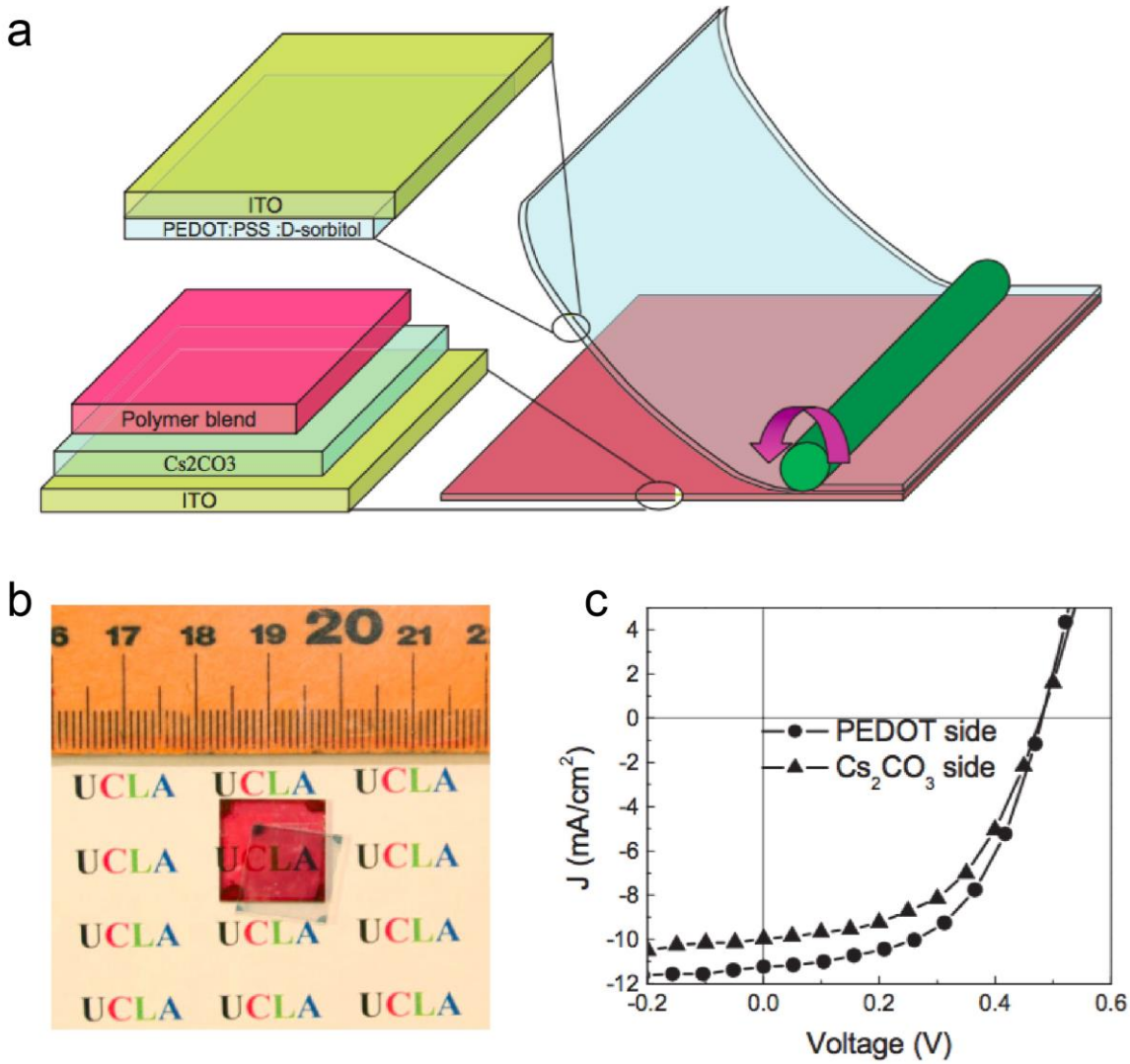

Figure 7. (a) Schematic illustration of device fabrication. (b) Photograph and (c) J-V curve of a ST device. Reproduced with permission.[46]

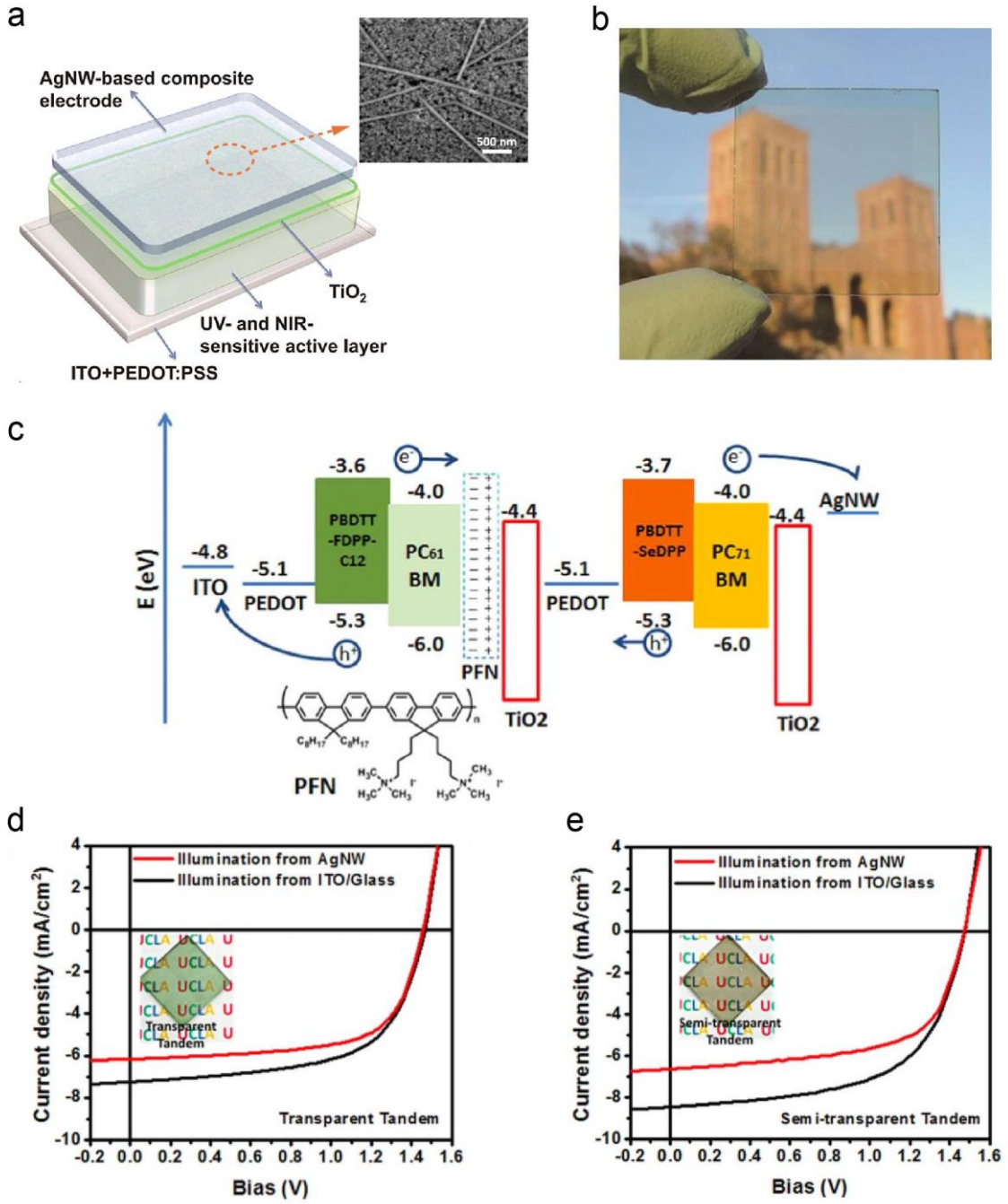

Figure 8. (a) Schematic of the device architecture and SEM image of AgNW-based composite electrode. (b) Photograph of a single junction transparent solar cell. Reproduced with permission.[53a] Copyright 2012, American Chemical Society. (c) Energy diagram of the tandem solar cell. (d, e) Photos and J-V curves of tandem ST-OSCs with different device transparency. Reproduced with permission.[25] Copyright 2013, Royal Society of Chemistry.

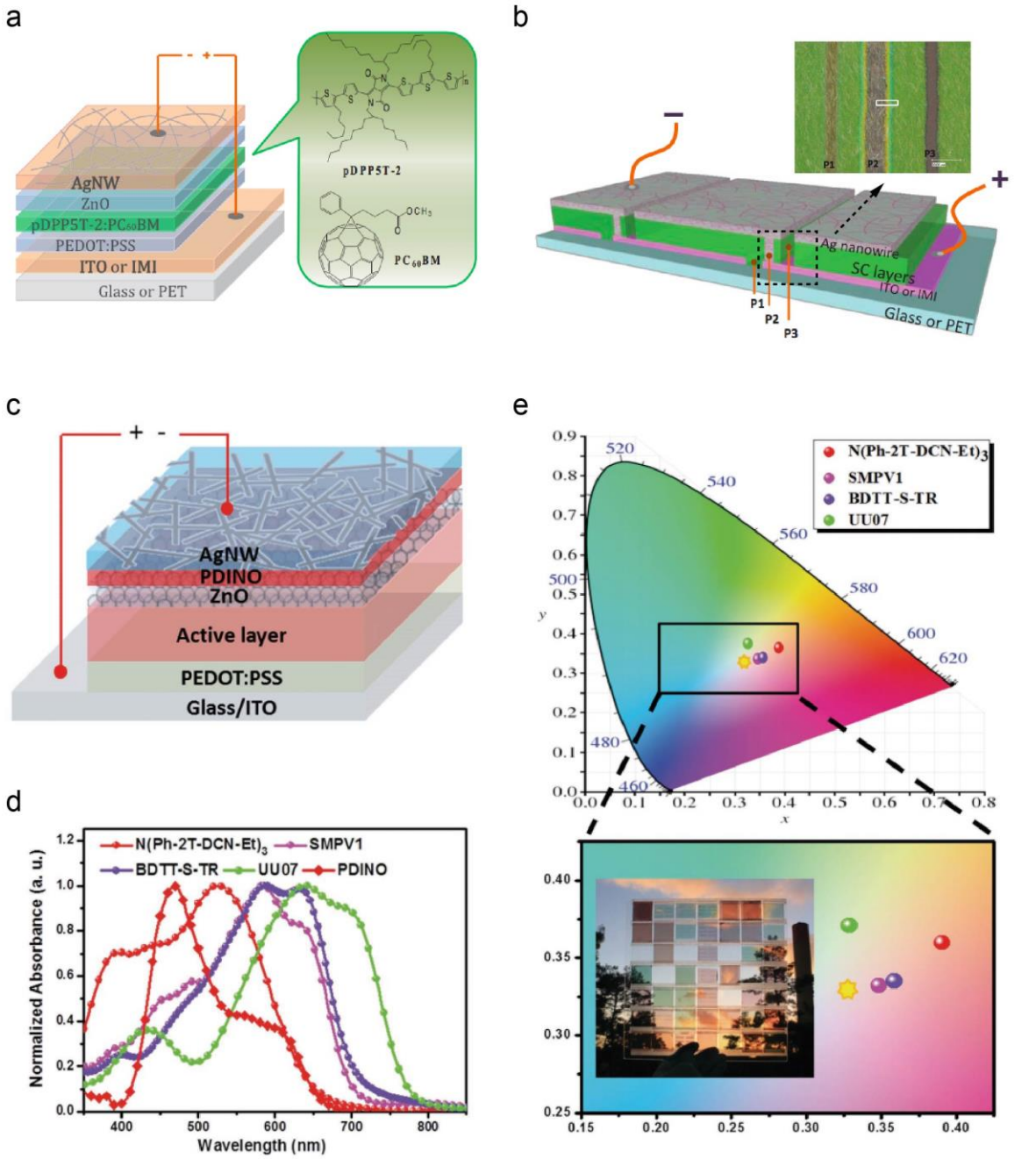

Figure 9. Schematic illustrations of (a) device structure and (b) semitransparent module for a ST-OSC based on pDPP5T-2:$PC_{60}BM$. Reproduced with permission.[51b] (c) Schematic of device structure, (d) absorption spectra of different donors, and (e) color coordinates of ST-OSCs based on different donors in CIE xy 1931 chromaticity diagram, in which a photograph taken through a module composed these ST-OSCs is inserted. Reproduced with permission.[53e]

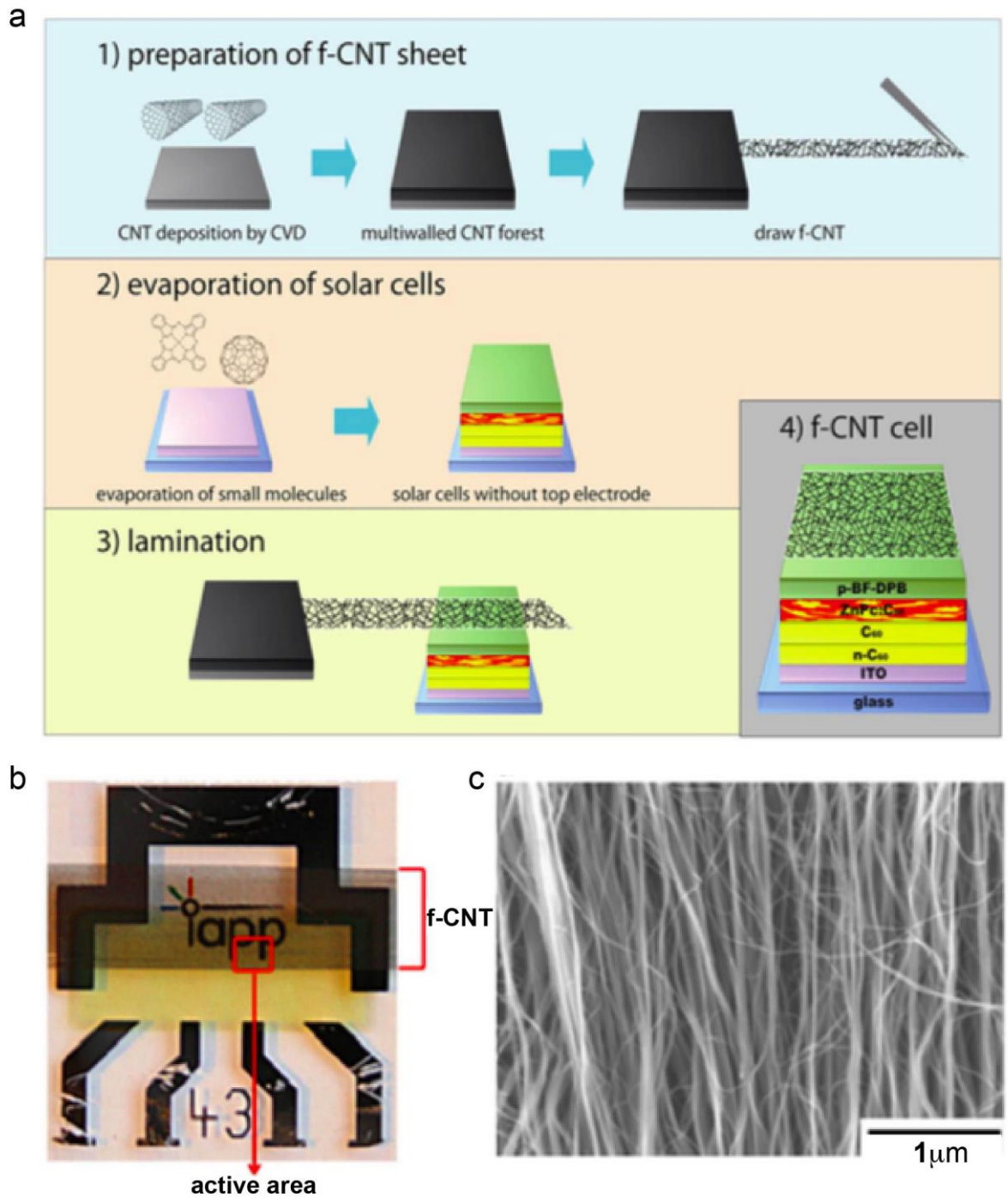

Figure 10. (a) Schematic illustration of device fabrication. (b) Photograph of a ST solar cell. (c) SEM image of the transparent CNT top electrode. Reproduced with permission.[29a] Copyright 2012, Elsevier.

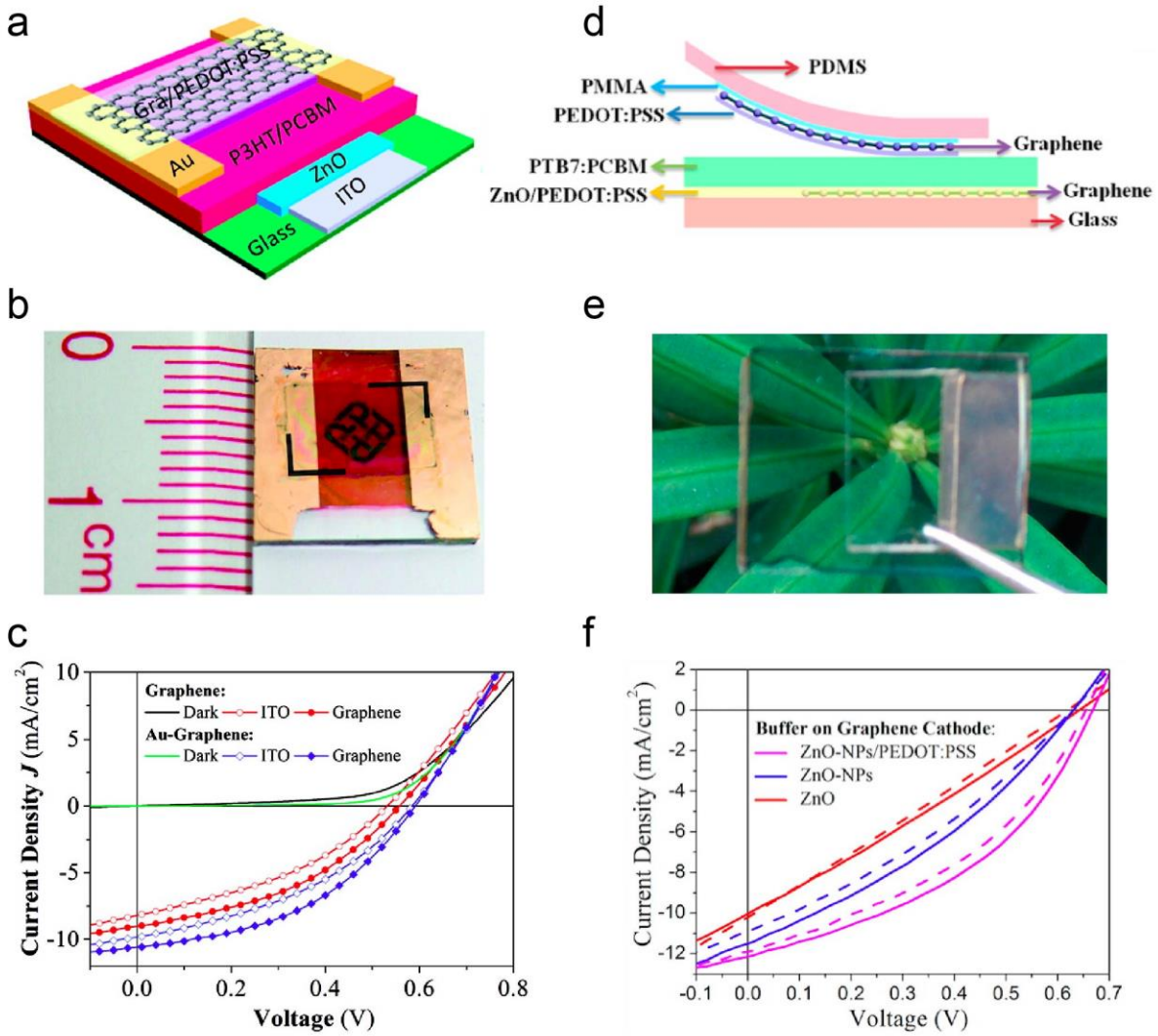

Figure 11. (a) Schematic illustration, (b) photograph, and (c) J-V curves of ST-OSC based transparent graphene top electrode. Reproduced with permission.[58] Copyright 2012, American Chemical Society. (d) Schematic illustration, (e) photograph, and (f) J-V curves of all- graphene based ST-OSC. Reproduced with permission.[60] Copyright 2015, American Chemical Society.

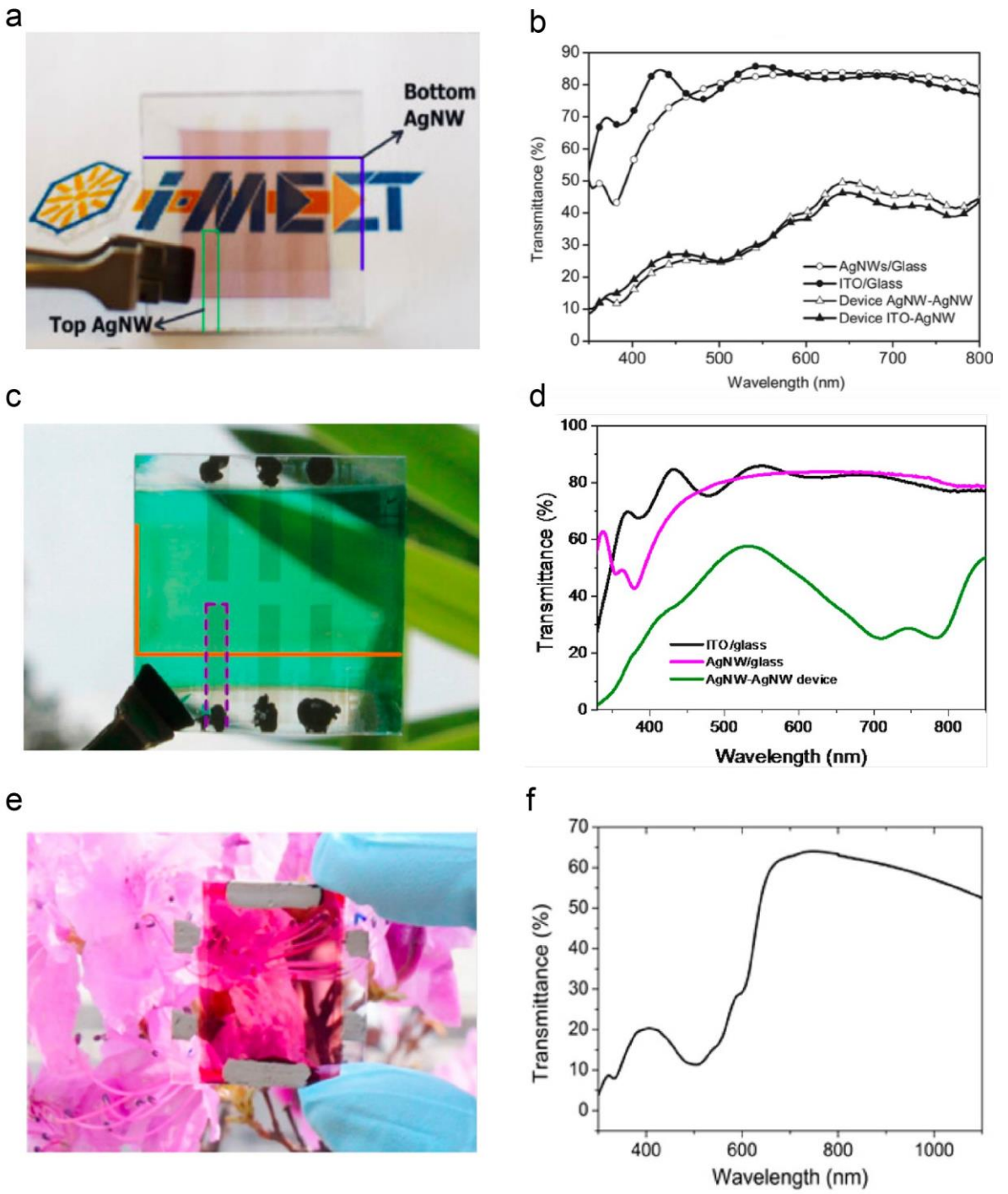

Figure 12 (a) Photograph and (b) transmittance of ST-OSCs with the structure ofAgNWs/AZO/P3HT:Si-PCPDTBT:$PC_{61}BM$/PEDOT:PSS/AgNWs. Reproduced with permission.[51a] (c) Photograph and (d) transmittance of ST-OSCs with the structure of AgNWs/PEDOT:PSS/PDD5T-2:$PC_{61}BM$/ZnO/AgNWs. Reproduced with permission.[65] Copyright 2014, American Chemical Society. (d) Photograph and (e) transmittance of ST-OSCs with the device structure of AgNWs/TiO_x/ZnO/P3HT:$PC_{61}BM$/PEDOT:PSS:GO/ PEDOT:PSS solar cell. Reproduced with permission.[66] Copyright 2014, American Chemical Society.

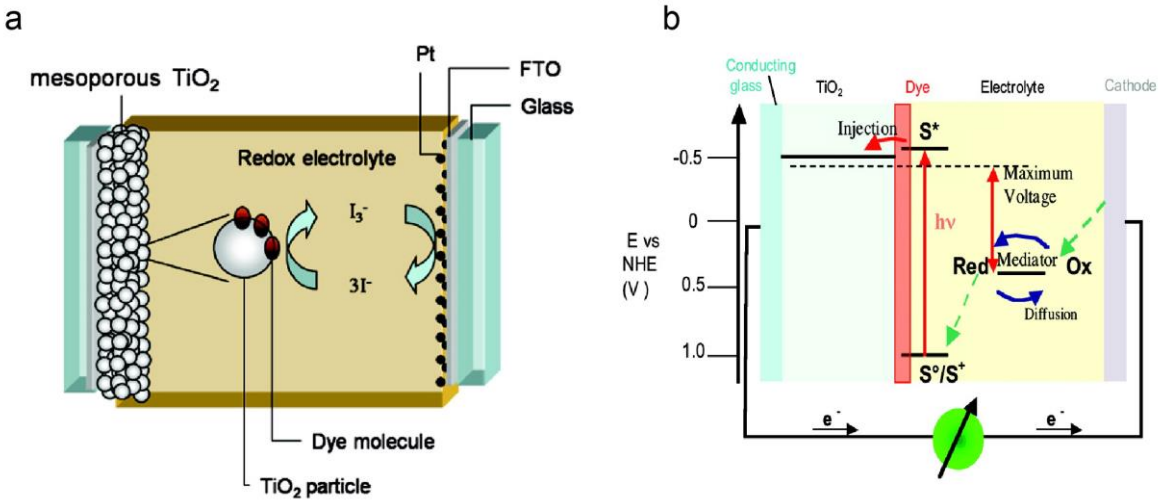

Figure 13 Schematic illustration of (a) structure, Reproduced with permission.[5b] Copyright 2010, American Chemical Society. (b) working mechanism of a typical DSC. Reproduced with permission.[1a] Copyright 2009, American Chemical Society.

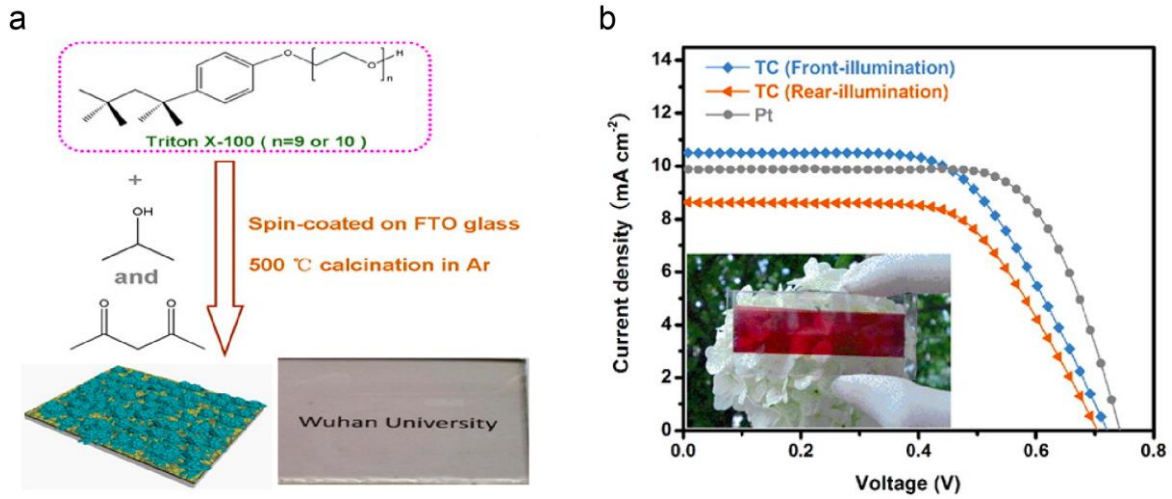

Figure 14 (a) Schematic illustration of the preparation and photograph of the transparent carbon CE. (b) J-V curves and photograph of a ST-DSC based on transparent carbon CE. Reproduced with permission.[83] Copyright 2013, American Chemical Society.

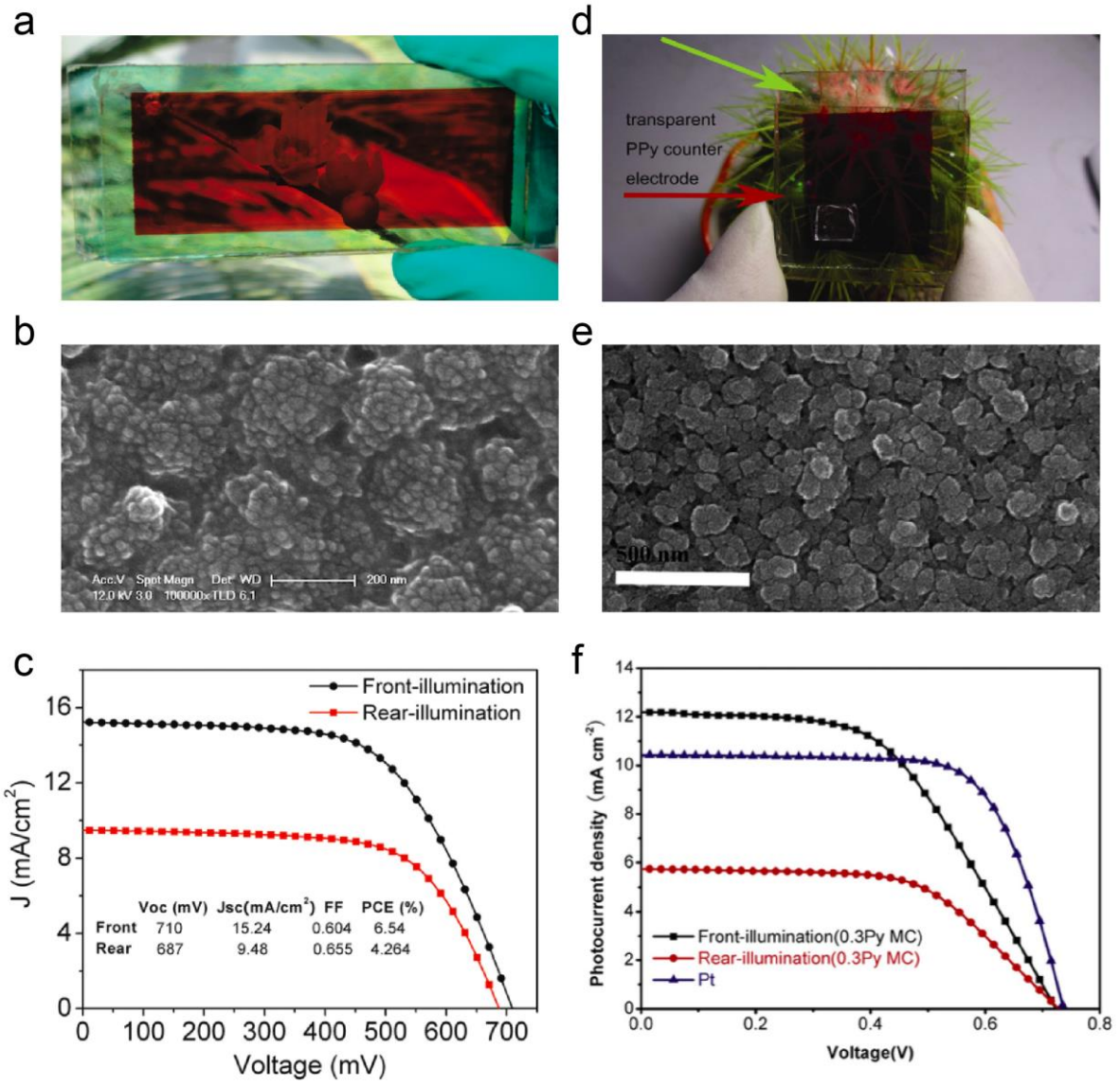

Figure 15 (a) Photograph of a ST-DSC based on transparent PANI CE. (b) SEM image of aPANI film. (c) The corresponding J-V curves of the PANI based device. Reproduced with permission.[84] Copyright 2011, American Chemical Society. (d) Photograph of a ST-DSC based on transparent PPy CE. (e) SEM image of aPPy film. (f) The corresponding J-V curves of the device with a PPy CE. Reproduced with permission.[87] Copyright 2013, Elsevier.

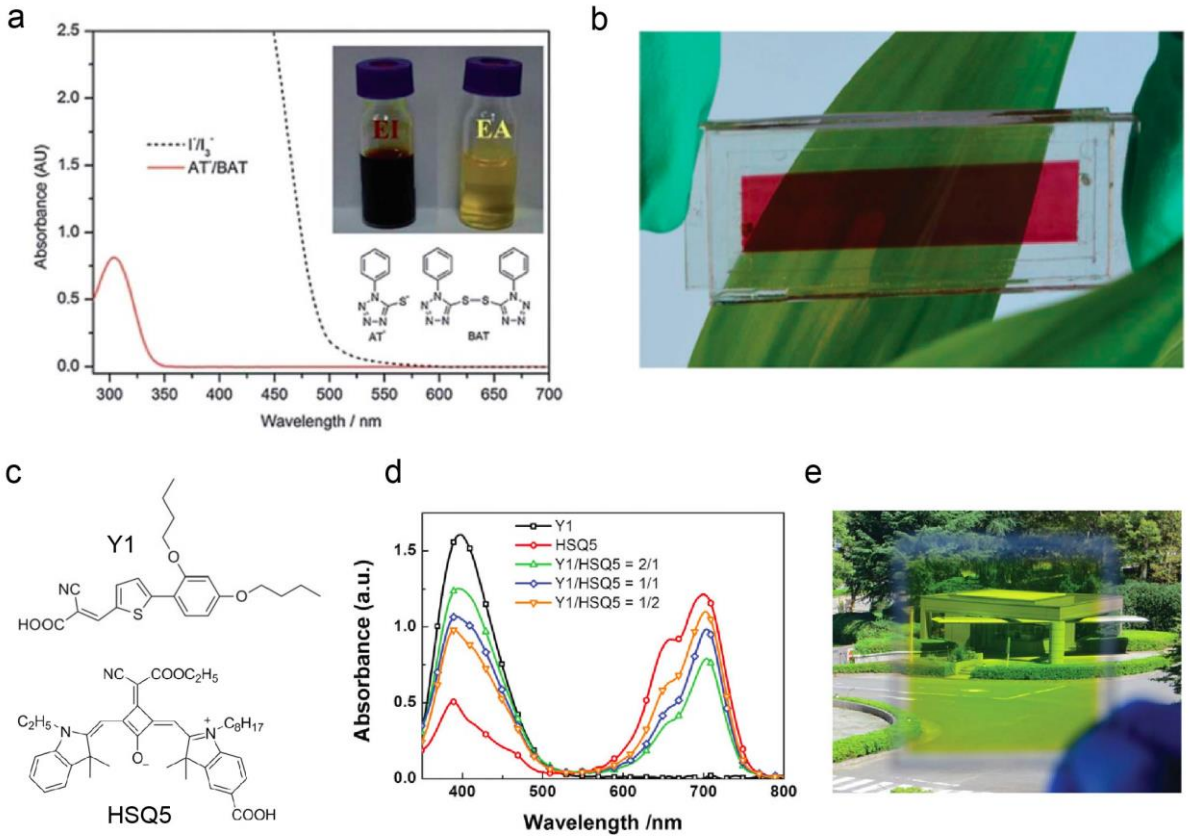

Figure 16 (a) Absorption spectra and photograph of AT^-/BAT and I^-/I_3^- electrolytes. (b) Photograph of ST-DSC based on transparent PEDOT CE and AT^-/BAT electrolyte. Reproduced with permission.[92] Copyright 2012, Royal Society of Chemistry. (c) Chemical structure of Y1 and HSQ5 dyes. (d) Absorption spectra of TiO_2 films sensitized by dye cocktails of Y1 and HSQ5 with different molar ratios. (e) Photograph of a ST-DSC based on Y1/HSQ5 cocktail dye using transparent Pt CE. Reproduced with permission.[107]

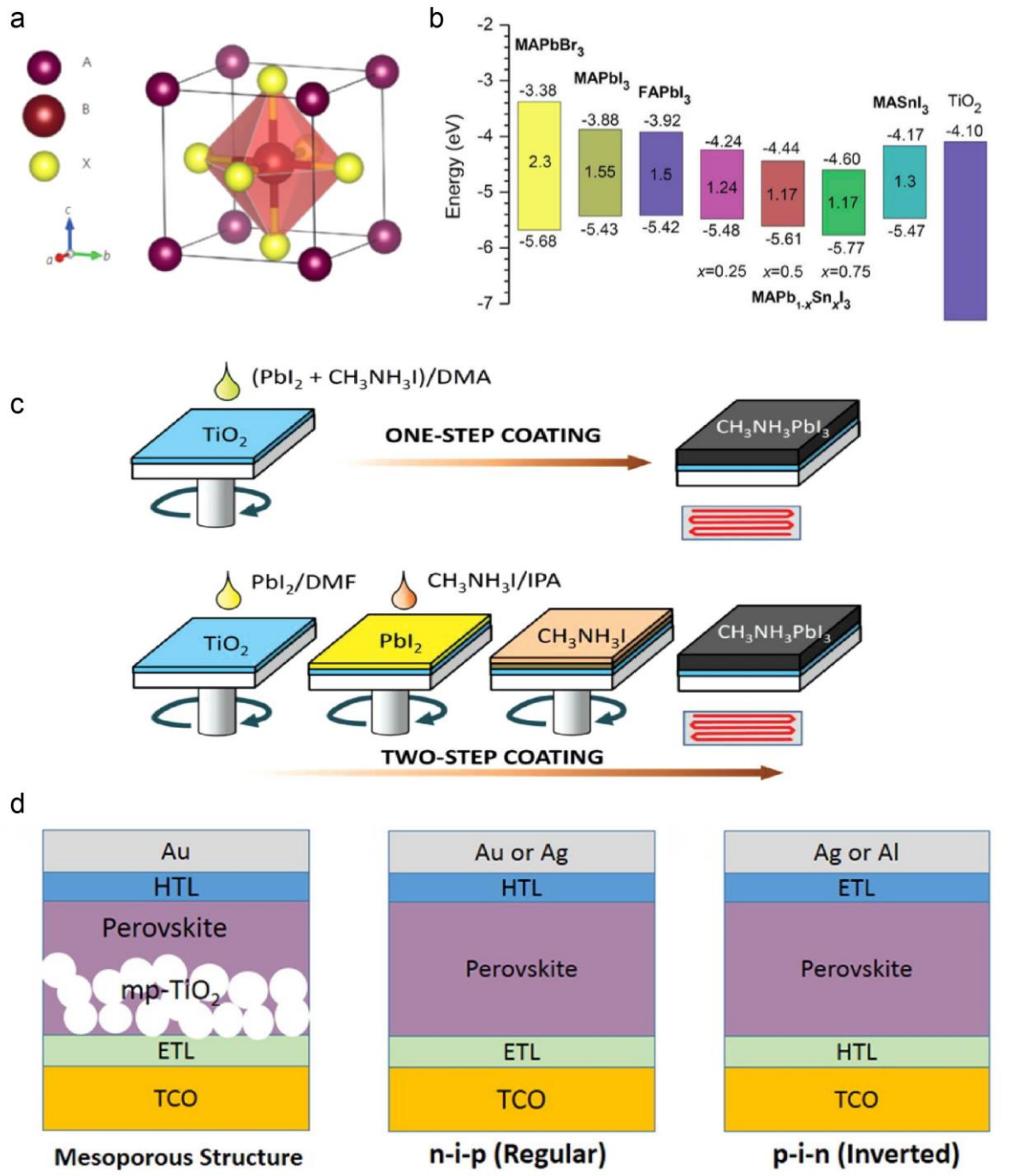

Figure 17 (a) Crystal structure of ABX_3perovskite, A is usually $CH_3NH_3^+$ (MA), $HC(NH_2)_2^+$ (FA) or mixture thereof, B is Pb or Sn and X is typically I^-, Cl^-, Br^- or mixture thereof. Reproduced with permission.[9k] Copyright 2014, Nature Publishing Group. (b) Schematic energy level diagram of perovskites with different compositions. Reproduced with permission.[9l] (c) Schematic illustration of one- and two-step methods for the deposition of perovskite films.[9l] (d) Schematic illustration of three typical structures of PSCs. Reproduced with permission.[9m] Copyright 2016, American Chemical Society.

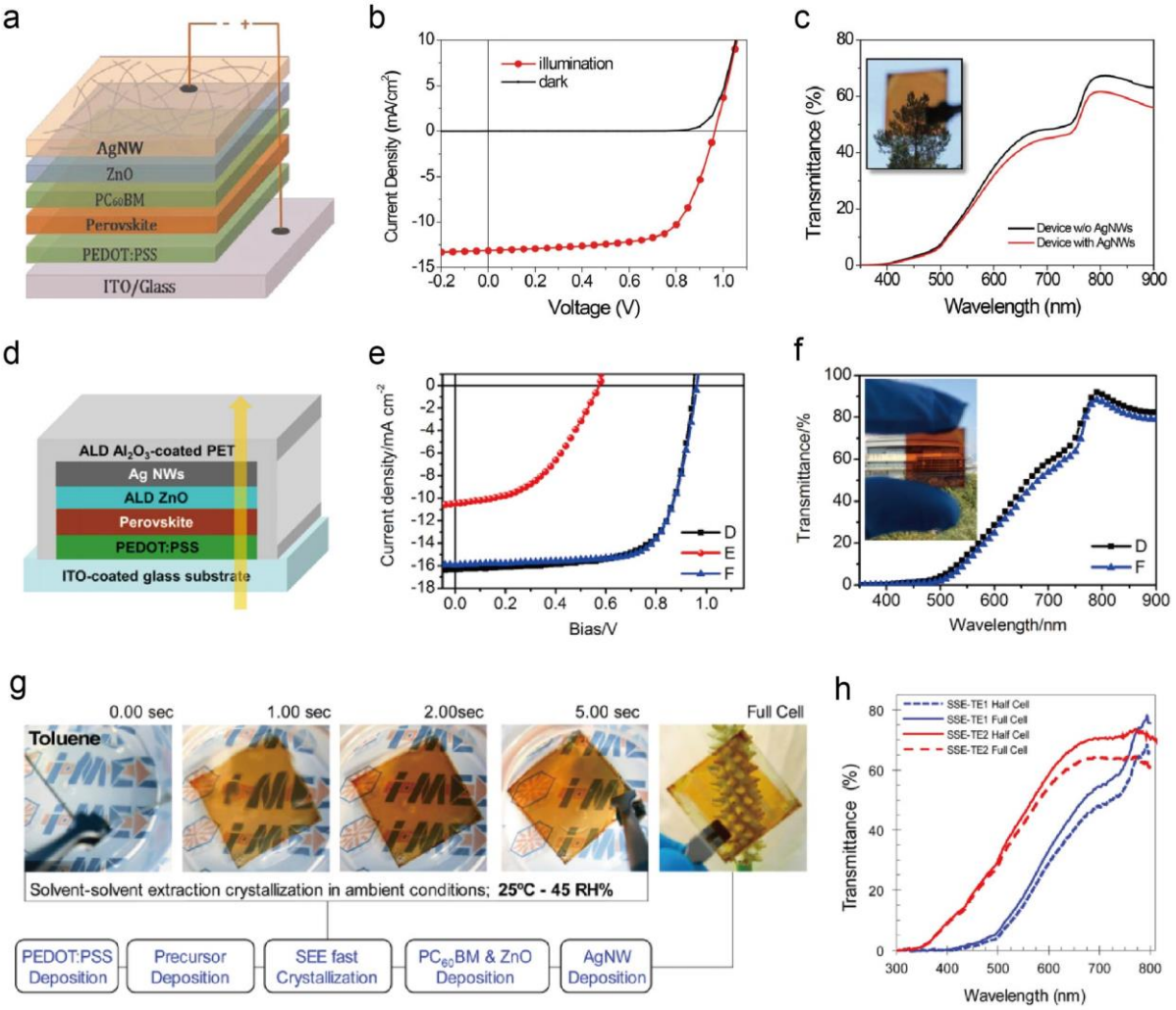

Figure 18 (a) Schematic structure of ST-PSC based on transparent AgNW top electrode. (b) J-V curve and (c) photograph and transmittance of the corresponding device. Reproduced with permission.[123] Copyright 2015, Royal Society of Chemistry. (d) Structure of ST-PSC using transparent AgNW top electrode coated with ALD-Al_2O_3 encapsulation layer (e) J-V curve, (f) photograph and transmittance of the corresponding device. Reproduced with permission.[124] Copyright 2015, American Chemical Society. (g) Demonstration of the SSE method with 5 seconds crystallization and photograph of a completed ST-PSC. (h) Transmittance of ST devices with and without AgNW top electrodes. Reproduced with permission.[126] Copyright 2015, Royal Society of Chemistry.

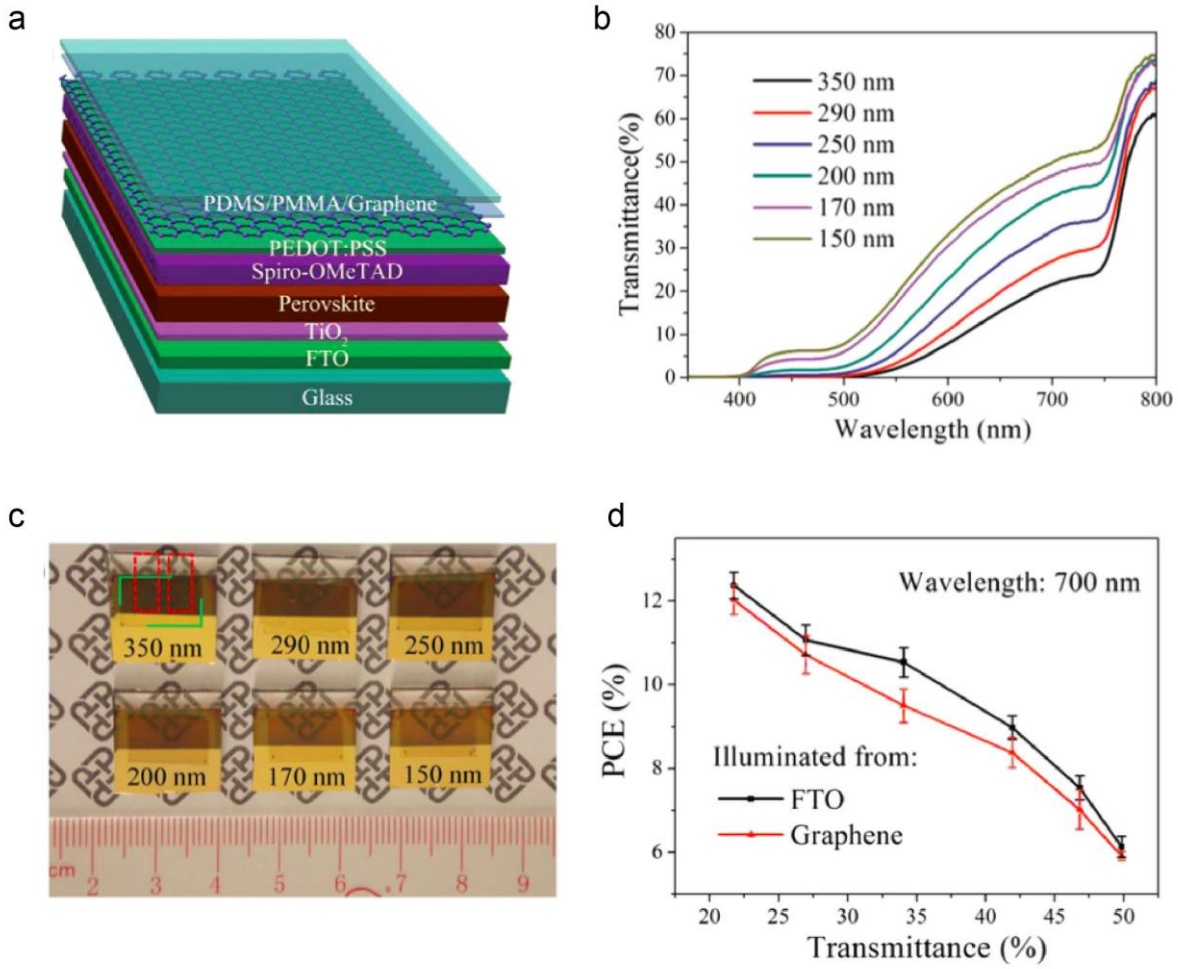

Figure 19 (a) Schematic structure of ST-PSCs based on transparent graphene top electrodes. (b) transmittance of perovskite layers with different film thickness. (c) Photographs of graphene-based ST-PSCs with different transparency. (d) Dependence of the PCE of ST-PSCs on device transmittance (the thickness of the perovskite layer). Reproduced with permission.[129]

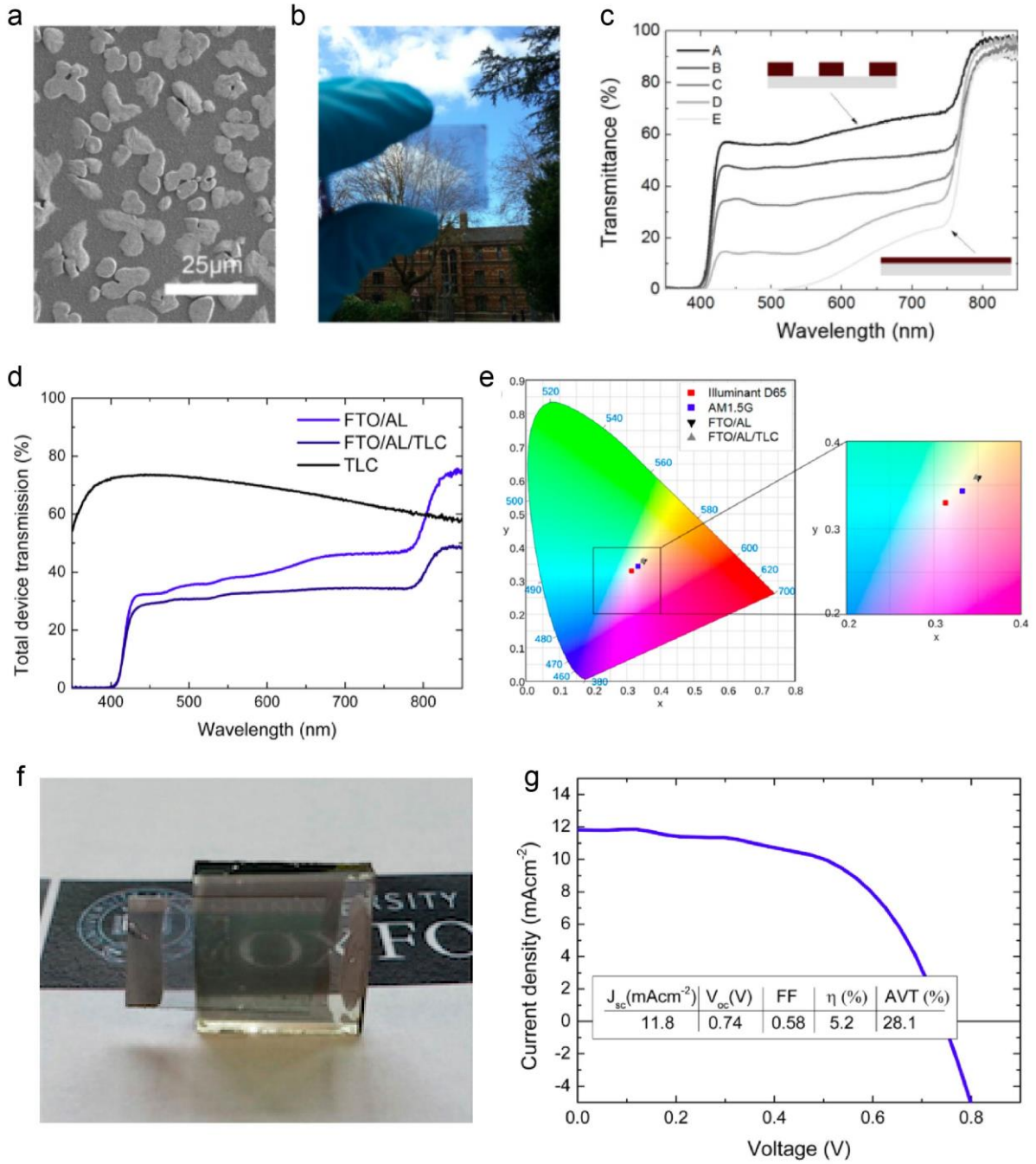

Figure 20 (a) SEM image and (b) photograph of a typical film of $MAPbI_3$perovskite islands. (c) Dependence of the transmittance of active layer on the coverage of $MAPbI_3$ perovskite film. Reproduced with permission.[131] Copyright 2014, American Chemical Society. (d) Transmittance of FTO/$FAPbI_3$, TLC electrode, and FTO/$FAPbI_3$/TLC and (e) the corresponding color coordinates of these films in CIE 1931 xy chromaticity diagram. (f) Photograph and (g) J-V curve of $FAPbI_3$ based neutral color ST-PSC. Reproduced with permission.[132] Copyright 2015, American Chemical Society.

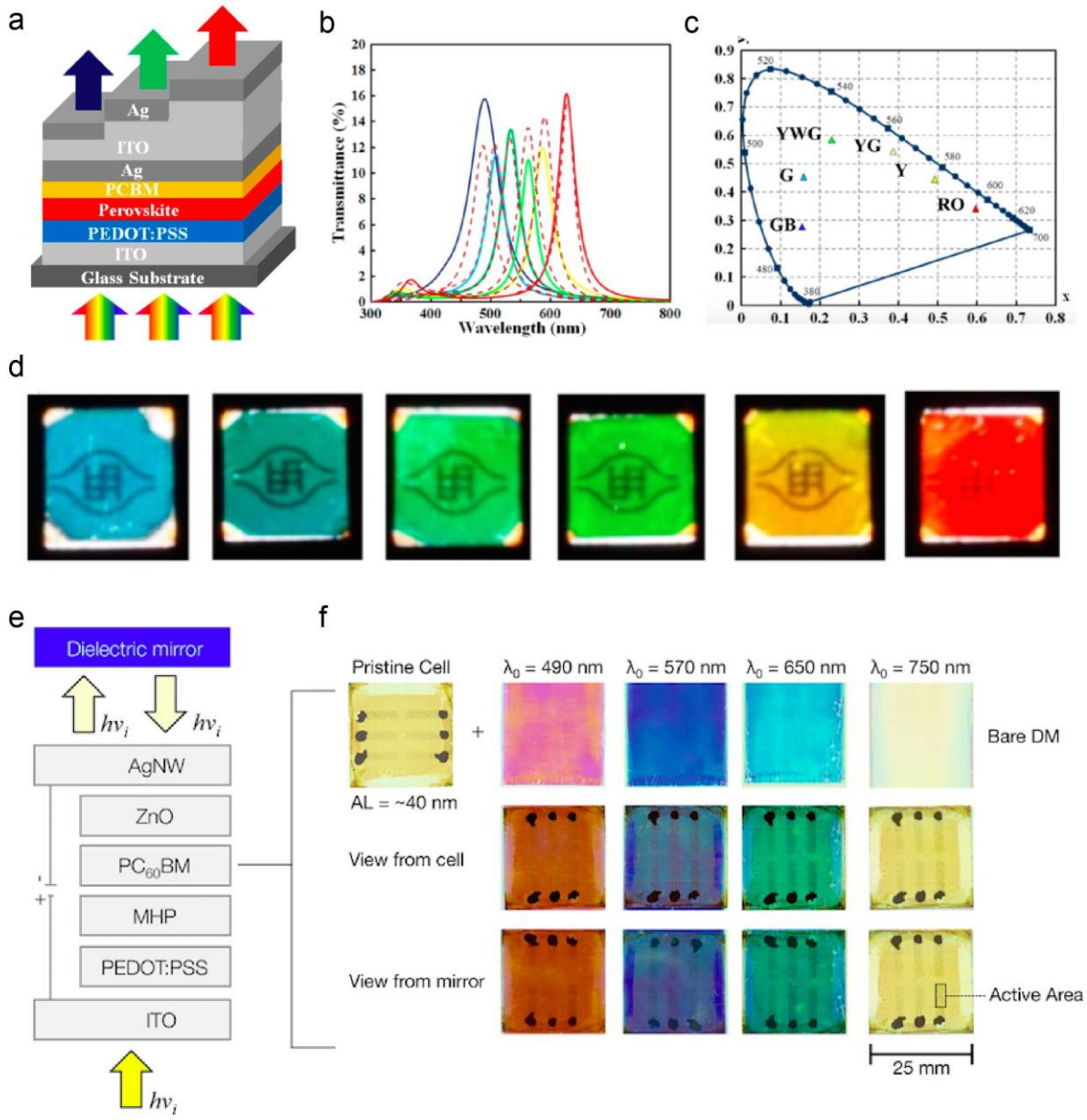

Figure 21 (a) Schematic illustration of microcavity-based ST-PSCs. (b) Measured (solid line) and simulated (dashed line) transmittance, (c) Color coordinates in CIE 1931 xy chromaticity diagram, and (d) photographs of microcavity-based ST-PSCs with different color appearances. Reproduced with permission.[20c] Copyright 2016, American Chemical Society. (e) Schematic structure of ST-PSCs employing dielectric mirrors. (f) Demonstration of the color-tuning of ST-PSC with dielectric mirrors of different optical responses, the views from solar cell and dielectric mirror sides are both presented. Reproduced with permission.[21] Copyright 2016, American Chemical Society.

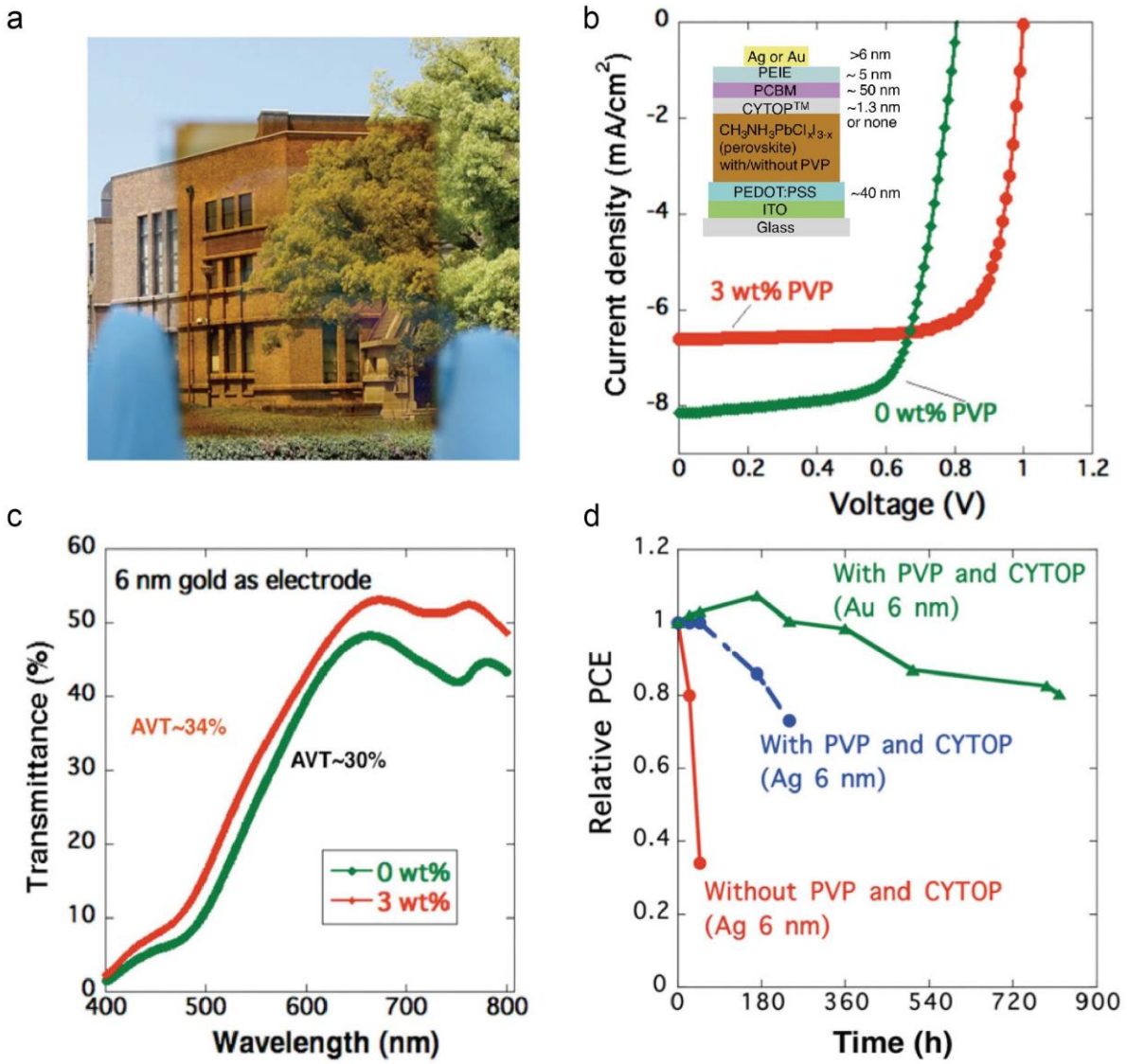

Figure 22 (a) Photograph of a PVP and CYTOP modified ST-PSC. (b) J-V curves, (c) transmittance, and air stability of ST-PSCs with and without PVP and CYTOP modification. Reproduced with permission.[140]

Table 1. Comparison of different materials for transparent electrodes used in solar cells.

Material	Transmittance (%)	Sheet resistance (Ω sq^{-1})[a]	Advantages	Disadvantages
ITO[13b]	85	<15	Good transparency and conductivity	Expensive, brittle, unstable to acid
FTO[13d]	80	15	Good transparency,conductivity and stability	Brittle, high roughness, low NIR transparency
AgNWs[13b]	90	<15	Solution processible, excellent transparency, couductivity and flexiblity	High roughness, poor adhesion
CNT[13c]	90	100	Solution processible, excellent transparency,couductivity ,flexiblity and stability	Low output, high resistance and roughness
Graphene[13d]	90	30	Excellent transparency, couductivity and flexiblity	Low doping stability
PEDOT:PSS[13e]	>80	<65	Soulution processible, low cost	Low environmental stability

[a] sheet resistance measured on glass substrate

Table 2. Summary of the representative ST-OSCs.

Top electrode	Device structure	PCE (%)[a)]	AVT (%)	Ref
Thin film Au	ITO/Cs_2CO_3/P3HT:$PC_{61}BM$/V_2O_5/Au	0.85	-	[34]
	AZO/ZnO/P3HT:$PC_{61}BM$/MoO_3/Au/MoO_3	2[b)]		[18]
Thin film Ag	ITO/PEDOT:PSS/ZnPc/PyF/Cr/Ag/ZnPc	0.5	~40 (400-550 nm)	[35]
	ITO/C_{60}:NDNI/C_{60}/F_4-ZnPc:C_{60}/DiNPB/DiNPB:NDP9/ C_{60}:NDNI/C_{60}/DCV6T:C_{60}/BPAPF/BPAPF:NDP9/ DiNPB:NDP9/ C_{60}:NDNI/Ag/Al/Alq_3	4.9	24	[37]
	ITO/ZnO/C_{60}-SAM/PBDTTT-C-T:$PC_{71}BM$/MoO_3/Ag	6	25	[19]
	ITO/ZnO/C_{60}-SAM/PCPDTFBT:$PC_{71}BM$/PEDOT:PSS/Ag	5	47.3	[38]
	ITO/PEDOT:PSS/PIDT-PhabQ:$PC_{71}BM$/C_{60}-bis/Ag	4.2	32	[29d]
	PET/ITO/ TiO_2/C_{60}-SAM/PSEHTT:ICBA/PANI/Ag	6.87	36	[39]
	ITO/ZnO/PDBTT-DPP:$PC_{71}BM$/MoO_3/Ag/Si NPs/Alq_3	6.22	32	[40]
	ITO/TiO_2/PCDTBT:$PC_{71}BM$/WO_3/Ag/photonic crystal	5.2-5.3	30-25	[26a]
	ITO/PEDOT:PSS/PTB7:$PC_{71}BM$/bathocuproine (BCP)/Ag/ non-periodic photonic crystal	5.6	30	[29c]
	ITO/TiO_2/P3HT:$PC_{61}BM$/MoO_3/Ag /MoO_3	1.4	-	[43a]
	ITO/TiO_2/P3HT:$PC_{61}BM$/WO_3/Ag /WO_3	1.9	-	[28]
	ITO/TiO_2/P3HT:$PC_{61}BM$/V_2O_5/Ag / V_2O_5	1.79	-	[42b]
	ITO/ p-BF-DBP/ ZnPc:C_{60}/ C_{60}/ n-C_{60}/Ag	2.2	28	[55]
	Glass/AgNWs/ p-BF-DBP/ ZnPc:C_{60}/ C_{60}/ n-C_{60}/Ag	2.1[b)]	23	[55]
	Glass/PEDOT:PSS/ p-BF-DBP/ ZnPc:C_{60}/ C_{60}/ n-C_{60}/Ag	1.9[b)]	29	[55]
TCO	ITO/TiO_2/P3HT:$PC_{61}BM$/MoO_3/ITO (sputtered)	1.9	80 (650-800 nm)	[45]
	ITO/Cs_2CO_3/P3HT:$PC_{61}BM$/PEDOT:PSS:D-sorbitol/ITO	3	70 (650-800 nm)	[46]
	ITO/PEDOT:PSS/PCDTBT:$PC_{71}BM$/TiO_x/AZO	4	34	[47]
AgNWs	ITO/AZO/P3HT:$PC_{61}BM$/PEDOT:PSS/AgNWs	2	-	[53b]
	ITO/PEDOT:PSS/PDBTT-DPP:$PC_{61}BM$/TiO_2/AgNWs -ITO NPs composite	4	61 (400-650 nm)	[53a]
	ITO/PEDOT:PSS/PBDTT-FDPP-C_{12}:$PC_{61}BM$/PFN/TiO_2/PEDOT:PSS/PBDTT-SeDPP:$PC_{61}BM$ ($PC_{71}BM$)/TiO_2/ AgNWs-ITO NPs composite	6 (7)	40 (30)	[25]
	ITO/MoO_x/PBDTTPD:$PC_{71}BM$/ZnO/AgNWs	5	34	[53c]
	ITO glass (PET)/PEDOT:PSS/pDD5T-2:PC61BM/ZnO/AgNWs	2-2.7[c]	~50 (450-650 nm)	[51b]
	ITO/PEDOT:PSS/BDTT-S-TR:$PC_{71}BM$/ZnO/PDINO/AgNWs	3.62	~30	[53e]
	AgNWs/AZO/P3HT:Si-PCPDTBT:$PC_{61}BM$/PEDOT:PSS/AgNWs	2.2[b]	33	[51a]
	AgNWs/PEDOT:PSS/pDDP5T-2:$PC_{61}BM$/ZnO/AgNWs	2.9[b]	41	[65]
	Graphene/PEDOT:PSS/PSEHTT:ICBA/ZnO/PEDOT:PSS/PBDTT-DPP:$PC_{71}BM$/TiO_2/AgNWs	8.02[b]	45	[67]
CNTs	ITO/n-C_{60}/C_{60}/ZnPc:C_{60}/p-BF-DBP/CNTs	1.5	-	[29a]
	ITO/ p-BF-DBP/ ZnPc:C_{60}/ C_{60}/ n-C_{60}/CNTs	1.3	24	[55]
	Glass/PEDOT:PSS/ p-BF-DBP/ ZnPc:C_{60}/ C_{60}/ n-C_{60}/CNTs	1.1[b)]	22	[55]
	ITO/ZnO/PTB7:$PC_{71}BM$/MoO_3/CNTs	3.7-4.1	-	[56]
Graphene	ITO/ZnO/P3HT:$PC_{61}BM$/GO/graphene	1.8-2.5	-	[57]
	ITO/ZnO/P3HT:$PC_{61}BM$/PEDOT:PSS/graphene	3	-	[58]
	Glass/graphene/PEDOT:PSS/ZnO/PTB7:$PC_{71}BM$/PEDOT:PSS/Graphene	3.4[b)]	40	[60]
PEDOT:PSS	ITO/ZnO/C_{60}-SAM/P3HT:$PC_{61}BM$/PEDOT:PSS/PH500	2.51	-	[63a]
	ITO/ZnO/P3HT:$PC_{61}BM$/PAH-D/PH500	1.68	-	[63b]
	ITO/ZnO/P3HT:$PC_{61}BM$/PEDOT:PSS:PH1000	~2.4	~70 (650-800 nm)	[63d]
	Glass/PH1000/ZnO/P3HT:PC61BM/PEDOT:PSS/PH1000	1.8[b)]	~55 (650-800 nm)	[63c]
	Glass/AgNWs/TiOx/ZnO/P3HT:$PC_{61}BM$/PEDOT:PSS/GO/PH1000	2.3[b)]	~60 (650-800 nm)	[66]

[a)] PCEs obtained with illuminations from the bottom electrode. [b)]These are ITO-free devices.

[c)]The PCE varies with glass and PET substrates as well as the device areas.

Table 3. Summary of the representative ST-DSCs.[a)]

CE material	Device structure	PCE (%)[b)]	AVT (%)	Ref
Pt	FTO/c-TiO_2/mp-TiO_2/N719/(I^- /I_3^-) /Pt/FTO	6.17	~10 (600-800 nm)	[75]
	FTO /mp-TiO_2/Y1-HSQ5/(I^- /I_3^-) /Pt/FTO	3.66	60 (500-600 nm)	[107]
	FTO/ c-TiO_2/mp-TiO_2/N719/(I^- /I_3^-) /Pt/FTO	3.5	24	[108]
	FTO/c-TiO_2/mp-TiO_2/photonic crystal/N719/(I^- /I_3^-) /Pt/FTO	4.5	9.5	[108]
Carbon	FTO/c-TiO_2/mp-TiO_2/N719/(I^- /I_3^-) / Carbonized FTO	6.07	-	[83]
Conducting polymer	FTO /mp-TiO_2/N3/(I^- /I_3^-) /PANI/FTO	6.54	-	[84]
	FTO /mp-TiO_2/N3/(I^- /I_3^-) /PPy/FTO	5.74	-	[87]
	FTO/c-TiO_2/mp-TiO_2/N719/(AT^- /BAT) / PEDOT/FTO	6.07	-	[92]
AgNWs	FTO/c-TiO_2/mp-TiO_2/D35/Spiro-MeOTAD/ PEDOT:PSS/ AgNWs	3.6	-	[97]

[a)]This table only summarizes ST-DSCs with photographs or transmittance spectra presented in the original papers, bifacial DSCs are not included, as the transparency of these devices is unknown. It is noteworthy that bifacial DSCs can be easily made semitransparent by reducing the thickness of the photoactive layers.[b)]PCEs obtained with illuminations from the bottom electrode.

Table 4. Summary of the representative ST-PSCs.

Top electrode	Device structure	PCE (%)[a)]	AVT (%)	Ref
Thin film Au	ITO/PEDOT:PSS/$MAPbI_3$/$PC_{61}BM$/Au/LiF	7.3 (6.4)	22 (29)	[109]
	FTO/ c-TiO_2/mp-TiO_2/$MAPbI_3$grid/Spiro-MeOTAD/Au	4.9 (0.38)	19 (67)	[110]
	FTO/ c-TiO_2/$MAPbI_3$/Spiro-MeOTAD/MoO_3/Au/MoO_3	13.6 (5.3)	7 (31)	[111]
	Glass/Au/PEDOT:PSS/ $MAPbI_3$/$PC_{61}BM$/ MoO_3/Au//Ag/ MoO_3/Alq_3	8.67 (4.11)	15.9 (31.6)	[112]
	FTO/ c-TiO_2/$MAPbI_3$ islands/ Spiro-MeOTAD/Au	8 (3.5)	7 (30)	[131]
	FTO/ c-TiO_2/$MAPbI_3$ islands (OTS)/ Spiro-MeOTAD/Au	6.1	38	[133]
	ITO/PEDOT:PSS/$MAPbI_3$-PVP/CYTOP/$PC_{61}BM$/PEIE/Au	5.36	34	[140]
Thin film Ag	ITO/CuSCN/$MAPbI_3$/$PC_{61}BM$/Bis-C_{60}/Ag	10.7 (7.5)	13 (37.5)	[113]
	ITO/PEDOT:PSS/$MAPbI_3$/$PC_{61}BM$/MUTAB/Ag	11.8	20.8	[114]
	ITO/PEDOT:PSS/$MAPbI_3$/$PC_{61}BM$/PTCBI/Ag/WO_3/PTCBI/Ag	3.86	-	[20b]
	ITO/PEDOT:PSS/$MAPbI_3$/$PC_{61}BM$/Ag/ITO/Ag	7.6	~8	[20c]
	ITO/PEDOT:PSS (thiourea treated)/$MAPbI_3$/$PC_{71}BM$/C_{60}/ AUH/Ag	9.4 (8.2)	29 (34)	[115]
TCOs	FTO/ c-TiO_2/$MAPbI_3$/PTAA/ITO/glass	15.8 (12.6)	6.3 (17.3)	[117a]
	FTO/c-TiO_2/mp-TiO_2/$MAPbI_3$/Spiro-MeOTAD/MoO_x/ITO	6.2	-	[117b]
	ITO/PEDOT:PSS/$MAPbI_3$/$PC_{61}BM$/AZO/ITO	12.3	-	[117c]
	FTO/ZnO/$PC_{61}BM$/$MAPbI_3$/MoO_3/IO:H	14.1	-	[118]
	ITO/SnO_2/PEIE/$PC_{61}BM$/$MAPbI_3$/Spiro-MeOTAD/MoO_x/IO:H/ITO	16.3	-	[122]
	FTO/c-TiO_2/mp-TiO_2/$MAPbI_3$/Spiro-MeOTAD/MoO_x/IZO	10.36	-	[119]
	FTO/c-TiO_2/mp-TiO_2/$MAPbI_3$/Spiro-MeOTAD/MoO_3/AZO/Ni-Al grid/MgF_2	12.1	-	[120]
	FTO/ c-TiO_2/$MAPbI_3$ islands (PS treated)/PEDOT:PSS/ITO /glass	6.17±2.32	20.9	[134]
AgNWs	ITO/PEDOT:PSS/$MAPbI_3$/$PC_{61}BM$/ZnO/AgNWs	8.5	28.4	[123]
	ITO/PEDOT:PSS/$MAPbI_3$/ ALD-ZnO/AgNWs/ALD-Al_2O_3	10.55	22.5	[124]
	FTO/ c-TiO_2/$MAPbI_3$/Spiro-MeOTAD/ Au/AgNWs	11.07	-	[125]
	ITO/PEDOT:PSS/$MAPbI_{3-x}Cl_x$/$PC_{61}BM$/ZnO/AgNWs	8.12 (3.55)	28 (46)	[126]
CNT	FTO/ c-TiO_2/mp-TiO_2/$MAPbI_3$/CNTs	6.29	-	[127]
	FTO/ c-TiO_2/mp-TiO_2/$MAPbBr_3$/CNTs	4.84	-	[128]
	FTO/ c-TiO_2/mp-TiO_2/$MAPbBr_3$/CNTs/PMMA	5.33	-	[128]
Graphene	FTO/ c-TiO_2/ $MAPbI_{3-x}Cl_x$/ Spiro-MeOTAD/PEDOT:PSS/ Graphene	12.02	-	[129]
PEDOT:PSS	FTO/ c-TiO_2/mp-TiO_2/$MAPbI_3$/ Spiro-MeOTAD /PEDOT:PSS	10.1/2.9[b)]	7.3	[130]

[a] PCEs obtained with illuminations from the bottom electrode. [b] The 10.1 and 2.9 % PCE corresponds to device area of 0.06 and 2.4 cm^2, respectively.

Dr. Qidong Tai is currently an assoicate researcher at Institute for Interdisciplinary Research, Jianghan University. He obtained his PhD in materials physics and chemistry from Wuhan University in 2012. From 2014-2015, he joined Prof. Feng Yan's group at The Hongkong Polytechnic University as a postdoctoral research fellow. His current research interests include transparent conductive electrode materials and solar cells.

Prof. Feng Yan has research interests on thin film transistors, solar cells, 2D materials, organic electronics, biosensors and smart materials. He received his PhD degree in physics from Nanjing University in China. Then he joined the Engineering Department of Cambridge University in Feb 2001 as a Research Associate and joined National Physical Laboratory in UK in April 2006 as a Higher Research Scientist. He became an Assistant Professor at the Department of Applied Physics of the Hong Kong Polytechnic University in September 2006 and was promoted to Full Professor in 2016.

Recent developments of semitransparent organic solar cells, dye-sensitized solar cells, and perovskite solar cells are reviewed with a focus on different device design, transparent top electrode materials and the corresponding device fabrication techniques. Key issues related to the optimization of the efficiency, color, and transparency of the semitransparent photovoltaic devices are discusssed in details.

Keywords: semitransparent, organic solar cells, dye-sensitized solar cells, perovskite solar cell

Q. D. Tai and F. Yan*

Title: Emerging Semitransparent Solar Cells: Materials and Device Design

ToC figure ((Please choose one size: 55 mm broad × 50 mm high **or** 110 mm broad × 20 mm high. Please do not use any other dimensions))